



## **Design and Analysis of a Network Arch Bridge**

**Bernardo Morais da Costa**

Thesis to obtain the Master of Science Degree in

**Civil Engineering**

**Examination Committee**

Chairperson: Professor José Manuel Matos Noronha da Câmara

Supervisor: Professor José Joaquim Costa Branco de Oliveira Pedro

Member of the Committee: Professor Francisco Baptista Esteves Virtuoso

**October 2013**



# Abstract

The present dissertation aims the design and analysis of the hanger arrangement and the structural stability of a Network arch bridge – a tied-arch bridge with inclined hangers that cross each other at least twice. A comparative analysis with other types of hanger arrangements is also performed.

Possible solutions with respect to spans, materials and deck cross-section typology are presented and succinctly discussed. Modeling using a tridimensional finite element model of the main bridge is described.

A detailed analysis of the hanger arrangement influence on the structural behavior is performed for the adopted solution. Four different arrangements of hangers – a vertical, a Nielsen and two different Network arrangements – are compared in terms of stress distributions, deflections, hangers' relaxation and fatigue behavior.

The linear stability analysis is finally performed for the four different models, comparing their buckling modes and discussing the results with respect to different load patterns and load increments. The critical loads are evaluated using the European standards formulation, a simplified method and FEModel models.

**Keywords:** Network arch bridge, Tied-arch bridge, Bowstring bridge, roadway bridge design, hanger arrangement, arch buckling, arch stability analysis



## Resumo

Na presente dissertação apresenta-se o projeto base de uma ponte em arco superior do tipo *Network* – uma ponte do tipo *Bowstring* com pendurais inclinados que se cruzam entre si pelo menos duas vezes. São também analisados e comparados outros tipos de arranjo dos pendurais.

Possíveis soluções relativamente aos vãos, aos materiais e à secção transversal do tabuleiro são apresentadas e sucintamente discutidas. A modelação, usando um modelo de elementos finitos da ponte, é descrita.

É analisada a influência do tipo de arranjo dos pendurais na resposta estrutural do modelo. Quatro tipos diferentes de arranjos: um vertical, um *Nielsen* e dois arranjos *Network* diferentes são comparados em termos das distribuições de esforços, deformações, comportamento à fadiga e relaxação dos pendurais.

Finalmente foi realizada uma análise linear de estabilidade para os quatro modelos diferentes, comparando os seus modos de instabilidade e discutindo os resultados para diferentes distribuições e incrementos de carga. As cargas críticas são avaliadas adotando diferentes procedimentos do Eurocódigo, um método simplificado e análises lineares e não lineares de um modelo de elementos finitos.

**Palavras-chave:** ponte *Network*, ponte *Bowstring*, ponte em arco superior, arranjo de pendurais, dimensionamento de ponte rodoviária, estabilidade do arco, instabilidade do arco



## Acknowledgements

I want to first express my gratitude towards Professor José Oliveira Pedro for giving me the opportunity of studying this subject and continuously guiding me throughout the entire duration of this dissertation, and to Professor Angel C. Aparicio Bengoechea. Only with these esteemed professors continuous help, amazing knowledge, motivating personalities and inspiring teachings I was able to develop the design and analysis here presented. Along with Professor Francisco Virtuoso, the three were my personal favorite professors during my entire career, and to have two of them actually guiding and supporting my project is a true blessing.

Acknowledgments also to Professors Joan Ramon Casas and Philippe Van Bogaert, Eng. Pedro Gonçalves and mostly to Diogo Tomás Peixoto, for his true contribute and incentives.

The result of this dissertation was only possible thanks to Per Tveit, Benjamin Brunn, Frank Shanack and several other researchers' intensive work on the subject and their will to share it on numerous publications. For that I am honestly grateful. Though, my most special thanks go to my parents, not for the thesis, but for the person who made it, that they, kindheartedly, designed! And I hope to show that to them, every day.

Finally, I send my appreciations to all the people who use bridges as metaphors for good things, as they, in a certain way, contribute to a more pleasant and gratifying result from the study of this type of structures.





# Contents

1. Introduction.....	1
1.1 General Overview.....	1
1.2 Main Objectives.....	3
1.3 Document Outline .....	4
2. Alternative and Adopted Solution.....	5
2.1 Local Constraints .....	5
2.2 Alternative Solutions .....	6
2.2.1 Options for the Bridge Spans .....	6
2.2.2 Deck Cross-Section Solutions .....	8
2.3 Adopted Solution .....	8
2.3.1 General Layout .....	8
2.3.2 Composite Deck Advantages.....	13
2.3.3 Structural Elements.....	14
2.3.3.1 Slab.....	14
2.3.3.2. Tie (Longitudinal Beam) .....	15
2.3.3.3. Rib (Transversal Beam).....	16
2.3.3.4. Arch .....	16
2.3.3.5. Hangers (Network Arrangement).....	18
2.3.3.6. Secondary Elements – (Bracing Beams and End-Cross-Girders).....	24
2.3.4 Deck Support Conditions.....	25
2.3.5 Constructive Procedures .....	26
2.3.6 Comparison with Built Tied-Arch Bridges .....	31
3. Design Actions and Modeling.....	35
3.1 Actions.....	35
3.1.1 Traffic Loads .....	35
3.1.1.1 Approach Viaduct.....	36

3.1.1.2 Bowstring Bridge .....	38
3.1.2 Wind Load .....	39
3.1.3 Seismic Action .....	40
3.1.4 Temperature Actions.....	41
3.1.5 Combinations of Actions .....	42
Ultimate Limit State (ULS) .....	42
Serviceability Limit State (SLS) .....	43
3.2 Modeling .....	43
4. Structural Analysis.....	47
4.1 Overview .....	47
4.2 Deck Slab Analysis .....	47
4.3 Ribs Analysis .....	54
4.4 Ties Analysis .....	58
4.5 Arches Analysis.....	69
4.6 Hangers Analysis .....	73
4.7 Expansion Joints .....	81
5. Hanger Arrangements and Arch Instability Investigations .....	85
5.1 Overview .....	85
5.2 Hanger Arrangements' Investigations.....	86
5.3 Arch Instability Analysis.....	94
5.3.1 Load cases and sequence of application .....	94
5.3.2 Critical loads and buckling modes.....	96
5.3.3 Other forms of evaluating the arch critical load .....	105
5.3.4 Discussion of the results.....	111
6. Conclusions and Future Developments.....	113
6.1 General Conclusions.....	113
6.2 Future Developments.....	114
References.....	115
Appendixes.....	A-1

Appendix A – Bowstring Bridge Characteristics and Loads .....	A-3
Appendix B – Combination of Actions $\Psi$ Factors .....	A-7
Appendix C - Approach Viaduct Structural Verifications .....	A-9
C.1 Deck Slab .....	A-9
C.2 Longitudinal Beams .....	A-11
C.3 Columns.....	A-13
Appendix D – Bowstring Arch Main Columns Verifications .....	A-15
Appendix E – Expansion Joint Definition.....	A-17

# List of Figures

Figure 1 – Arch mechanism, expressed as a “will to open”, when sustaining loads.....	1
Figure 2 – Arch bridge with a higher deck.....	1
Figure 3 – Tied-arch bridge. ....	1
Figure 4 – Nielsen arrangement of hangers. 1 set of hangers. ....	2
Figure 5 – Hangers cross each other once. 2 sets of hangers. ....	2
Figure 6 – Network arrangement of hangers – most hangers cross each other twice. 3 sets of hangers.....	2
Figure 7 - Steel weight comparison between different steel bridge types - <i>Per Tveit (2011)</i> . ....	2
Figure 8 - The Brandanger Sound Bridge - by <i>Per Tveit</i> . 220 m Span.....	3
Figure 9 – Plan view of the Llobregat River, with the plan alignment. ....	5
Figure 10 – Elevation view of the Llobregat River, with the bridge road profile. ....	5
Figure 11 – Road deck cross-section. ....	5
Figure 12 – Future high speed train cross-section. ....	6
Figure 13 – Future highway cross-section.....	6
Figure 14 – 1st Solution. Bowstring Bridge with 190 meters span. ....	6
Figure 15 – 2 <sup>nd</sup> Solution. Bowstring Bridge with piers inside the river. ....	7
Figure 16 – 3 <sup>rd</sup> Solution. Approach bridge supports require a small railway displacement. ....	7
Figure 17 – 4 <sup>th</sup> Solution. Lateral approach viaduct spans too long. ....	7
Figure 18 – Central suspended solution for the deck cross-section. ....	8
Figure 19 - Plan view of the river and bridge proposed.....	9
Figure 20 – Deck cross-section detailing of the adopted solution (m). ....	10
Figure 21 – Elevation view of the entire adopted solution (m). ....	10
Figure 22 – Elevation view of the arch span (m).....	11
Figure 23 – Top view of the arch span (m).....	11
Figure 24 – Adopted cross-section (m). ....	12
Figure 25 – Concrete slab and longitudinal reinforcement adopted.....	14
Figure 26 – Steel ties cross-section adopted in the main span.....	15
Figure 27 – Steel longitudinal beams cross-section, adopted in the approach viaducts.....	15
Figure 28 – Rib’s center cross-section adopted. ....	16
Figure 29 - Rib’s end cross-section adopted. ....	16

Figure 30 – Steel arch cross-section characteristics.....	17
Figure 31 – Hanger cross-section and characteristics of the adopted solution. *Tension Rod Type 860, 80 mm diameter, $N_{R,d}$ according to EC3. PFEIFER Cable Structures.....	18
Figure 32 – Optimal arrangement of hangers on a concrete deck, using constant spacing between hangers at the arch level.....	19
Figure 33 – 0.55 ratio of load length to span length.....	21
Figure 34 – Ratio of live load / dead load and ratio of load length / span length combinations that make at least one hanger relax, in a 200 m span bridge, designed for the IABSE Congress in Vienna (1980), according to <i>Per Tveit (2011)</i> .....	21
Figure 35 – Adopted hanger’s slope to prevent relaxation, <i>Per Tveit (2011)</i> .....	22
Figure 36 – Influence line for shear force over A-A, used to manually obtain the crossed hanger’s axial force. ....	23
Figure 37 – Hangers final layout: Constant 5 m spacing on the tie; Parallel hangers with a slope of $65^{\circ}$ .....	23
Figure 38 – Bracing beams and end-cross-girder location.....	24
Figure 39 – Bracing beam cross-section (m). ....	24
Figure 40 – End cross girder - End cross-section.....	25
Figure 41 – End cross girder - Middle cross-section. ....	25
Figure 42 – Bowstring bridge deck constraints. ....	25
Figure 43 – Approach bridge constraints (left deck displayed). The inferior left corner of the figure is the point fixed to the abutment. ....	26
Figure 44 – Arch construction on the riverside, and floating cranes erecting the steelwork – <i>Pentele Bridge (2006)</i> .....	26
Figure 45 – Arch being lifted into position by small cranes over the approach spans. Lake Champlain Bridge (2011).....	27
Figure 46 – The Fort Pitt Bridge (1959), during its construction phase. ....	27
Figure 47 – Rotation of the arch scheme. ....	27
Figure 48 – New Sado Railway River Crossing.....	28
Figure 49 – Approach viaduct constructive process. ....	28
Figure 50 – Proposed constructive process - pushing the arch through the approach viaduct. Image sequence from <i>Per Tveit (2011)</i> .....	29
Figure 51 – Composite slab solution example. ....	29
Figure 52 – Precast concrete slab solution examples. ....	30
Figure 53 – Definition of Load model 1, according to <i>EN1991-2</i> . ....	35
Figure 54 –Tandem System “TS(123R_R)”.....	36
Figure 55 –Tandem System “TS(R31_2R)”.....	36

Figure 56 - 1 <sup>st</sup> Lane positioning for: UDL1 + TS(R31_2R).....	37
Figure 57 - 2 <sup>nd</sup> Lane positioning for: UDL2 + TS(R31_2R).....	37
Figure 58 – 3 <sup>rd</sup> Lane positioning for: UDL2 + TS(123R_R).....	37
Figure 59 – 4 <sup>th</sup> Lane positioning for: UDL1 + TS(123R_R).....	37
Figure 60 – Load combination: “UDL-All + TS(123R_R)”.....	38
Figure 61 – Uniformly distributed load “UDL(1R_R)”.....	39
Figure 62 – Uniformly distributed load “UDL(R1_R)”.....	39
Figure 63 – Deck’s wind exposed area. Scheme of the deck’s cross-section.....	39
Figure 64 - Response spectrum introduced in SAP2000 software.....	41
Figure 65 – Different views of the final model of the bowstring bridge.....	43
Figure 66 – Rib, ties and slab sketch.....	44
Figure 67 – Model of the rib with stiff elements. Rib frame element in red and stiff elements in purple.....	44
Figure 68 – Extrude view of the rib as composite beam. Slab in green, steel beam in red, stiff elements in purple.....	44
Figure 69 – Deck Model. Ribs and ties.....	45
Figure 70 – Deck Model. Ribs, ties and slab.....	45
Figure 71 – Introduction of the arch, hangers and bracing beams to complete the model.....	45
Figure 72 - Slab's $m_{11}$ due to SDL (only left-half deck is shown).....	48
Figure 73 - Slab's $f_{11}$ due to SDL (only left-half deck is shown).....	49
Figure 74 - Slab's $m_{11}$ max envelope, due to TS(R31_2R) (only left-half deck is shown).....	50
Figure 75 - Slab's $m_{11}$ min envelope, due to TS(R31_2R) (only left-half deck is shown).....	50
Figure 76 - $f_{11}$ on the slab, due to wind load (all deck is shown).....	51
Figure 77 – $f_{11}$ on the slab, due to negative uniform temperature (Deck: $-22^{\circ}$ ; Arches and hangers: $-29^{\circ}$ ).....	51
Figure 78 – $f_{11}$ on the slab, due to positive uniform temperature (Deck: $29^{\circ}$ ; Arches and hangers: $41^{\circ}$ ).....	51
Figure 79 – Neutral axis location. Longitudinal reinforcement and concrete stress for the ULS verification ( $N_{ed}=1036$ kN/m ; $M_{ed}=189$ kNm/m).....	52
Figure 80 - Longitudinal reinforcement stress for the ULS verification. Support section with: $N_{ed}=2790$ kN/m and $M_{ed}=0$ .....	53
Figure 81 – Crack analysis of the slab for the SLS. Conventional section with $N_{ed}=453$ kN/m and $M_{ed}=108$ kNm/m.....	53
Figure 82 – Crack analysis of the slab for the SLS. Support slab section with $N_{ed}=1375$ kN.....	53
Figure 83 - $M_{33}$ in rib’s critical section for DL. $M_{Ed}=3198$ kN.....	55

Figure 84 - Resultant $V_{22}$ forces in rib for DL. $V_{Ed}=451\text{kN}$ .	55
Figure 85 - $M_{33}$ in rib's critical section for UDL(R1_R). $M_{Ed}=525\text{kNm}$ .	55
Figure 86 - $M_{33}$ envelope in the rib for TS(R31_2R).	55
Figure 87 – Resultant axial force in rib's critical section for UDL(R1_R). $N_{Ed}=724\text{Kn}$ .	56
Figure 88 – Resultant axial force envelope in the rib for TS(R31_2R).	56
Figure 89 - Cross-section selected for the conditioning axial stresses.	57
Figure 90 – Effective cross-section for DL axial stresses only.	57
Figure 91 – Effective cross-section for SDL and LL axial stresses.	57
Figure 92 – Weight from vertical loads (except DL) being transferred directly to the tie.	59
Figure 93 – SDL weight directly transferred to the tie.	59
Figure 94 - Axial Force Diagram for all Dead Loads (concrete modeled without stiffness).	60
Figure 95- $M_{3-3}$ diagram for DL (concrete modeled without stiffness).	60
Figure 96 - Torsion diagram for all Dead Loads. Concrete modeled without stiffness.	61
Figure 97 - Axial Force Diagram for SDL.	62
Figure 98 - $M_{3-3}$ diagram on the most requested tie, for UDL(1R_R)- <b>All</b> .	62
Figure 99 - $M_{3-3}$ diagram on the most requested tie, for UDL(1R_R)- <b>Half</b> .	63
Figure 100 - $M_{3-3}$ envelope for the TS(123R_R) on the more loaded tie.	63
Figure 101 – $M_{3-3}$ due to HPP2.	64
Figure 102 - Axial force under wind load.	64
Figure 103 - Deformed shape when wind is applied.	65
Figure 104 - Top view of the bridge's approximately deformed shape, when wind is applied.	65
Figure 105 – In-plane bending moments $M_{2-2}$ on the arches, when acting wind force.	66
Figure 106 – Deformation of a 2D model created on <i>Ftool</i> software, subjected to positive uniform temperature (no stresses).	66
Figure 107 –Axial forces. Positive uniform temperature variation (Deck: $29^{\circ}\text{C}$ ; Arch and hangers: $41^{\circ}\text{C}$ ).	66
Figure 108 – Ties tangential stress distributions.	68
Figure 109 – In-plane bending moment $M_{2-2}$ diagram for Dead Loads. View of both arches and bracing beams.	70
Figure 110 – Bending moments $M_{3-3}$ (on the left) and $M_{2-2}$ (on the right) of the arch when applied a vertical uniform load over the entire span (conditioning load distribution, from Chapter 5).	72
Figure 111- Hanger's numeration.	74
Figure 112 – Model of a truss beam (the leaning inwards diagonals are compressed).	74
Figure 113 - Hangers axial force due to Steel DL.	75

Figure 114 – Axial forces on the hangers, for “DL+SDL”. Cracked concrete stiffness (approximation). .....	77
Figure 115 - Hanger forces for “DL + SDL + HPP2 + 1.35*[UDL(Half) + TS(123R_R)]”. Traction forces only. Detail of the 8 <sup>th</sup> leaning inwards hanger, counting from the right. ....	78
Figure 116 – Axial force on hangers for ULS: 1.35*[DL+SDL+UDL(Half)+TS(123R_R)] + HPP2. Detail of the 2 <sup>nd</sup> , from the left, leaning outwards hanger. $N_{Ed,Max}=1209$ kN. ....	79
Figure 117 - Axial force on hangers for ULS: 1.35*[DL+SDL+UDL(All)+TS(123R_R)] + HPP2. Detail of the 2 <sup>nd</sup> , from left, leaning outwards hanger. $N_{Ed,Max}=1146$ kN. ....	<b>Error! Bookmark not defined.</b>
Figure 118 - Axial Force on hangers for ULS: (Dead+SDL+UDL 1R_R All+TS 123R_R+ HPP2)*1.0. Detail of the 3 <sup>rd</sup> , from the right, leaning outwards hanger.....	80
Figure 119 – LM3 for fatigue verification, according to <i>EN1991 Part-2</i> . ....	80
Figure 120 – Hanger’s axial force’s envelope, when subjected to the fatigue load model. ....	81
Figure 121 – Different hanger arrangements models investigated. ....	85
Figure 122 – Representation of both Load Distributions to be applied.....	86
Figure 123 – Normal forces and bending moments diagrams for the Live Load LM4 on all or half deck span.....	88
Figure 124 – Highest axial forces and bending moments in the arch and ties for the Live Load LM4 applied on all or half deck span.....	89
Figure 125 – Hangers $N_{max} / N_{Rd}$ and axial force amplitude variation. ....	91
Figure 126 – Nielsen arrangement, when LD-Half is applied and compressed hangers are iteratively removed. $M_{33,Max} = -10616$ kNm. ....	93
Figure 127 – Load Distributions applied in this section, to assess the arch instability. ....	94
Figure 128 – Comparison of the stability analysis results.....	96
Figure 129 – Comparison of the stability analysis results.....	96
Figure 130 – In-plane buckling mode. ....	97
Figure 131 – Out-of-plane buckling mode. ....	97
Figure 132 Optimized Network Model. Buckling shape for LD1. $\lambda=16.30$ . ....	97
Figure 133 Optimized Network Model. Buckling shape for LD2. (Load applied on left half of the span). $\lambda=26.22$ . ....	97
Figure 134 – Bending moments 3-3 and axial force diagrams, on Optimized Network Model, for the LD2. (Load applied on left half of the span).....	97
Figure 135 – Hangers’ axial force on the Optimized Network Model (Left) and on the Network Model (Right) for the LD2. (Load applied on left half of the span). $N_{min} = -168$ kN (Network Model). .....	98
Figure 136 – Compressed Hangers $\lambda$ - Buckling factor given by SAP2000 without taking into account relaxation. Real $\lambda$ – Buckling factor given by a multi-step analysis where hangers cannot	



mobilize compression. No Compressed Hangers $\lambda$ – Buckling factor given by SAP2000 with a model where compressed hangers were previously removed. ....	98
Figure 137 – Geometrical initial imperfections ( $\Theta_0$ ) and their consequences on the displacement ( $\Theta$ ) when loading (P) acts. ....	99
Figure 138 – Network Model and its hangers’ axial forces for the LD2, after iteratively removing compressed hangers. ....	101
Figure 139 – Buckling mode of the Network Model after being removed all compressed hangers. Very similar to the previously seen Compressed Hangers Model buckling mode.....	101
Figure 140 - Vertical Hangers' Model. Buckled shape for LD2 (Load applied on left half of the span). $\lambda=22.01$ .....	101
Figure 141 – Bending moment 3-3 Diagram on Vertical Hangers' Model, for the LD 2 (Load applied on left half of the span). ....	102
Figure 142 - Axial Force Diagram on Vertical Hangers' Model, for the LD 2 (Load applied on the left half of the span). ....	102
Figure 143 – Nielsen Hangers Arrangement Model. Compressed hangers removed. Buckled Shape for LD2 (Load applied on the left half of the span). $\lambda=28.19$ . ....	103
Figure 144 - Comparison between bending moment 3-3 diagrams, due to LD1. (All diagrams have the same scale factor). ....	104
Figure 145 – Wind portal arch frames (darker and colored). ....	107
Figure 146 – FE Network Model, with effective wind-bracing frames. These frames were modeled with a rigid material. ....	107
Figure 147 – FE Network Model, with effective wind-bracing frames. First buckling mode for LD1. $\lambda=29,51$ .....	107
Figure 148 – Example of an efficient bracing system. Waikato River Network Arch Bridge. ....	108
Figure 149 – Network Model without wind-bracing. LD1 buckling analysis. $\lambda=3,27$ .....	108
Figure 150 – Left approach viaduct model.....	A-9
Figure 151 - Global and Local deflections. ....	A-9
Figure 152 – Column shared between the bowstring and the approach viaduct. Detail of the main reinforcement - 55 $\phi$ 25.....	A-15

## List of Tables

Table 1 – Live Loads and Dead Loads comparison, in the tied-arch span.....	20
Table 2 – Wind equivalent static loads acting on each of the structural elements.....	40
Table 3 – Different winter and summer air and structure temperature, in °C.....	41
Table 4 – Slab - DL – [simply supported slab].....	48
Table 5 – Slab - SDL .....	48
Table 6 – Slab – UDL(R1_R)-All.....	49
Table 7 – Slab - TS(R31_2R).....	50
Table 8 – Slab - Wind.....	51
Table 9 – Slab - Positive Uniform Temperature .....	51
Table 10 – Slab - ULS .....	52
Table 11 – Slab - SLS.....	52
Table 12 - Slab - SLS - Deflection .....	54
Table 13 - Ribs - Acting Forces and ULS.....	56
Table 14 – Ribs – Cross-sections characteristics and ULS stresses .....	57
Table 15 - Ribs – SLS - Deflection .....	58
Table 16 - DL - [non-stiff concrete slab] .....	59
Table 17 - Ties - SDL.....	62
Table 18 – Ties - UDL(1R_R) + TS(123R_R).....	63
Table 19 – Ties – HPP2 .....	64
Table 20 – Ties – Wind Action .....	64
Table 21 – Ties - Negative Uniform Temperature Gradient.....	67
Table 22 – Ties – Forces in the ULS .....	67
Table 23 – Ties – Corner Cross-Section Elastic Verification .....	67
Table 24 - Service Limit State - Deflection .....	69
Table 25 – Arch - DL- [non-stiff concrete slab].....	69
Table 26 – Arch - SDL.....	70
Table 27 – Arch - HPP2 .....	70
Table 28 – Arch - UDL-All + TS(123R_R) .....	70
Table 29 – Arch - Wind .....	71
Table 30 – Arch - Positive Uniform Temperature Gradient .....	71

Table 31 – Arch – Forces in the ULS .....	71
Table 32 – Arch - Corner Cross Section Elastic Verification .....	71
Table 33 – Arch - Moment, Reduction and Interaction Factors, according to <i>EN1993-1-1 6.3</i> .....	72
Table 34 - Hangers’ Supported Loads .....	73
Table 35 – Hangers Influence Matrix [kN] – [No concrete slab on the model].....	75
Table 36 – Hangers Influence Matrix [kN] – [Cracked stiffness concrete].....	75
Table 37 - Hangers Prestress Phase 1 .....	76
Table 38 - Hangers Prestress Phase 2 .....	78
Table 39 – Decks Horizontal Displacements (m).....	82
Table 40 – Hangers Characteristics on the Different Models .....	86
Table 41 – Main forces and displacements on the different hanger arrangements. ....	87
Table 42 – Hanger axial forces for different hanger arrangements.....	91
Table 43 - Fatigue assessment between arrangements .....	92
Table 44 – Relaxed hangers on the different arrangements .....	92
Table 45 – Instability Analysis Results.....	96
Table 46 – Design buckling resistance comparison for the 4 hangers’ geometries.....	111

# Notation

Tie – Longitudinal beam of the deck.

Rib – Transversal beam of the deck.

End Cross Girders – First and last ribs of the deck, which have a different cross-section.

Bracing Beams - The 7 beams that connect the two arches, holding them one against the other.

LD – Load Distribution.

DL (Steel) – Dead Loads from steel elements only.

DL (Concrete) - Dead Load from the concrete slab only.

DL – Dead Loads, including all steel and concrete elements.

SDL – Superimposed Dead Loads.

UDL – Uniformly Distributed Loads

TS – Tandem System

LL – Live Loads. They refer to both the UDL and the TS.


CS<sub>x</sub> – Construction Stage number *x*


H<sub>x</sub> - Hanger number *x*

HPP<sub>x</sub> – Hanger Prestress Phase *x*

FEM – Finite Element Method

FEModel – Finite Element Model

 Tension or positive V, M or T

 Compression or negative V, M or T

# 1. Introduction

## 1.1 General Overview

Arch bridges in general have outwardly directed horizontal forces on the arch ends. These important forces, proportional to the weight being carried out, the relation between bending and axial stiffness of the arch, the rise, and several other factors, can be visually understood from Figure 1, by the “will” of the loaded arch to “open”.

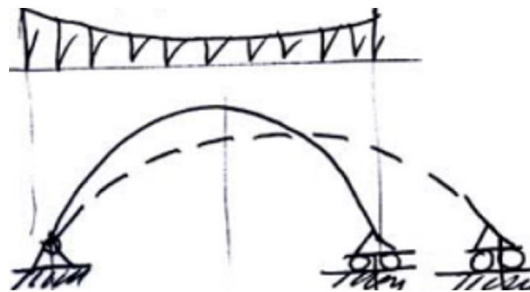


Figure 1 – Arch mechanism, expressed as a “will to open”, when sustaining loads.

When the arch is under the deck, these forces are usually transmitted directly to the ground, by compression, requiring a great capacity of the soil underneath or big concrete foundations. Tied-arch bridges, also known as *Bowstring* bridges, get their name from the way they withstand these forces. These bridges use the deck as a tie (string) in tension to “hold” the top compressed arch (bow).

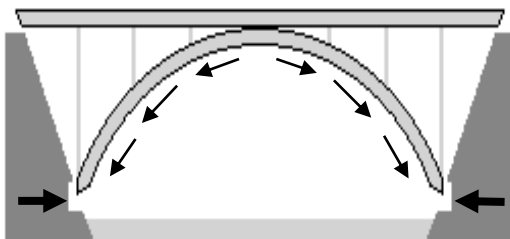


Figure 2 – Arch bridge with a higher deck.

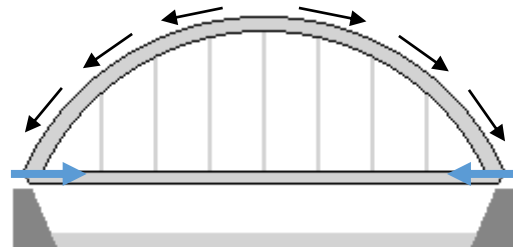


Figure 3 – Tied-arch bridge.

## Chapter 1. Introduction

Network arch bridges are tied-arch bridges with inclined hangers that cross each other at least twice. To better understand it, this arrangement can be disassembled into three or more simpler sets of hanger arrangements, as for example the Nielsen arrangement of hangers, from Figure 4 to Figure 6, with hangers not necessarily with the same slope.

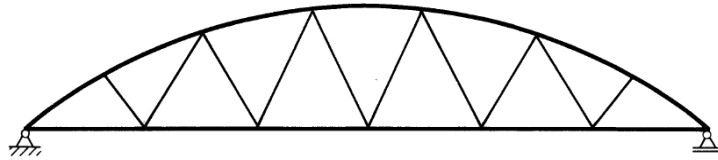


Figure 4 – Nielsen arrangement of hangers. 1 set of hangers.

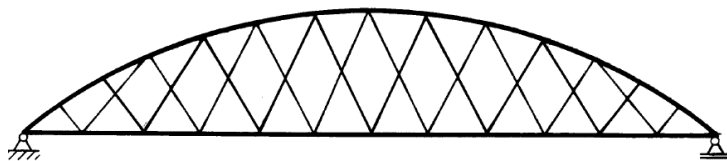


Figure 5 – Hangers cross each other once. 2 sets of hangers.

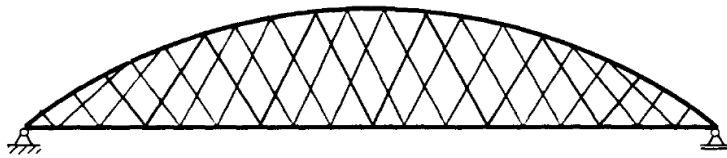


Figure 6 – Network arrangement of hangers – most hangers cross each other twice. 3 sets of hangers.

Using the Network arrangement of hangers in a tied-arch bridge, *Per Tveit (2011)* refers it is possible to save between 40 % and 50 % of the cost of the superstructure, when comparing with other steel bridges. The same author presents a comparison of steel weight between different bridges, for deck spans up to 300 m (Figure 7).

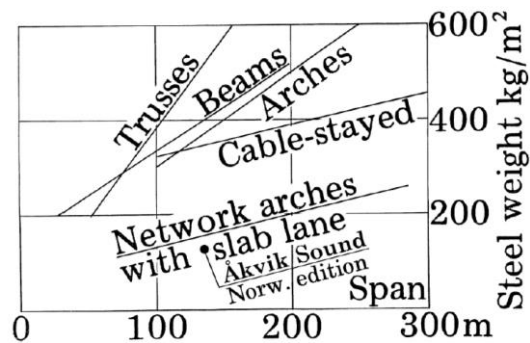


Figure 7 - Steel weight comparison between different steel bridge types - *Per Tveit (2011)*.

Several tied arch bridges with network hangers arrangements have been built, impressing by their high slenderness. The best example of this bridge typology may be the world's record slenderest bridge, designed by *Per Tveit*, with a 220 m span (Figure 8) - *Per Tveit (2011)*.



Figure 8 - The Brandanger Sound Bridge - by *Per Tveit*. 220 m Span

It is therefore comprehensible that this type of bridge can get very competitive. Yet, it seems, engineers still have some way to go in fully “understanding” and optimizing this type of bridges, as the number of examples is still quite small.

## 1.2 Main Objectives

The first aim of this thesis consists on designing a Network arch bridge that crosses Llobregat River, in Barcelona (Spain), 170 meters wide. This bridge should have a total length of around 300 m, considering the approach spans on both sides, for crossing also a set of railway and roadway lanes. For aesthetical reasons and environmental integration of the total bridge solution, these approach spans are also studied. Indeed, this dissertation intends to identify the advantages or disadvantages of adopting a Network arrangement of hangers and in which situations should it be considered.

A second aim of this work is to investigate the structural influence of the different hangers' arrangements on the bridge behavior. Four different hangers arrangements are studied using tridimensional SAP2000 FEModels, namely: i) a Vertical hangers arrangement, ii) a Nielsen hangers arrangement, iii) a Network hangers arrangement with constant slope, and iv) a Network hangers arrangement with variable slope. The influence of the following aspects are investigated:

## Chapter 1. Introduction

i) resulting stresses distributions on the arch, ties and hangers, ii) total stiffness of the structure and expected deflections, iii) number and importance of relaxing (compressed) hangers, and iv) global stability of the structure.

Finally, it is also a main objective of this work to investigate the stability of the arch, describing and comparing the multiple possible approaches. A linear stability analysis is performed, for the different models and arrangements studied, considering five different load patterns, and discussing the different ways of incrementing the bridge loads until buckling. The different procedures to obtain the buckling load are also investigated from the one proposed in the European standards and from a simplified method proposed by *Outtier et al. (2010)*, comparing the results with the ones obtained using FEModel linear and nonlinear analysis.

### 1.3 Document Outline

Chapter 1 begins with a general introduction to Network arch bridges and presents the main objectives of the current study.

Chapter 2 starts with the discussion about the possible solutions, then presents in detail the adopted solution, namely all its structural elements, support conditions and constructive process. At the end of this chapter, this solution is compared with constructed tied arch bridges.

Chapter 3 defines the loads, criterions of design and finite element model used.

Chapter 4 presents structural analysis of the main bowstring span of the bridge, concerning the slab, the ribs, the ties, the arches, the hangers, and the expansion joints that separate the approach spans from the bowstring span.

Chapter 5 studies the influence of the hanger arrangement on the structural behavior, by means of comparison of four different arrangements with respect to stress results, deflections, fatigue behavior and relaxation issues on the hangers. It then studies instability, performing a linear stability analysis with *SAP2000*, and finally examines the differences between assessing instability with the FEModel, with the European standards' procedure and with a simplified method proposed by *Outtier et al. (2010)*.

Chapter 6 provides overall conclusions and possible future developments.



## 2. Alternative and Adopted Solution

### 2.1 Local Constraints

The local constraints and terms of the design, the necessary information, the cross-section of the river and the required deck road cross-section are presented in Figure 9 to Figure 11.

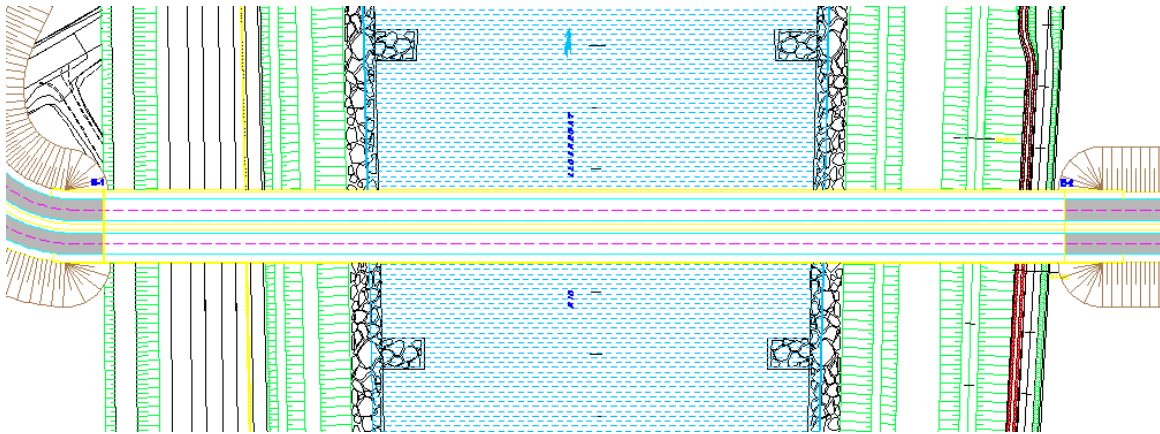


Figure 9 – Plan view of the Llobregat River, with the plan alignment.



Figure 10 – Elevation view of the Llobregat River, with the bridge road profile.

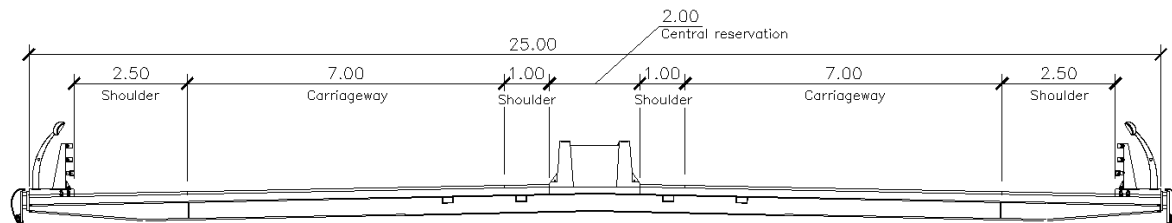


Figure 11 – Road deck cross-section.

A small road on each side of the river and a small embankment already exist in each side of the river, so bridge supports should be carefully positioned. Moreover, there should be considered the future construction of both a 2 lanes railway and a highway on the left bank. A 14 m width reservation was assumed for this future high-speed train corridor.

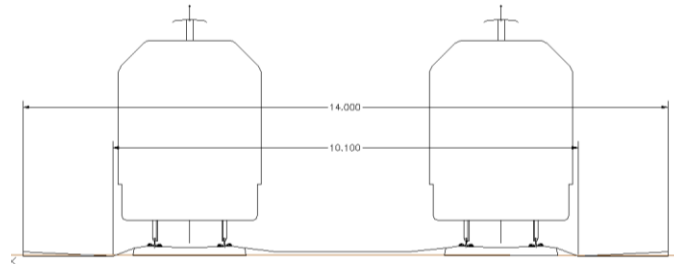


Figure 12 – Future high speed train cross-section.

A 24 m wide highway has also to be planned with a typical cross-section presented in Figure 13.

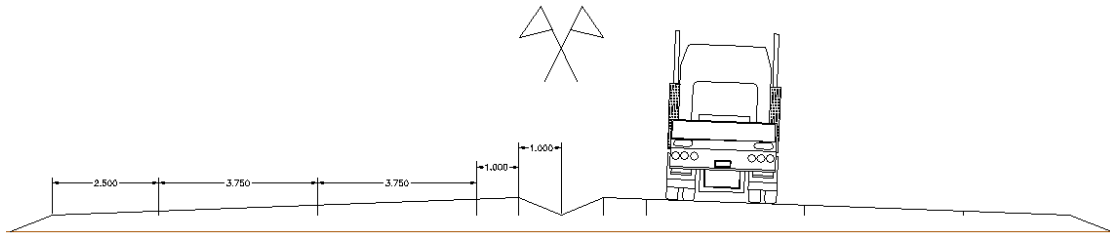


Figure 13 – Future highway cross-section.

## 2.2 Alternative Solutions

### 2.2.1 Options for the Bridge Spans

When deciding on the best solution, the variables taking into account are: aesthetics, constructive process, symmetry of the approach bridges, total bridge length and cost, allowance for a future high speed train and a highway, and possibility and interest of adopting the same deck cross-section in the main span and approach bridges.

Several solutions were studied, using a tied arch bridge for the main span and a more classical continuous span viaduct for the approach bridges:

1<sup>st</sup> Solution – Aesthetic and simple solution but an increase of the arch span length implies a non-linear increase of the bridge cost and a 190 m arch span start to deviate from the optimal economic range, from 80 to 170 m according to *Per Tveit (2011)*. Furthermore, the future highway would have a column on the central strip, but the high speed train is perfectly possible.

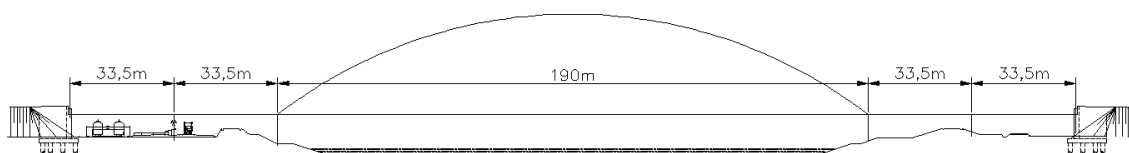


Figure 14 – 1st Solution. Bowstring Bridge with 190 meters span.

2<sup>nd</sup> Solution – Smaller approach spans are used to facilitate the adoption of the same deck cross-section in the approach bridges and the main span. Three span approach viaducts with equilibrated spans are considered and a good total bridge length is achieved. The arch-span is also perfectly inside the optimal economic interval, but bridge supports are situated, in relation to the riverside, more than 12 to 14 meters inside the river, which is a major drawback of this solution from a hydraulic and construction point of view. Finally, an equilibrated economically solution but probably less aesthetic, and with the undesirable interference with the river.

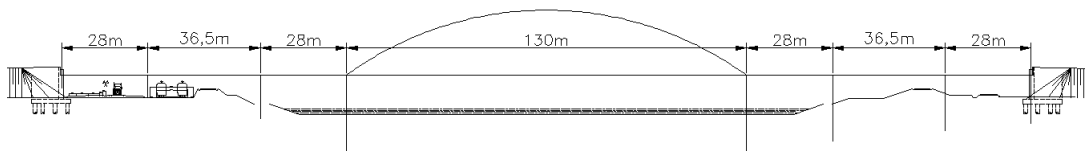


Figure 15 – 2<sup>nd</sup> Solution. Bowstring Bridge with piers inside the river.

3<sup>rd</sup> Solution – This solution is a balance between the 1<sup>st</sup> and 2<sup>nd</sup> solutions but has the need for a future small displacement of the high speed railway corridor. Similar to the 1<sup>st</sup> Solution, this solution avoids the supports at the central strip of the highway and has the advantage of a 10 m shorter arch span, avoiding still the main bridge pier supports to be placed on the embankments.

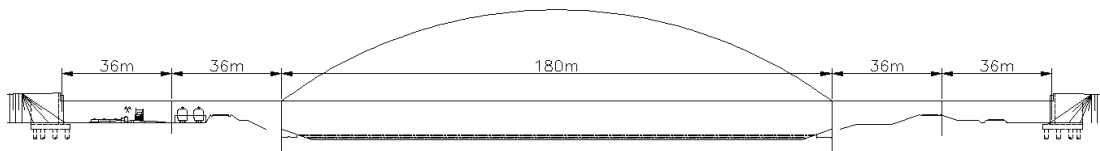


Figure 16 – 3<sup>rd</sup> Solution. Approach bridge supports require a small railway displacement.

4<sup>th</sup> Solution – A smaller arch-span could even be envisaged on this 4<sup>th</sup> solution. But, longer approach spans are required which imply a different deck cross-section for these structures from the arch deck, which is less aesthetic and increases the difficulty of the deck construction.

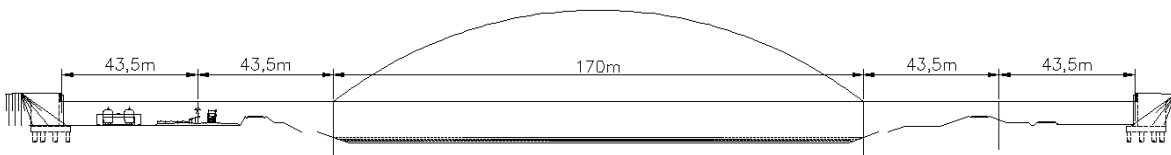


Figure 17 – 4<sup>th</sup> Solution. Lateral approach viaduct spans too long.

## 2.2.2 Deck Cross-Section Solutions

A central suspended deck cross-section can be envisaged alternatively to the adopted lateral suspended deck solution exposed in sub-chapter 2.3. A central suspended deck solution has mainly an aesthetical advantage but it also provides more space for sidewalks. Using central suspension a single centered longitudinal box-girder should resist to the longitudinal bending moments, with the contribution of the slab, if both elements are connected, making it a composite girder. Two additional longitudinal box-girders are placed on each edge of the deck, mainly to control differential deflections between ribs. Transversely, the deck behaves as a cantilever on each side, which brings the worst of this solution: High transversal negative bending moments require heavy ribs and therefore prove expensive. Moreover a single central arch should be adopted, which for an 180 m long span would result in an impressively strong arch section, to avoid important instability issues.

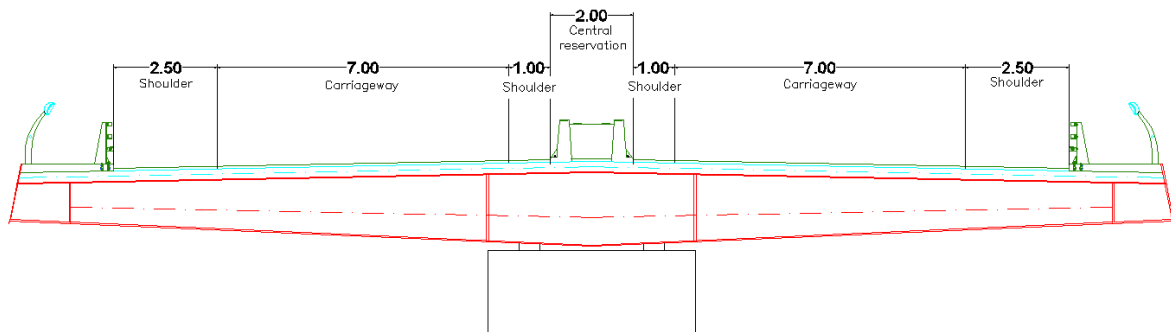


Figure 18 – Central suspended solution for the deck cross-section.

## 2.3 Adopted Solution

### 2.3.1 General Layout

A 5th Solution was then envisaged. The 180 m main span was kept but the approach viaducts were divided in 3 spans for a more economical and structural efficient solution (Figure 19 and Figure 20). Except for the total length of the bridge and a slightly out of the economic interval arch span, this was decided to be the best solution since it allows the crossing of both railway and highway

lanes, and, as will be demonstrated, allows the same deck structure typology on both the approach viaducts and the main span. For academic purpose, a longer arch span will enhance study results and comparisons such as the consequences of the hangers' arrangement, the instability issues, the supporting conditions issues and the influence of a lighter/heavier deck. The adopted solution is illustrated in Figure 19 to Figure 24.

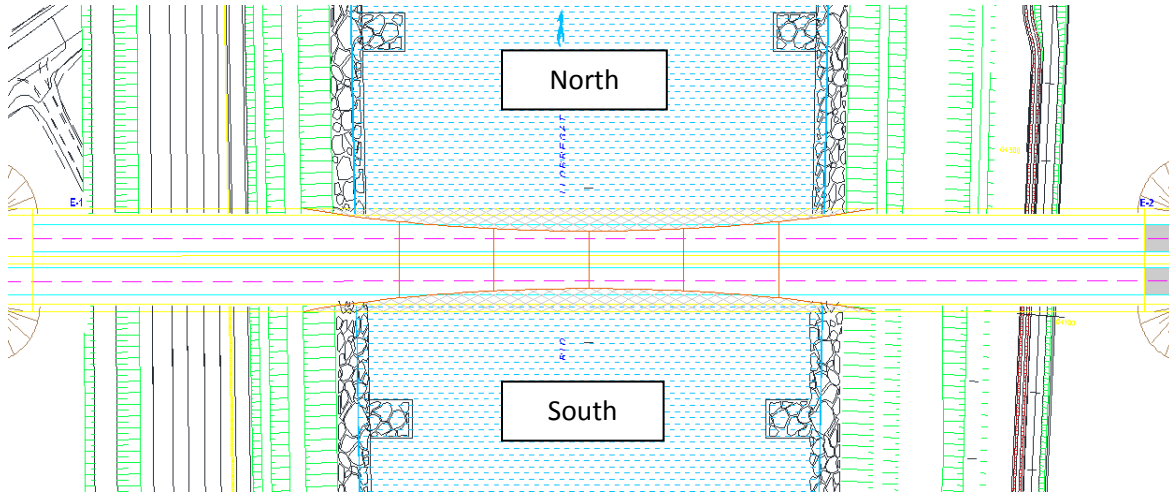


Figure 19 - Plan view of the river and bridge proposed.

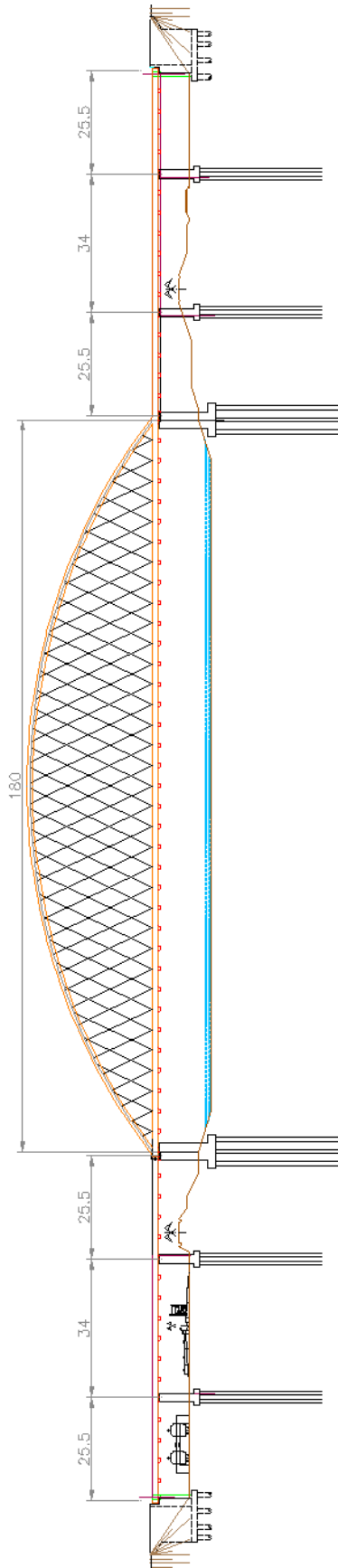


Figure 20 – Elevation view of the entire adopted solution (m).

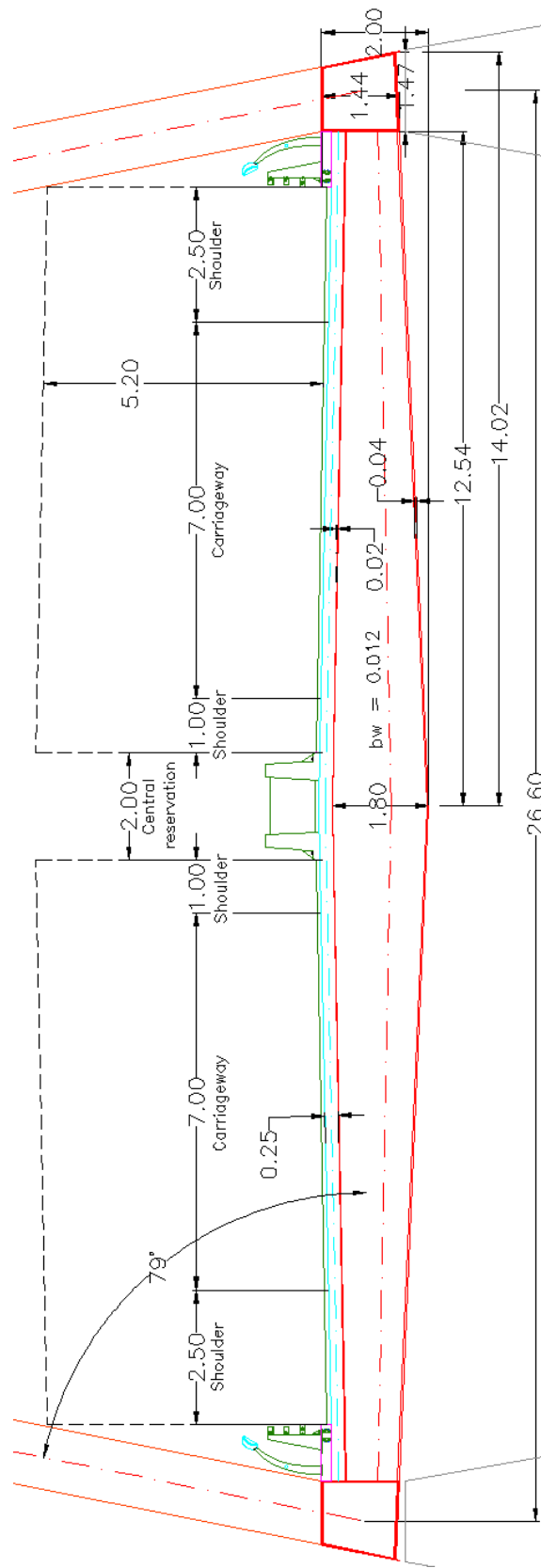


Figure 21 – Deck cross-section detailing of the adopted solution (m).

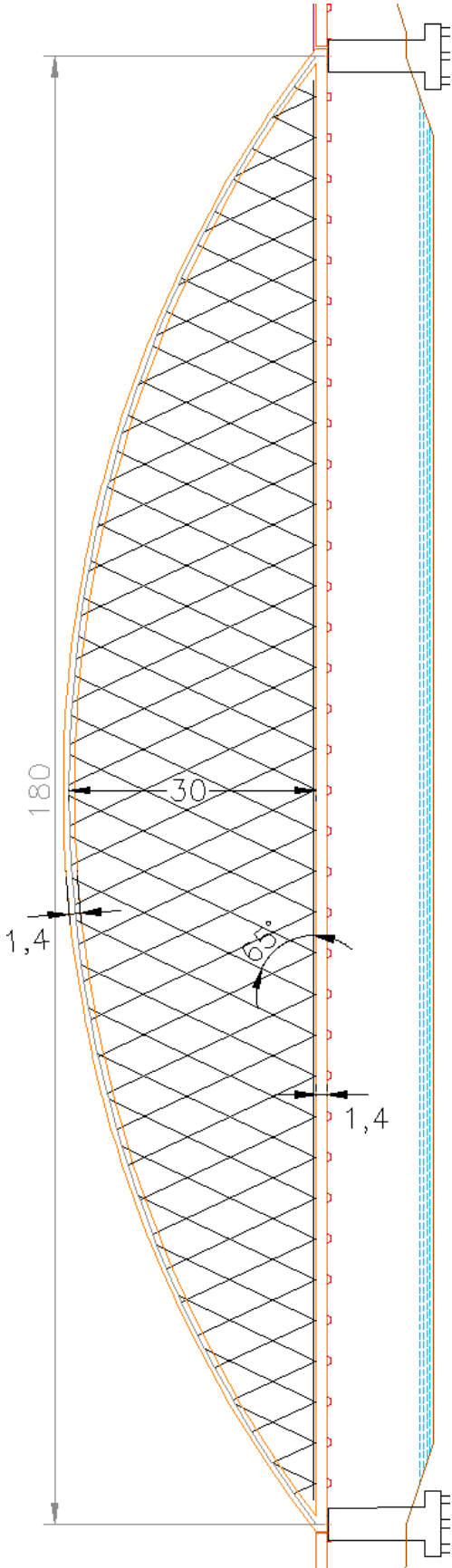


Figure 23 – Elevation view of the arch span (m).

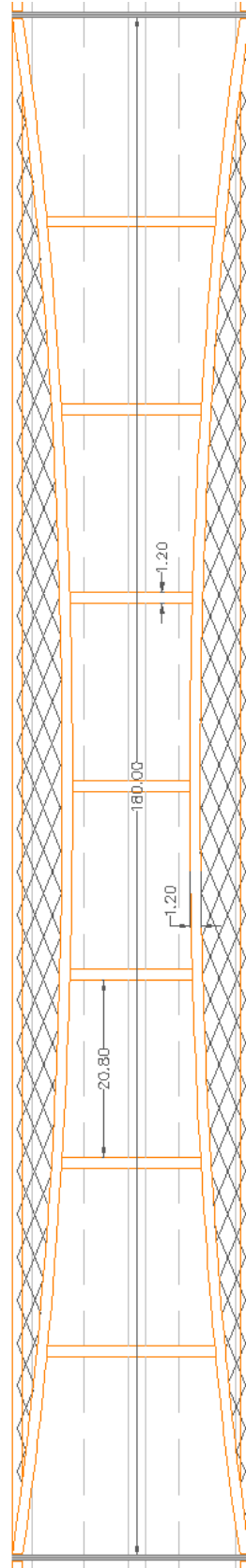


Figure 22 – Top view of the arch span (m).





The portion of the superficial concrete next to the tie that supports the railings and lighting (pink colored rectangle in Figure 24) was chosen to be made of light concrete and won't be considered as resistant on the structural analysis.

The approach spans and the bowstring span are divided by an expansion joint, making them structurally independent from each other. For this reason, the approach spans on each side of the bowstring span are often designated as the approach viaducts, and the bowstring span as a bowstring bridge or tied-arch bridge.

The main characteristics of the bowstring bridge are found in Appendix A.

### 2.3.2 Composite Deck Advantages

One of the important decisions of the design is the deck section type adopted. Since the most commonly types adopted are composite and concrete deck solutions, they are briefly compared.

Considering the large deck's width, approximately 26.6 m, a concrete made deck would be required with a thick slab, packed with lots of pre-stressing cables in both directions, to avoid cracking and assure durability. Certainly it would be heavy and probably a more expensive and un-esthetical solution.

About this subject, *Per Tveit* states: *"When there is less than 15 to 18 meters distance between the arches, the tie should be a concrete slab with longitudinal partial prestress. The author does not think much of steel beams in the tie when the distance between the arches is less than 15 m."* – *Per Tveit (2011)*.

In fact, the only competitive concrete solution would be one with 3 arches, which means an extra arch in the middle of the deck's width. In the author's opinion, this 3 arch solution would compromise aesthetics. Also, this would result, according to *Per Tveit's* pre-design advices of concrete decks, in an approximately 32cm thick slab with transversal prestress, which corresponds to an increase of 38 kN/m compared with the adopted 25 cm thick slab, resulting in a heavier solution.

## Chapter 2. Alternative and Adopted Solution

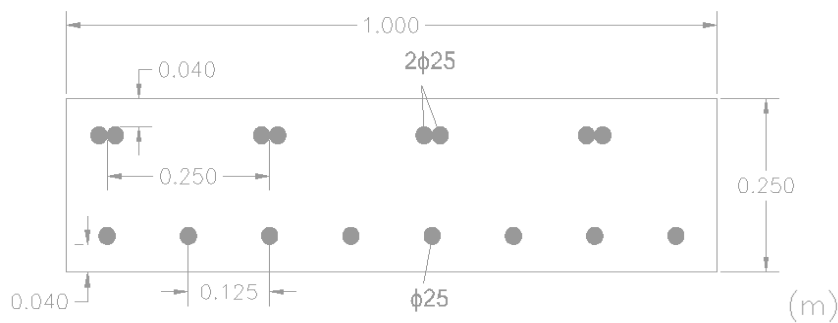
Therefore, the composite section solution can be the lightest, the fastest to build, the one with better aesthetics and also possibly the most economic one, though requiring eventually more maintenance works due to the tensioned slab.

A composite deck solution solves several of these issues: i) is lighter than the all concrete deck solution; ii) is not so expensive as the all steel solution; iii) solves the issue related with the lack of adherence between the asphalt layer and the orthotropic steel slab of the all steel deck solution; iv) is faster to build than a concrete deck section, since steel parts of the deck are modular, and can therefore be prefabricated during the time of infrastructure construction, and even the slab can be prefabricated in panels using only the joints to be cast in situ.

### 2.3.3 Structural Elements

#### 2.3.3.1 Slab

The adopted concrete slab, settled over steel ribs longitudinally spaced 5 m from each other and connected both to the ribs and ties, and its main longitudinal reinforcement is presented in Figure 25. The top rebars are grouped in pairs to facilitate the concreting. A highly reinforced concrete slab solution is essential to allow a thin slab and a light overall solution.

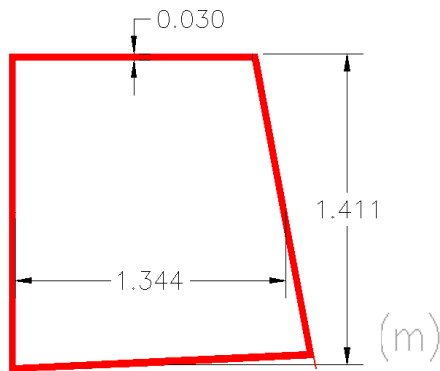


Concrete		C40/50		Reinforcement		A500	
$f_{cd}$	MPa	26.7		$f_{yd}$	MPa	435	
$f_{ck}$	MPa	40		$f_{yk}$	MPa	500	
$f_{ctm}$	MPa	3.5		$E_s$	GPa	200	
$E_{c,28}$	GPa	35		$A_{s\ sup}$	cm <sup>2</sup> /m	39.27	
				$A_{s\ inf}$	cm <sup>2</sup> /m	39.27	

Figure 25 – Concrete slab and longitudinal reinforcement adopted.

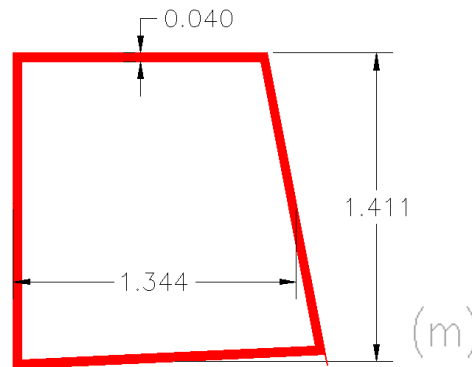
2.3.3.2. Tie (Longitudinal Beam)

The adopted steel tie cross-section in the main span is shown in Figure 26, and the adopted steel longitudinal beam cross-section in the approach viaducts is shown in Figure 27. A tiny steel plate can be seen in the inferior right corner of the cross-section in Figure 26. This prevents water to slide to the bottom flange of the tie and to the bottom flange of the ribs.



Steel S420		
$f_{yd}$	MPa	420
Area	m <sup>2</sup>	0.1622
$N_{rd}$	kN	57581
Inertia <sub>3-3</sub>	m <sup>4</sup>	0.0506
$W_{el\ 3-3}$	m <sup>3</sup>	0.06833
$M_{el,rd\ 3-3}$	kNm	24258
Inertia <sub>2-2</sub>	m <sup>4</sup>	0.0479
$W_{el\ 2-2}$	m <sup>3</sup>	0.05936
$M_{el,rd\ 22}$	kNm	21071

Figure 26 – Steel ties cross-section adopted in the main span.



Steel S420		
$f_{yd}$	MPa	420
Area	m <sup>2</sup>	0.2146
$N_{rd}$	kN	90132
Inertia <sub>3-3</sub>	m <sup>4</sup>	0.0661
$W_{el\ 3-3}$	m <sup>3</sup>	0.08929
$M_{el,rd\ 3-3}$	kNm	37501
Inertia <sub>2-2</sub>	m <sup>4</sup>	0.0624
$W_{el\ 2-2}$	m <sup>3</sup>	0.07731
$M_{el,rd\ 22}$	kNm	32472

Figure 27 – Steel longitudinal beams cross-section, adopted in the approach viaducts.

### 2.3.3.3. Rib (Transversal Beam)

The ribs have a variable cross-section to adjust them to the acting transversal bending moments. The end and the center cross-sections are illustrated in Figure 28 and Figure 29. These slender ribs will work mostly in tension, due to the composite transversal behavior of the slab and ties.

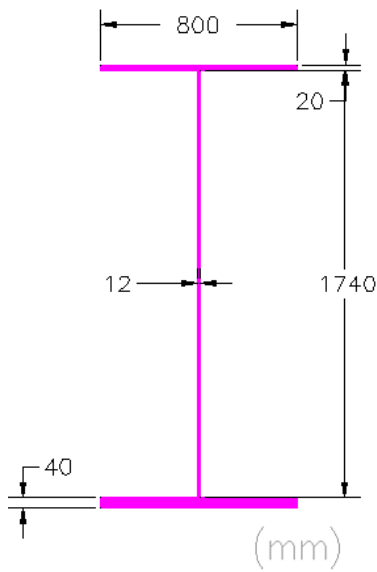


Figure 28 – Rib's center cross-section adopted.

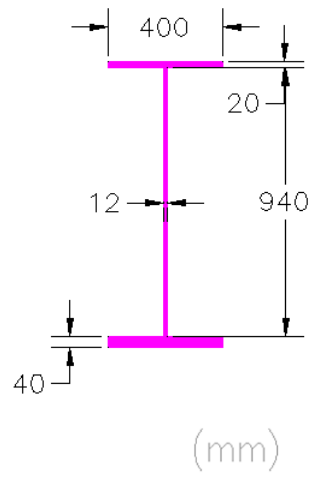


Figure 29 - Rib's end cross-section adopted.

Steel S355			
	Units	Rib Section	
		Center	End
$f_{yd}$	Mpa	355	355
Area	m <sup>2</sup>	0.069	0.035
$y_{sup}$	mm	1220	730
$y_{inf}$	mm	580	270
Inertia <sub>3-3</sub>	m <sup>4</sup>	0.04	0.006046
$W_{el\ 3-3}$	m <sup>3</sup>	0.033	0.008
$M_{el\ 3-3}$	KNm	11639	2940

### 2.3.3.4. Arch

The adopted cross-section for the arch has a shape of a parallelogram as a consequence of the arches 79° inclination inwards, according with Figure 30.

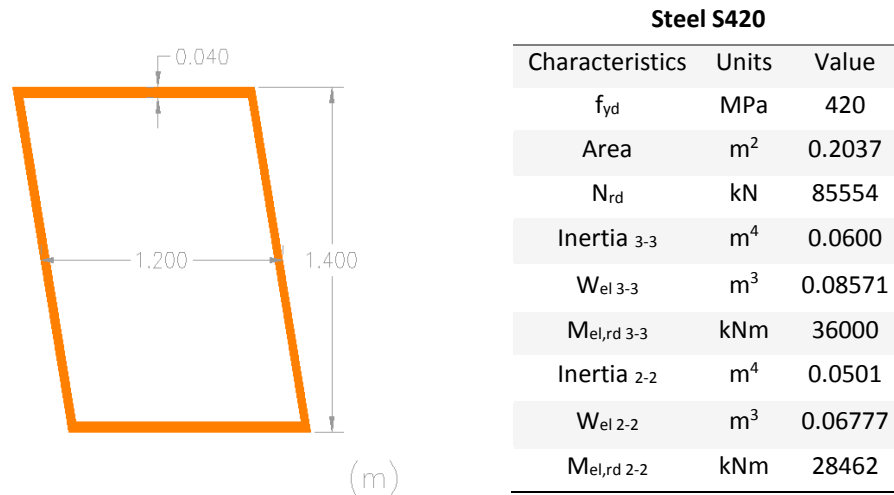


Figure 30 – Steel arch cross-section characteristics.

Attending to the arch local buckling resistance, the highest quotient of the internal compression fragment length and thickness is obtained from eq. (1):

$$\frac{c}{t} = \frac{1,346}{0,04} = 33,65 \sim 42\varepsilon = 31,5 \quad (1)$$

If the arch was submitted to axial compression only, it would be nearly a Class 3 section. In fact, with the significant bending moments that will act in both directions, it turns into Class 3 at the conditioning sections, so an elastic verification will be used. The option of using a steel with high strength instead of increasing the thickness of the arch is related with the structure self-weight savings, which will also keep the stress solicitations low. Also, when the thickness of the steel exceeds the adopted 40 mm, the design yield strength sees itself reduced, according to *EN1993-1-1 Section 3.2.2*.

The slenderness of the arch - its rise divided by its length - is defined as:

$$\text{Arch slenderness} = \frac{f}{l} = \frac{30 \text{ m}}{180 \text{ m}} = \frac{1}{6} = 0,167 \quad (2)$$

The whole network arch can be compared to a bending beam with a compression and a tension chord. This way, an increased rise in the arch will give smaller axial forces in the chords (ties and

## Chapter 2. Alternative and Adopted Solution

arches), and lower steel weights. Therefore, it is mainly due to aesthetic reasons that limits 1/6 to 1/8 are usually adopted for the slenderness. To this respect, the commonly adopted rise to span quotients on *Per Tveit's (2011)* examples are in this range. Other bowstring bridges (not necessarily network) have a slightly higher interval value for the arch slenderness, as seen in section 2.3.6 of this document from the database collected by *Gonçalves, P. (2012)*.

### 2.3.3.5. Hangers (Network Arrangement)

Hangers have all the same circular bar cross-section and use steel S460N (Figure 31)

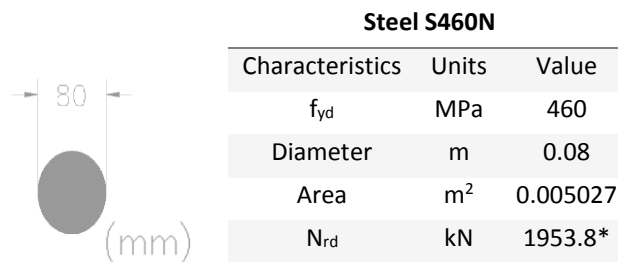


Figure 31 – Hanger cross-section and characteristics of the adopted solution. \*Tension Rod Type 860, 80mm diameter,  $N_{R,d}$  according to EC3. PFEIFER Cable Structures.

To evaluate the Network arrangement's advantages the adopted solution uses this hanger arrangement.

The main decisions concerning the hangers are: their sub-type of arrangement, their slope and the distance between their nodes. It is essential to carefully read the advices of *Per Tveit (2011)* and *Brunn & Schanack (2003)* on this topic.

The horizontal distance between two successive hangers is chosen to be the same as the distance between ribs, i.e. 5 meters. This is a common decision when the deck is composite and has equally spaced ribs supporting the concrete slab. This way, hanger nodes on the lower chord can be placed coincidentally with the rib-tie intersections, avoiding extra shear forces on the tie. If the hanger nodes' distance is set constant on the tie, then it will result inconstant on the arch and vice-versa. As for a concrete deck, according to *Per Tveit (2011)*, an ideal hangers' arrangement

would have kept equal distances between hanger's nodes on the arch, and thus different distances at deck level. This hangers' arrangement is presented in Figure 32.

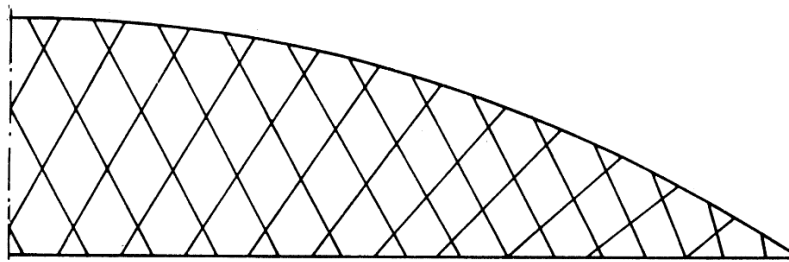


Figure 32 - Optimal arrangement of hangers on a concrete deck, using constant spacing between hangers at the arch level.

It is also needed to define the hangers display. There are two main ways of displaying the hangers, using the Network solution:

- 1- Hangers with constant slope, thus parallel to each other;
- 2- Hangers with variable slope.

Although the second arrangement would allow more even solicitations on the hangers, the first one is the simplest and the most commonly adopted when the distance between hangers is made constant along the tie - *Per Tveit (2011)*.

The first arrangement, with constant slope hangers is therefore adopted, although an analysis and comparison with the second arrangement and other arrangements is performed on chapter 5.

Finally, the slope angle of the hangers must also be defined. This issue is entirely related to the relation between dead and live loads as it pretends to accommodate all eccentric load positions, without overstressing the arch or compressing any hanger. The smaller the slope (angle between the hanger and the tie), i.e. the more horizontal the hanger, the less relaxation problems on the hangers, when loading only half of the span, but longer and more stressed hangers have to be used.

Therefore the proportion between dead and live loads must be first evaluated according to Table 1.

## Chapter 2. Alternative and Adopted Solution

**Table 1 – Live Loads and Dead Loads comparison, in the tied-arch span.**

UDL	12960	kN	72	kN/m
TS	1200	kN	26.67*	kN/m
Live <sub>total</sub>	14160	kN	98.67	kN/m
Dead <sub>total</sub>	55999	kN	311.1	kN/m

\*The Tandem System should be converted to an equivalent uniformly distributed load. For this, the approximated influence line illustrated slightly further in this chapter, in Figure 36, allows this conversion. Since it has a triangular shape, by positioning the concentrated load on the maximum negative (compression) value of the influence line, it would have the same effect as a UDL distributed over all the “compression length” (negative zone) of this influence line, with the value of:

$$TS_{equiv}[kN/m] = \frac{TS [kN]}{\text{“compression length” [m]}} \times 2 = \frac{1200}{180/2} \times 2 = 26,67 \text{ kN/m}$$

As it will be explained later, for the relaxation study in this document, a load in the left half of the span will be applied, so the “compression length” result is  $180/2=90$  m.

Additionally, from the “Live<sub>total</sub>” it is possible, by transversely eccentrically positioning the loads, to load more one arch than the other, so the true maximum live loads that will load one arch will be approximately 43 kN/m from “UDL” and 22.79 kN/m from the “TS”, resulting in a total of 65.79 kN/m, instead of Live<sub>Total</sub> / 2.

As for the dead loads, they are symmetrically applied and so they will load each arch with  $311.1 / 2 = 155.6$  kN/m. Therefore, the ratio between live and dead loads is:

$$\frac{\text{Live Loads}}{\text{Dead Loads}} = \frac{65.79}{155.6} = 0.42$$

Remembering that the slenderness of the arch is  $30 / 180 = 0.1667$  and this result it is possible to obtain the better slope to be adopted, thanks to *Per Tveit’s* propositions.

It’s still necessary to understand the ratio of load length to span length, and its effects. Load length is the same as saying the longitudinal length in which the live load is applied, starting from the left. In Figure 33, a ratio of 0.55 is exemplified.



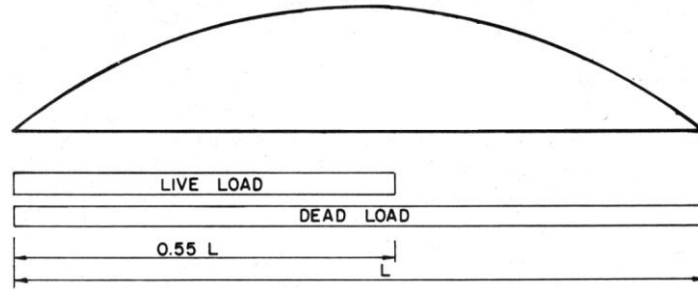


Figure 33 – 0.55 ratio of load length to span length.

Figure 34 presents the relation between ratios of load length with the ratio of live to dead load which determines the relaxation of hangers. The values were obtained for a 200 m span bridge illustrated in the same figure, designed for the IABSE Congress in Vienna (1980), according to *Per Tveit (2011)*.

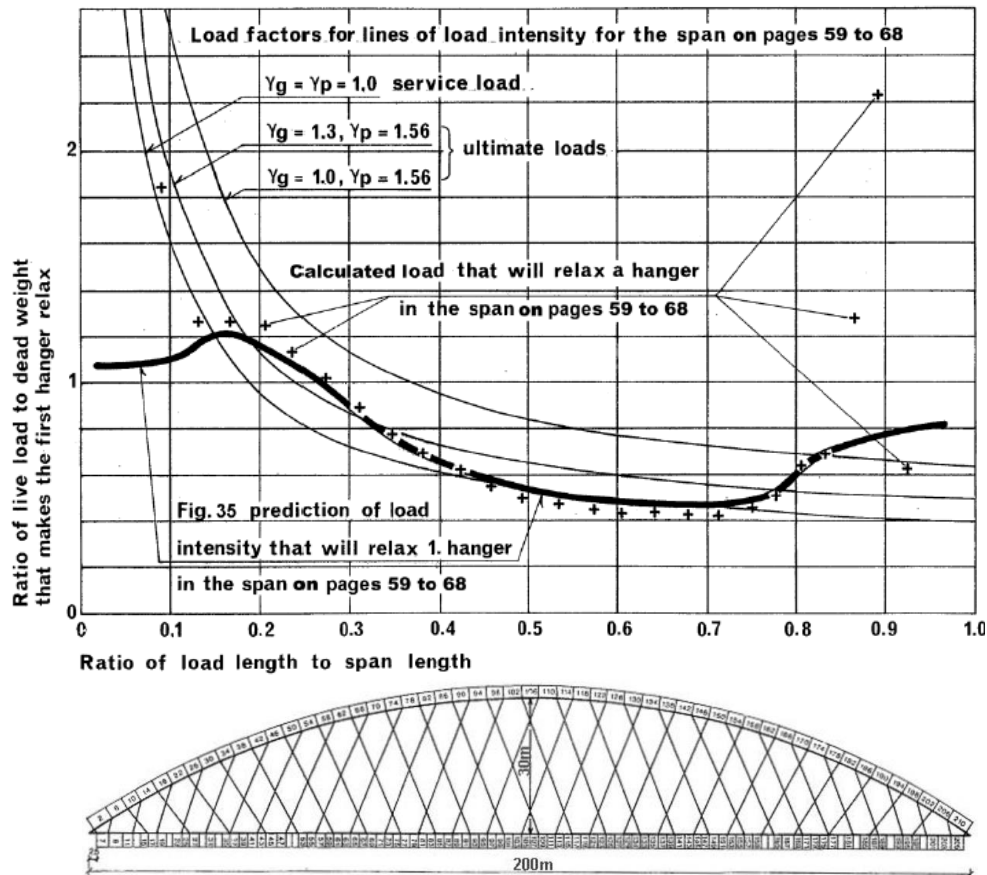


Figure 34- Ratio of live load / dead load and ratio of load length / span length combinations that make at least one hanger relax, in a 200 m span bridge, designed for the IABSE Congress in Vienna (1980), according to *Per Tveit (2011)*.

## Chapter 2. Alternative and Adopted Solution

From this figure, and assuming the behavior of the illustrated bridge similar to the designed bridge, it can be concluded that ratio of load length to span length between 0.5 and 0.75 will be the most demanding to verify that no relaxation occurs since smaller live loads are necessary to relax hangers. For simplicity, in this study, relaxation will only be verified for a 0.5 ratio of load length to span length.

Finally, the hanger's slope can be pre-designed. *Per Tveit* presents, in the same document, different graphic results for obtaining a first approach to the best slope to adopt in order to prevent relaxation, as a function of the arch rise/span quotient. Considering this quotient of 0.16 and a ratio of 0.42 between live and dead loads, a slope of  $60^\circ$  to  $65^\circ$  should be adopted.

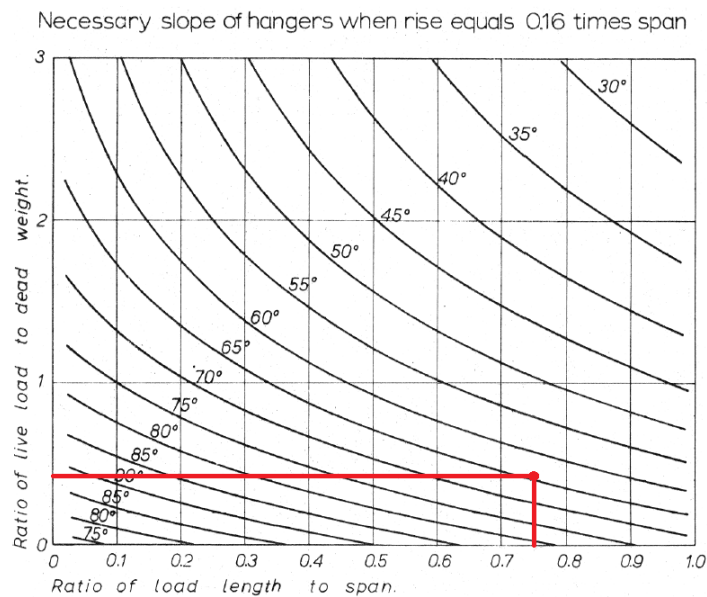


Figure 35 – Adopted hanger's slope to prevent relaxation, *Per Tveit (2011)*.

In respect to these graphics, according to *Per Tveit (2011)*, they “...can be used to find hangers' resistance in hangers that are not too near to the ends of the arches. Usually the resistance against relaxation in the hangers that are near to the ends of network arches is no problem”. This statement is in accordance with the results presented in Figure 34. Note that the methodology used to obtain the graphic in Figure 35 involved the calculation of an influence line for shear force, over an imaginary line A-A, as illustrated in Figure 36.

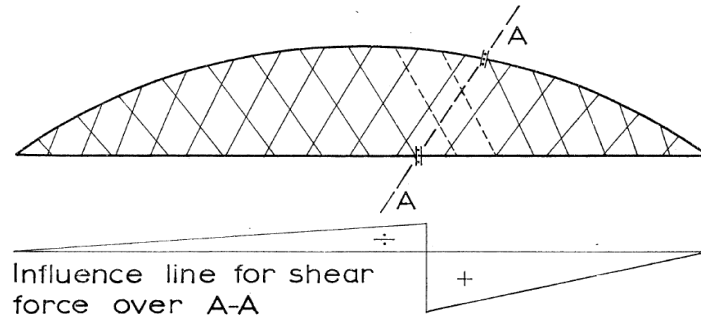


Figure 36 – Influence line for shear force over A-A, used to manually obtain the crossed hanger's axial force.

The hangers' real resistance to relaxation is slightly larger than the predicted by this method, due to the presence of shear and bending in the chords that are not considered.

In conclusion, a slope, between  $65^{\circ}$  and  $60^{\circ}$ , should be obtained considering that values over 0.75 won't be, as seen, critical. The adopted slope for the hangers is  $65^{\circ}$ . The final solution of the hangers is presented in Figure 37.

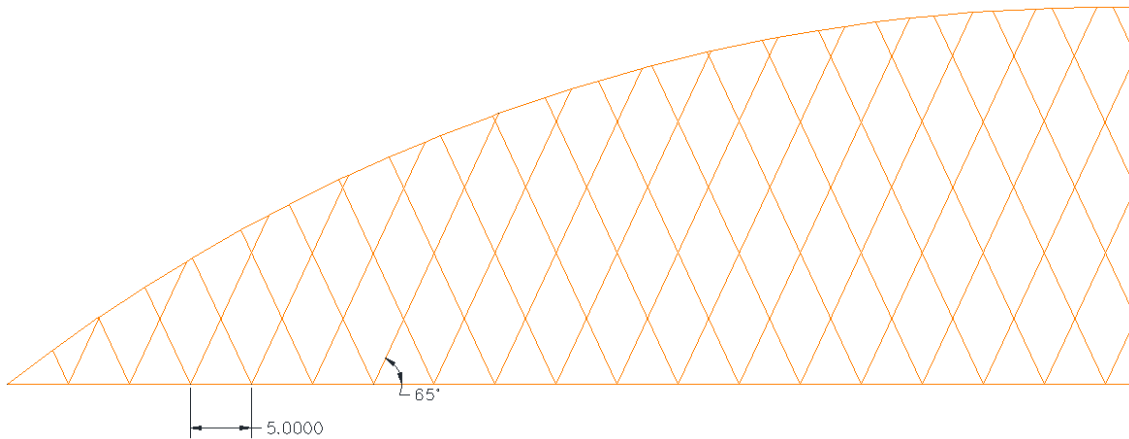


Figure 37 - Hangers final layout: Constant 5 m spacing on the tie; Parallel hangers with a slope of  $65^{\circ}$ .

2.3.3.6. Secondary Elements – (Bracing Beams and End-Cross-Girders)

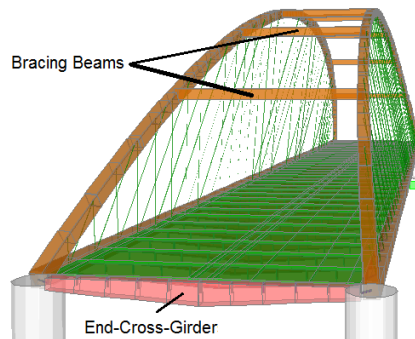


Figure 38 – Bracing beams and end-cross-girder location.

Seven bracing beams link both arches, preventing premature buckling of the arches and giving extra wind resistance. Additionally, two end-cross-girders are always adopted. These end-cross-girders are the first and the last rib of the deck, with a stronger and stiffer box section to better withstand the extra forces in this deck’s section, derived from the arch transversal bending moments, the torsional moment on the ties, and the rotational fixation of the first 5 m of slab, so that the slab behaves similarly in the first “local 5 m span” and in all other “local spans”.

These secondary elements are made of S355N steel and their safety was simply assured using the *SAP2000* “steel design/check” functionality.

The seven bracing beams’ cross-sections have the geometry presented in Figure 39.

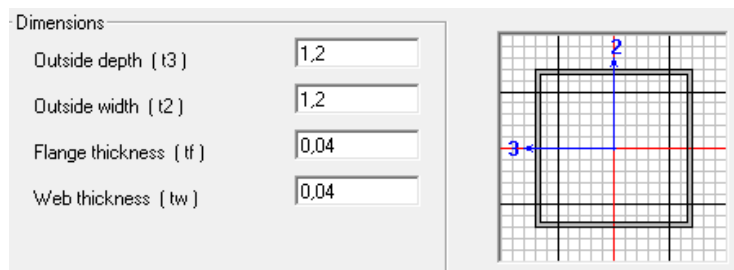


Figure 39 – Bracing beam cross-section (m).

The end cross-girders in the bowstring and approach viaducts, like the ribs, have a variable box section. Center and end cross-sections are given in Figure 40 and Figure 41 respectively.

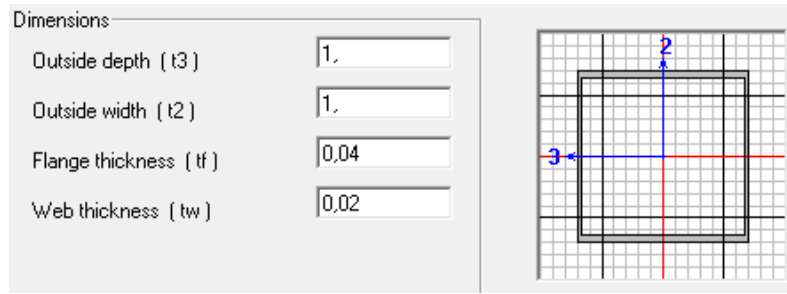


Figure 40 – End cross girder - End cross-section.

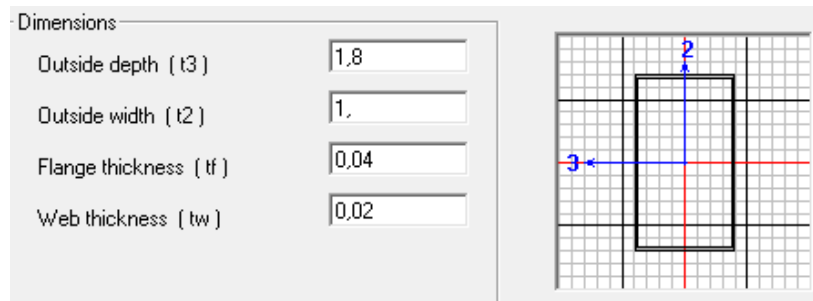


Figure 41 – End cross girder - Middle cross-section.

### 2.3.4 Deck Support Conditions

The adopted deck support conditions maximize the freedom of the structure to deform, while maintaining its ability to withstand vehicles' accelerations, wind forces and earthquake design actions. Figure 42 and Figure 43 illustrate the type of support conditions adopted on both the bowstring bridge deck and approach bridge deck.

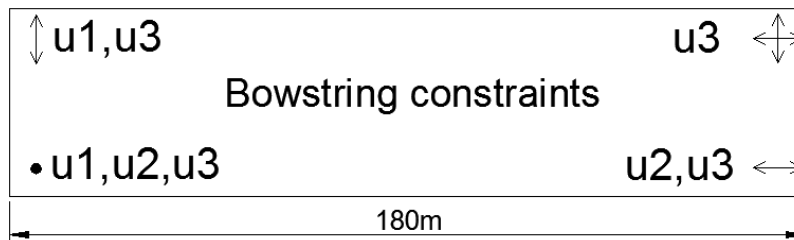


Figure 42 - Bowstring bridge deck constraints.

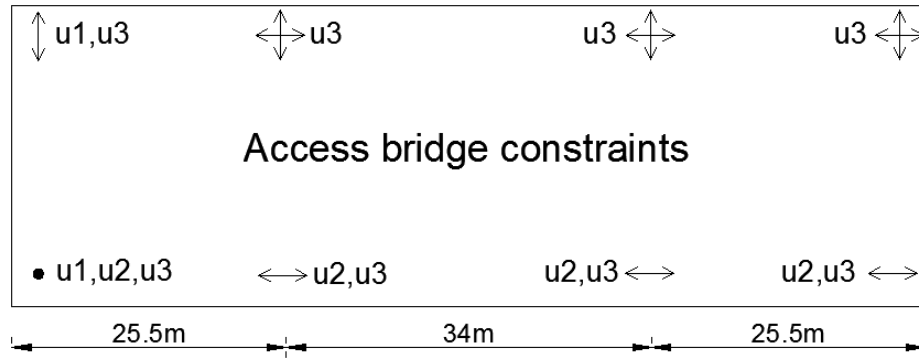


Figure 43 – Approach bridge constraints (left deck displayed). The inferior left corner of the figure is the point fixed to the abutment.

### 2.3.5 Constructive Procedures

Arches have been constructed over the years in many different ways. Several of these procedures were envisaged for the present bridge, namely:

- Big floating cranes erect the arch steelwork into place, after it being built off-site (Figure 44).



Figure 44 – Arch construction on the riverside, and floating cranes erecting the steelwork – *Pentele Bridge (2006)*.

- Small cranes, over the existing approach spans, erect the arch steelwork into place, after it being built off-site and floated into position by relatively small pontoons (Figure 45).



Figure 45 – Arch being lifted into position by small cranes over the approach spans. Lake Champlain Bridge (2011).

- Arch built in-site, with the help of provisory columns, cables and steel frames, above and under the deck (Figure 46).



Figure 46 - The Fort Pitt Bridge (1959), during its construction phase.

- Building the arch on the riverside, perpendicularly to its final position, above the ground, over a definitive column and provisional columns. Then, by transferring the weight on the provisional columns to a floating structure, and making it move to the final position, the bridge can rotate the  $90^0$ , with the base point on the definitive column (Figure 47).

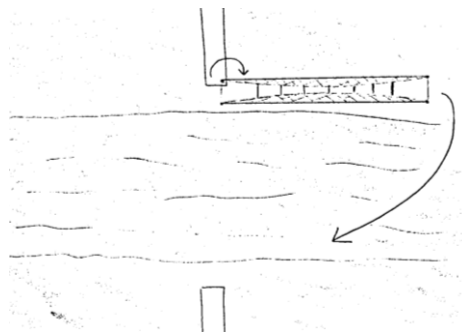


Figure 47 – Rotation of the arch scheme.

- Decks built by incremental launching followed by the erection of the arch by rotation, previously built over the deck (as it was recently done on the New Sado Railway River Crossing – Figure 48).

## Chapter 2. Alternative and Adopted Solution



Figure 48 – New Sado Railway River Crossing.

However, the final construction scheme (Figure 50), is different from the mentioned ones in these examples, and it's briefly explained next.

First the foundations, abutments and columns are erected. Since the distance of the bridge to the ground is small – slightly less than 10 m - scaffolding can be easily established under the approach spans (Figure 49). Then the ties and ribs are placed and welded.

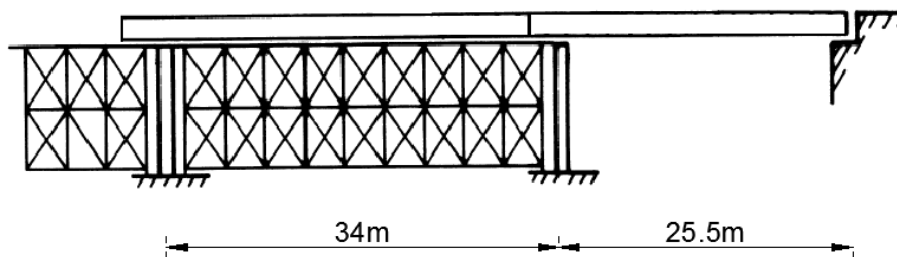


Figure 49 – Approach viaduct constructive process.

Next, or simultaneously, the arch span steelwork is erected on land, next to the end of the approach span. During the constructive process, temporary cranes and scaffolding aid the construction of all the steel elements.



The following constructive stage is to push the arch through the approach viaduct, until its final position, with the help of rolling mechanisms under the four arch span corners and a floating wagon or a pontoon (Figure 50).

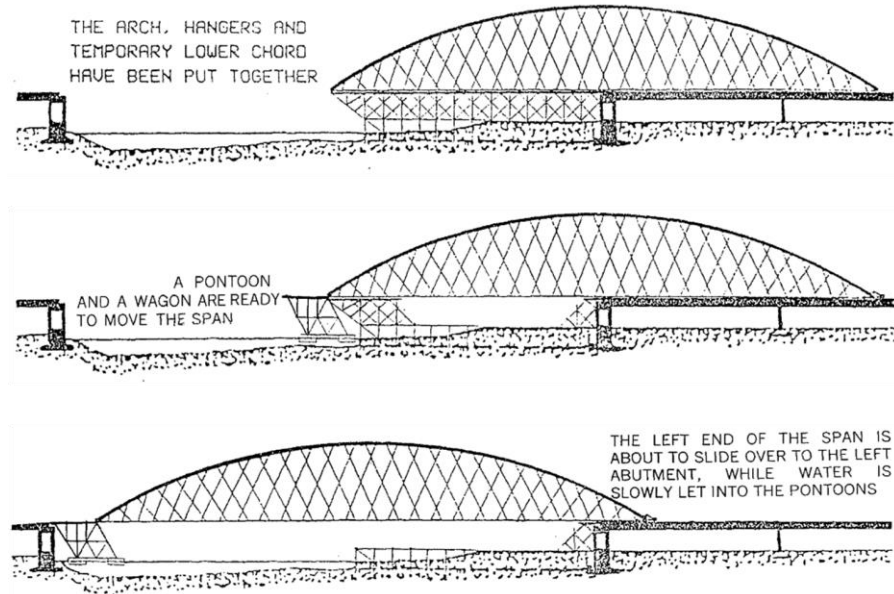


Figure 50 – Proposed constructive process - pushing the arch through the approach viaduct. Image sequence from *Per Tveit (2011)*.

Next, two different ways to build the concrete slab are presented:

- 1- Composite slab, with slim steel plates which can be previously prepared over the ribs, functioning as a lost formwork.

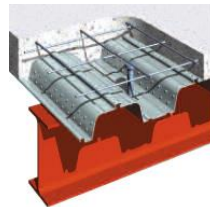


Figure 51 – Composite slab solution example.

- 2- Precast slabs. These will be put in place with a crane's support and will behave as simply supported for the concrete dead load. The overlapping should be made above the rib's top flange to avoid the need of formworks. Hook shaped rebars in the overlap zone should be used to accomplish this.

## Chapter 2. Alternative and Adopted Solution



Figure 52 – Precast concrete slab solution examples.

In this design phase, the second, precast slab method, is adopted and the overlap of the rebars is accomplished in the rib's top flange width (variable between 400 mm and 800 mm). At the end of the rib, where the top flange width is only 400 mm, there won't be negative moments since the tie and slab are connected, decreasing the overlap length, although the tension stresses from live loads oppose to this. Headed studs are placed both on the top flange of ribs and inner web of ties, to ensure the connection between these and the future concrete slab.

Finally, deck concreting operations are done in a symmetrical form with respect to the arch, starting from both ends to the center of the span, to avoid relaxing hangers and uncertain bending moments in the process, although the casting sequence might be different from project to project to avoid hanger relaxation during the construction stages, according to *Per Tveit (2011)*.

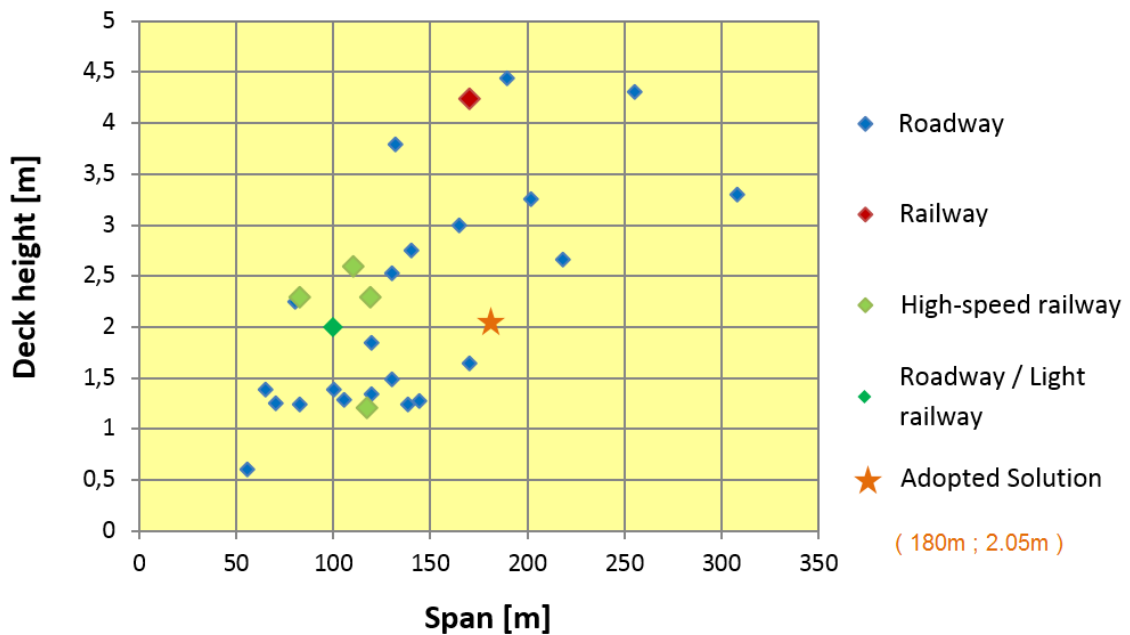
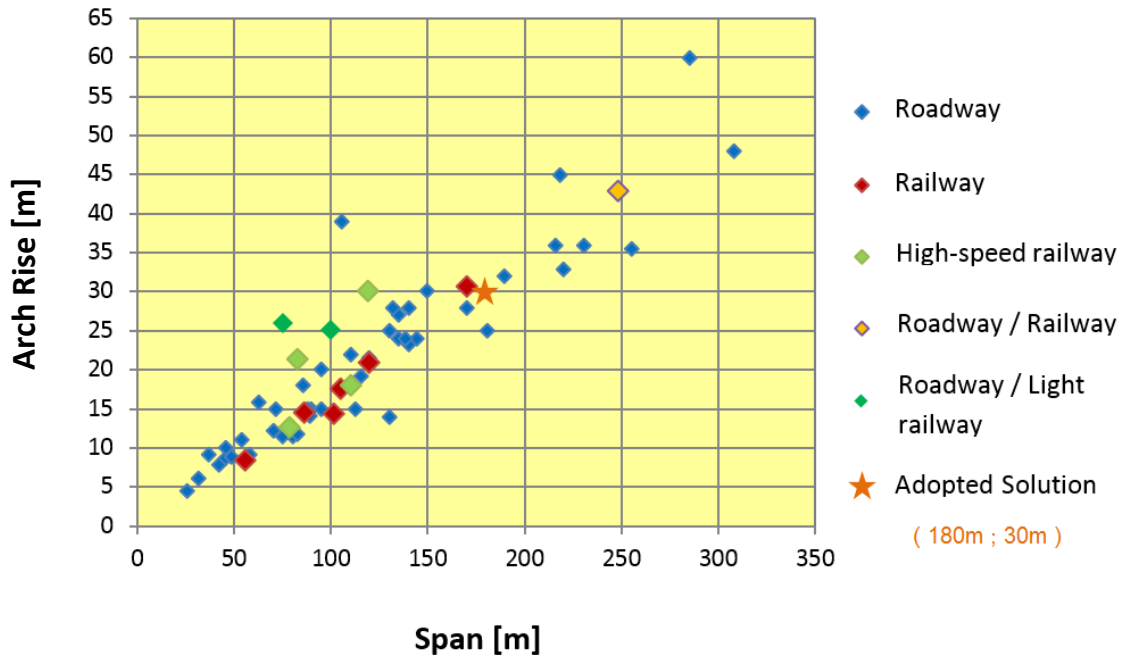
This solution, where the arch slides through the approach viaduct, is only possible since the total weight of the steel in the bowstring span is relatively small. A concentrated load of 25% of that total weight - simulating the support reaction of the bridge in one of its four corner - was applied in the most conditioning section of the tie, verifying that no yielding occurs. This simulates the concentrated forces of the arch weight on the provisional rolling supports under its four corners.

A combination of transversal wind effects with steel dead load was also considered applied to the arch to verify that no unbalance situation occurs. All reaction forces results on the four corners had upwards' direction, so the equilibrium is verified for this scenario.

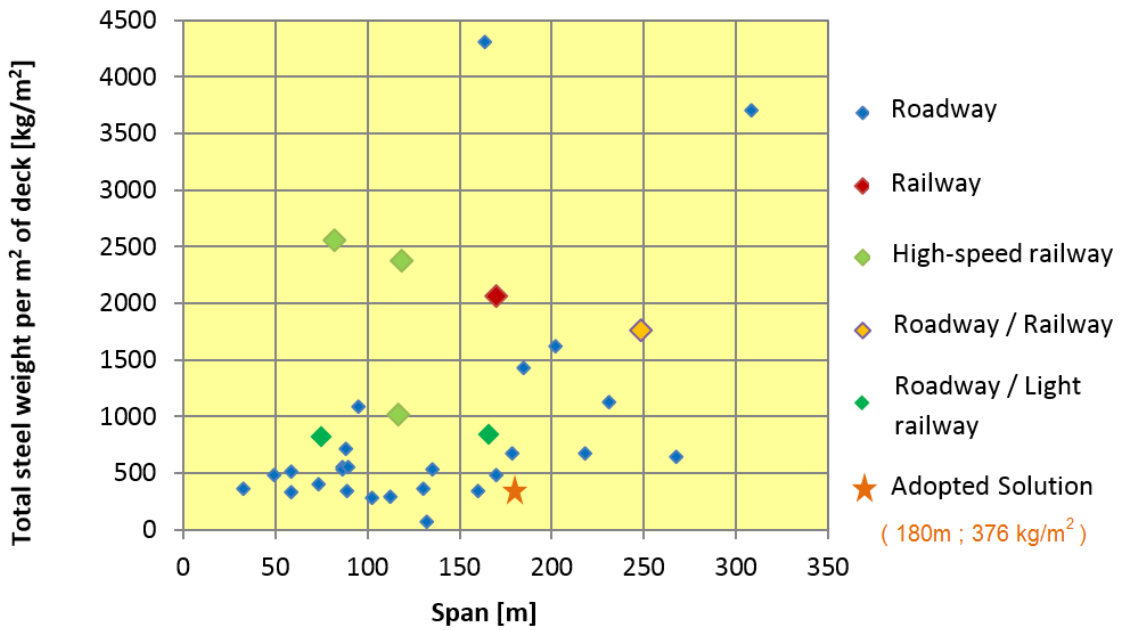
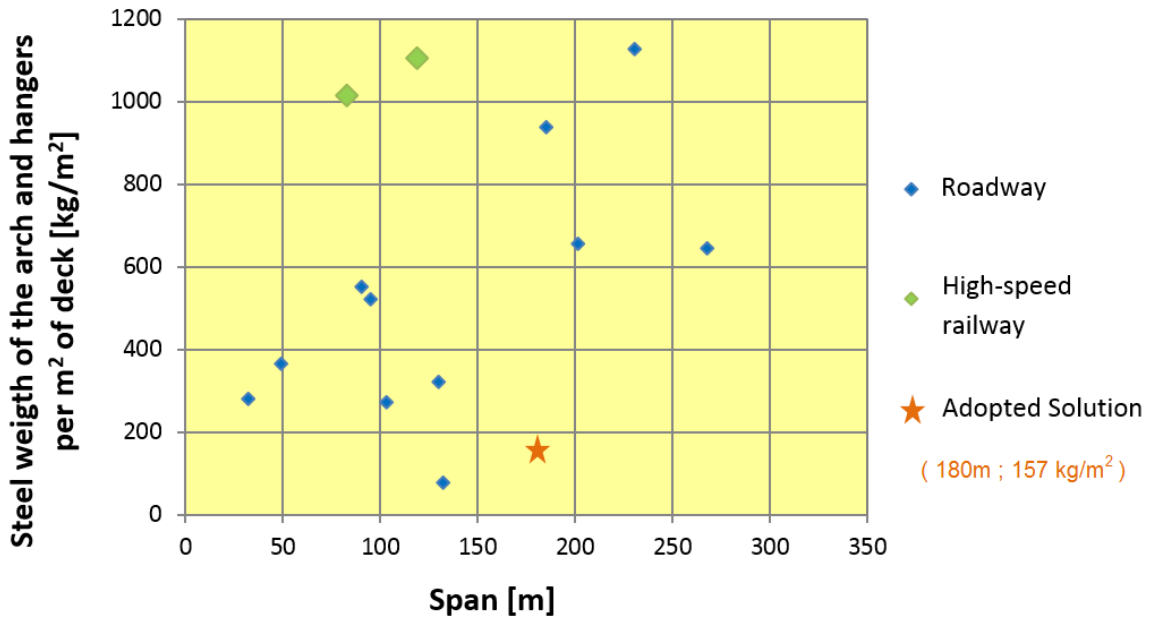
Pushing the arch through provisional columns on the river would also be an interesting option when a small river flow is predicted, although it would interfere with eventual traffic on the river. However, since columns would support the arch in different sections during the launching operations, severe hanger relaxations would occur. To overcome this, provisional compression resistant elements, connecting the upper and lower chords, should be required.

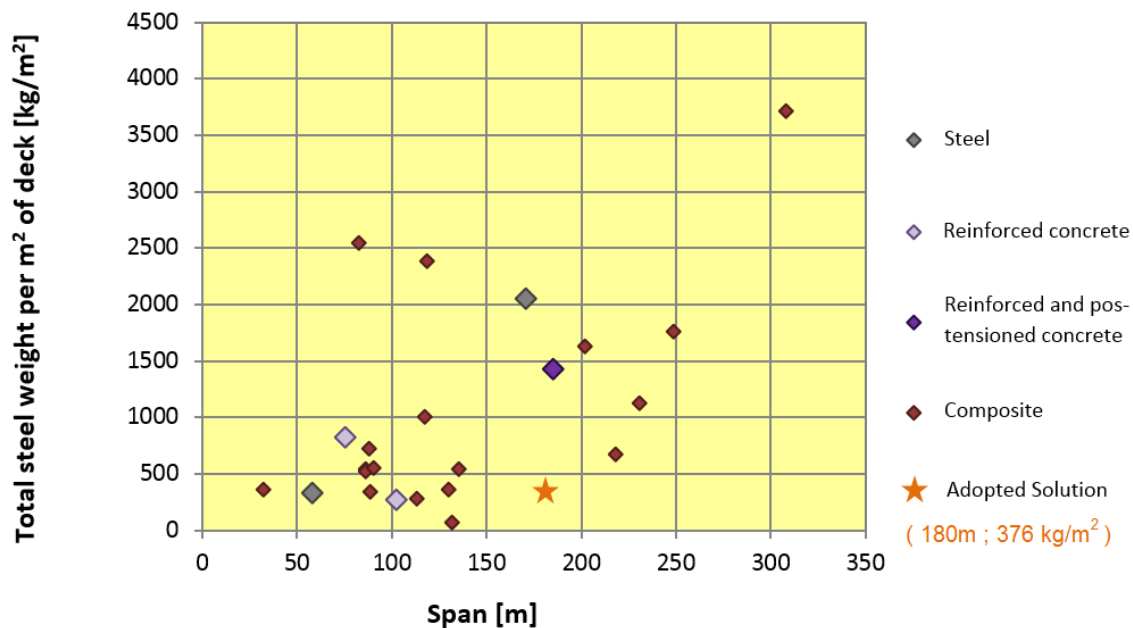
### 2.3.6 Comparison with Built Tied-Arch Bridges

The database collected by *Gonçalves, P. (2012)* compresses together useful information on several tied-arch bridges, not all necessarily with Network hangers arrangements or roadway. This makes possible a comparison between the adopted solution and many other tied-arch bridges, in respect to rise, slenderness and material quantities.



Chapter 2. Alternative and Adopted Solution





This database contains bridges from many different countries, with different requirements, demands, problems, standards, priorities and many different structural concepts.

It is apparent, however, that the adopted solution is very economic, when comparing to the other bridges, since it uses ratios of steel relatively low per square meter of the deck. The main reasons for these results are:

- There were no special architectural demands, so structural efficiency was the priority.
- Network arrangement of hangers is a very efficient structure option since bending moments on an arch of a bridge with vertical arrangement can be up to 15 times higher.
- Relatively high-strength steels were used on the arch (S420) and hangers (S460N).
- Many very light bridges, including the slender record breaker Brandanger network arch bridge in western Norway, are not included in the comparison of the steel weights (because no data was available).
- Dead and Live loads' multiplying factor adopted value of 1.35 for the ULS (a lower value than the widely adopted 1.5 factor for live loads).
- No significant earthquake forces were requested for this bridge (Barcelona, Spain), although this aspect would affect mainly the infrastructure design.

## Chapter 2. Alternative and Adopted Solution

- Careful design was performed with many iterations on the cross-sections' dimensions, exploring them nearly to their maximum capacity.

Finally, detail design should be performed to prove all pre-design options and decisions could be kept.

### 3. Design Actions and Modeling

#### 3.1 Actions

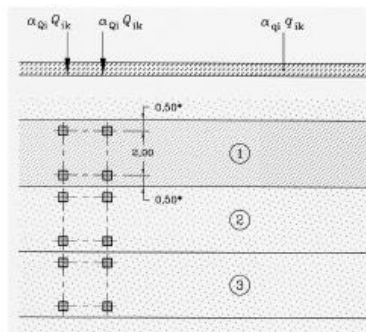
All permanent actions, i.e., DL- Dead Loads and SDL- Superimposed Dead Loads, and Live Loads such as the traffic UDL – Uniformly Distributed Load and the TS – Tandem System, have their values listed in *Appendix A*.

##### 3.1.1 Traffic Loads

The positioning of the UDL and the TS aims to maximize the resultant forces and deflections.

The TS was defined in *SAP2000 v14.2*, since this software allows the definition of moving loads. First, lanes were created along the bridge. Lanes are the geometrical places where the vehicles will pass through. The vehicles were defined according to the *EN1991-2*. The characteristic values and dimensions of these lanes and vehicles are illustrated in Figure 53.

Location	Tandem system <i>TS</i>	<i>UDL</i> system
	Axle loads $Q_{ik}$ (kN)	$q_{ik}$ (or $q_{ik}$ ) (kN/m <sup>2</sup> )
Lane Number 1	300	9
Lane Number 2	200	2,5
Lane Number 3	100	2,5
Other lanes	0	2,5
Remaining area ( $q_{ik}$ )	0	2,5



Key

(1) Lane Nr. 1 :  $Q_{1k} = 300$  kN ;  $q_{1k} = 9$  kN/m<sup>2</sup>

(2) Lane Nr. 2 :  $Q_{2k} = 200$  kN ;  $q_{2k} = 2,5$  kN/m<sup>2</sup>

(3) Lane Nr. 3 :  $Q_{3k} = 100$  kN ;  $q_{3k} = 2,5$  kN/m<sup>2</sup>

\* For  $w_l = 3,00$  m

Figure 53- Definition of Load model 1, according to *EN1991-2*.

### Chapter 3. Design Actions and Modeling

It is important to consider several positions, transversely and longitudinally, for these live loads, to access the higher stresses on the different structural elements of the bridge.

With respect to a transversal distribution of loads, two patterns of lanes were created, which are represented in Figure 54 and Figure 55, according with the lane numbers definition of *EN1991-2*. These patterns are simply entitled as “TS(123R\_R)” and “TS(R31\_2R)” respectively. This notation reflects directly the transversal position of loads.

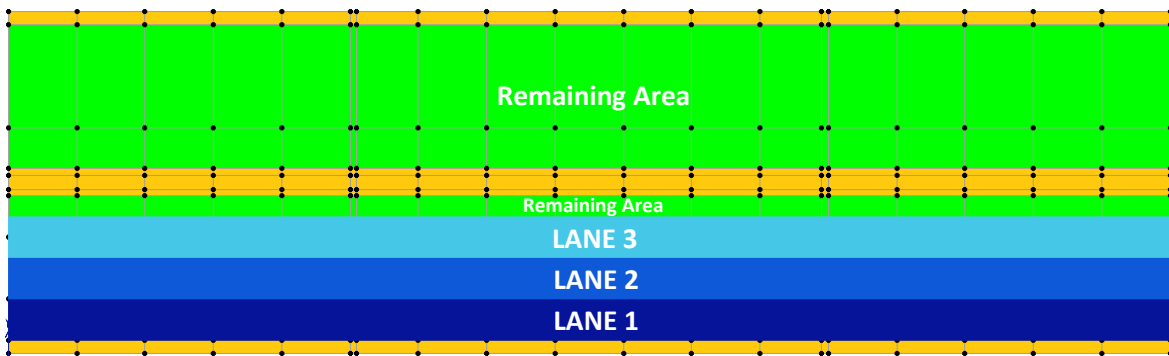


Figure 54 –Tandem System “TS(123R\_R)”.



Figure 55 –Tandem System “TS(R31\_2R)”.

#### 3.1.1.1 Approach Viaduct

With respect to the approach viaduct, 4 load distributions, combining different longitudinal and transversal positions, were defined according with schemes of next page (The red and green color represent respectively the uniform vertical distributed load of  $9 \text{ kN/m}^2$  and  $2.5 \text{ kN/m}^2$ ), considering that: i) UDL1 - Load pattern with only the central span loaded, and ii) UDL2 – Load pattern with the first two spans loaded.



Four combinations are possible (Figure 56 to Figure 59):

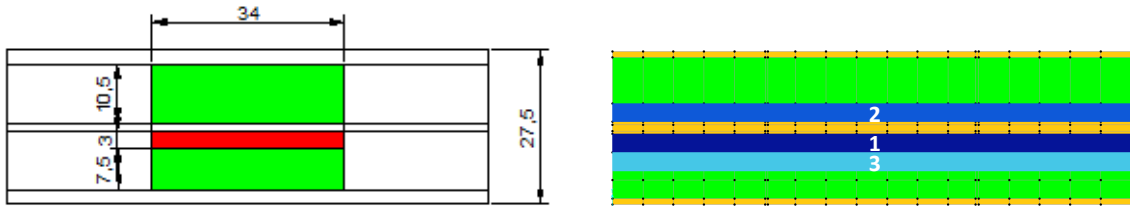


Figure 56 - 1<sup>st</sup> Lane positioning for: UDL1 + TS(R31\_2R).

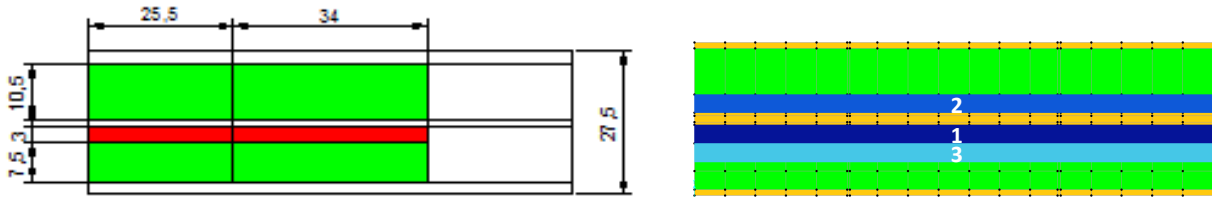


Figure 57 - 2<sup>nd</sup> Lane positioning for: UDL2 + TS(R31\_2R).

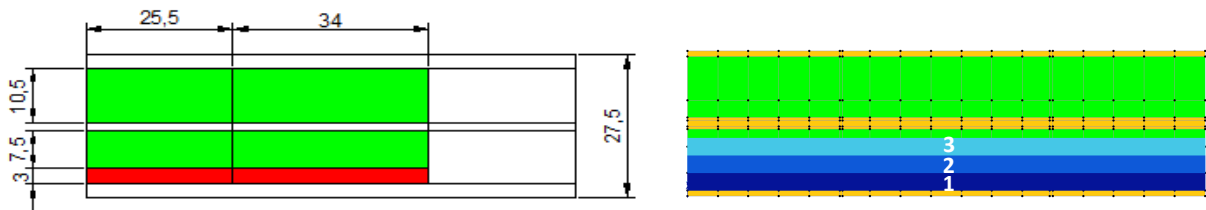


Figure 58 – 3<sup>rd</sup> Lane positioning for: UDL2 + TS(123R\_R).

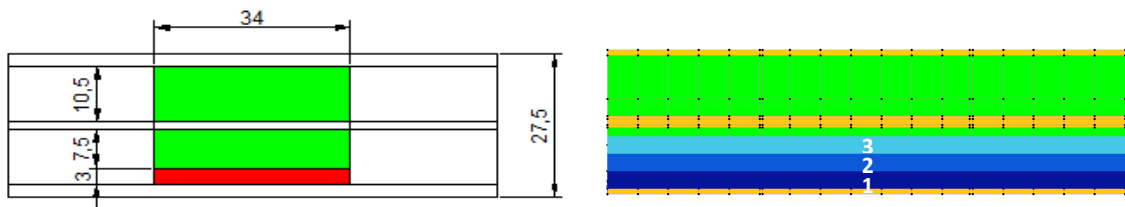


Figure 59 – 4<sup>th</sup> Lane positioning for: UDL1 + TS(123R\_R).

These load combinations are expected to generate the most demanding stress distribution on the different elements of the bridge deck, namely:

## Chapter 3. Design Actions and Modeling

1<sup>st</sup> Lane positioning for: UDL1 + (R31\_2R)

- Positive bending moment and tension in the rib (ULS).
- Possible positive longitudinal bending moment in the slab (ULS).
- Deflection of the ribs (SLS).

2<sup>nd</sup> Lane positioning for: UDL2 + (R31\_2R)

- No critical stresses are expected.

3<sup>rd</sup> Lane positioning for: UDL2 + (123R\_R)

- Negative longitudinal bending moment in the slab (ULS)
- Negative longitudinal bending moment and compression in the tie (ULS)
- Shear in rib (ULS)

4<sup>th</sup> Lane positioning for: UDL1 + (123R\_R)

- Positive longitudinal bending moment in the slab (ULS)
- Positive longitudinal bending moment and tension in the tie (ULS)
- Deflection of the tie (SLS)

The main results of each of these load distributions are presented in Appendix C.

### 3.1.1.2 Bowstring Bridge

The same transversal distributions are applied, together with two longitudinal patterns, namely:

- Load on the entire span (Notation - “UDL-All”).
- Load on the left half side of the span (Notation – “UDL-Half”).

An example for the load combination “UDL-All + TS(123R\_R)” is illustrated in Figure 60.

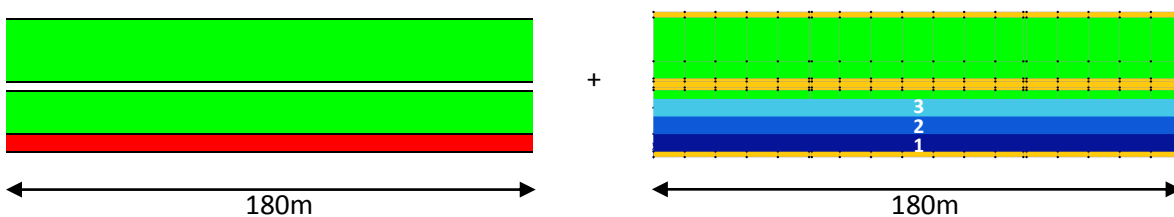


Figure 60 – Load combination: “UDL-All + TS(123R\_R)”.

When considering only the UDL load isolated, its transversal position is designated as “UDL(1R\_R)” or “UDL(R1\_R)” as in Figure 61 and Figure 62 respectively.

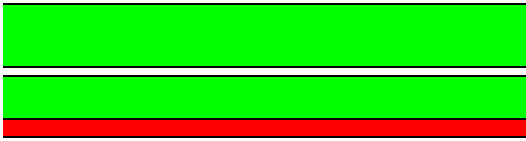


Figure 61 – Uniformly distributed load “UDL(1R\_R)”.

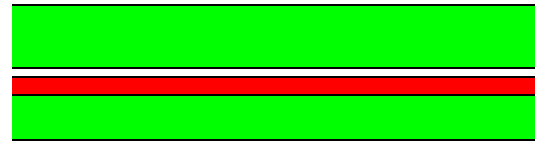


Figure 62 – Uniformly distributed load “UDL(R1\_R)”.

The different combinations and effects of each of these live loads will be carefully analyzed in Chapter 4.

### 3.1.2 Wind Load

The wind load is quantified using the equivalent reference basic speed value of  $v_{b,0} = 29 \text{ m/s}$  (Spain – Zone C).

Considering a return period of 100 years and a unitary directional and seasonal coefficient, the wind’s reference speed results in  $v_b = 1.04 \times 1 \times 1 \times 29 = 30.16 \text{ m/s}$ .

The exposing area, according with Figure 63, is  $d_{tot} = d + d_1 \approx 2 + 1 = 3 \text{ m}$ . The wind on vehicles was not considered.

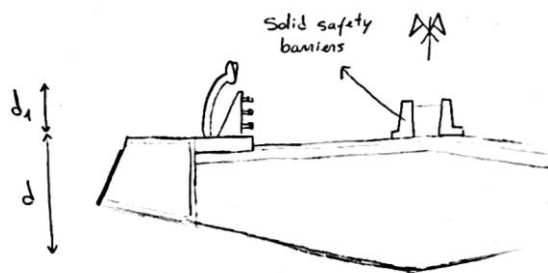


Figure 63 – Deck’s wind exposed area. Scheme of the deck’s cross-section.

Static equivalent wind force is evaluated by  $F_w = \frac{1}{2} \times \rho \times V_b^2 \times c_e \times c_f \times A_{ref}$ , where  $\rho = 1.25 \text{ kg/m}^3$ ,  $c_e$  is the exposure coefficient and  $c_f$  is the drag coefficient.

Using the *EN1991-1-4*, the coefficients and respective wind load results are presented in Table 2, for the deck, the arch, the hangers and the columns.

**Table 2 – Wind equivalent static loads acting on each of the structural elements**

	C <sub>e</sub>	C <sub>f</sub>	F <sub>w</sub> (kN/m <sup>2</sup> )	F <sub>w</sub> (kN/m)
Deck	2.81	1	1.598	4.794
Arch	3.04	2.24	3.871	5.4194
Hangers	3.04	1.2	2.074	0.1659
Columns	1.93	0.7	0.768	3.07

### 3.1.3 Seismic Action

The seismic action is defined according to *EN1998-1*.

The ground acceleration was obtained in the Spanish Annex. Its value for the region of Barcelona is only 0.05 m/s<sup>2</sup>.

It was considered a soil foundation type C, although more accurate information should be provided to classify the soil properly. The damping ratio was assumed as 3%.

The behavior factor, for the approach viaduct, was considered to be 1.2 and 1.5 respectively to the longitudinal and transversal direction. Both are considered to have limited ductility because the columns reinforcement is not designed using the capacity design procedure and, on the other hand, the bridge deck is fixed on a small number of columns so the capability to dissipate energy is not high. The different values are justified because in the longitudinal direction the bridge deck is fixed only on two columns while in the transversal direction the bridge deck is fixed on four columns.

The behavior factor of the arch bridge deck is considered 1.2 on both directions, since it is supported by only two columns in each direction.

The seismic action is defined by the response spectrum represented in Figure 64. The earthquake is applied in both directions simultaneously using the CQC modal and directional combination factor defined in *EN1998-1*.

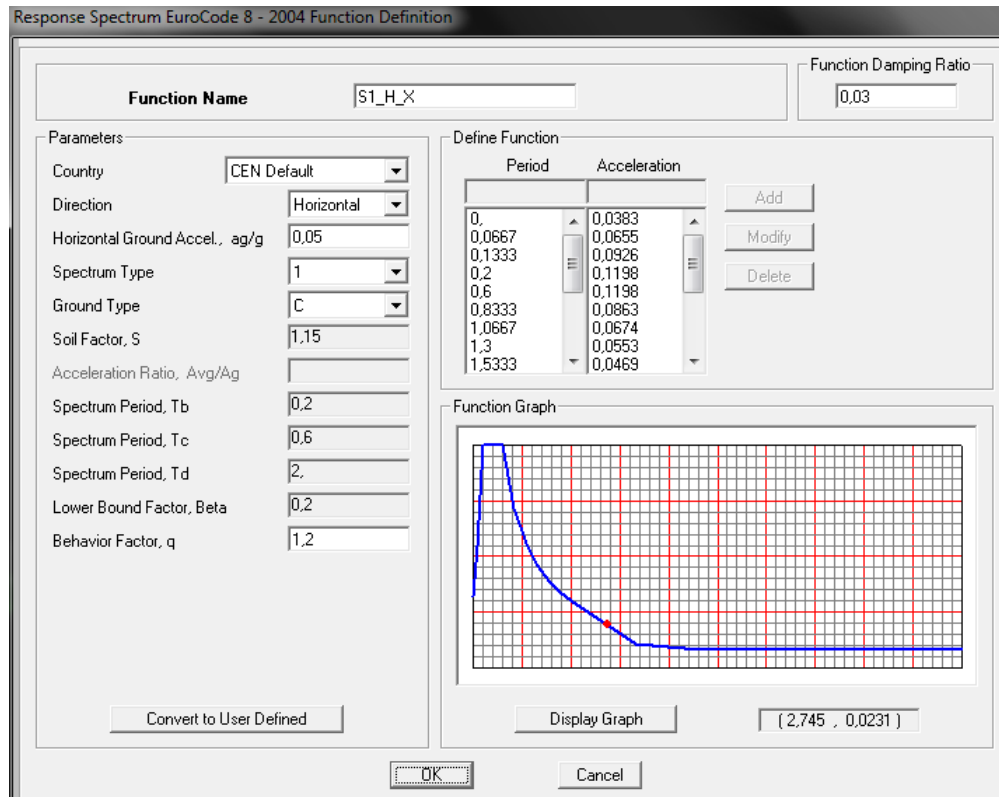


Figure 64 - Response spectrum introduced in SAP2000 software.

### 3.1.4 Temperature Actions

Only uniform temperature deck gradients are considered as differential temperature deck gradients do not have relevant effects on the tied-arch structure. Different uniform temperatures could be assigned to the concrete (slab) and to the steel part of the deck (ties and ribs), however the *EN1991-1-5* on section 6, refers that composite deck should be analyzed as a single block with the designation of *type2*, in which is applied a single uniform temperature according with Table 3, for the Barcelona region.

**Table 3 – Different winter and summer air and structure temperature, in °C**

	max	min
Air	40	-11
Composite	44	-7
Steel	56	-14

## Chapter 3. Design Actions and Modeling

Assuming that the average temperature during construction is 15<sup>0</sup>C, the following gradients to the maximum and minimum temperature values are applied on the composite deck and steel of the arch and hangers, obtaining the most adverse effects:

$$\text{Composite deck max. positive variation: } 44^0 - 15^0 = 29^0$$

$$\text{Composite deck max. negative variation: } (-7)^0 - 15^0 = -22^0$$

$$\text{Steel max. positive variation: } 56^0 - 15^0 = 41^0$$

$$\text{Steel max. negative variation: } (-14)^0 - 15^0 = -29^0$$

### 3.1.5 Combinations of Actions

#### *Ultimate Limit State (ULS)*

It was used the persistent and seismic combination of actions, which the expressions are respectively, according to *EN1990*, obtained by equations 3 and 4.

$$E_d = \sum_{i=1}^m \gamma_{gi} G_{i,k} + \gamma_q \left[ Q_{i,k} + \sum_{j=2}^n \psi_{0j} Q_{j,k} \right] \quad (3)$$

#### **Persistent combination of actions**

Attention should be made that the permanent and live load partial coefficients adopted value is 1.35.

$$E_d = \sum_{j=1}^m G_{k,j} + A_{Ed} + \sum_{i=1}^n \psi_{2,i} Q_{k,i} \quad (4)$$

#### **Seismic combination of actions**

### Serviceability Limit State (SLS)

The frequent combination of actions was adopted to verify deflection. This combination of actions is obtained by eq. 5.

$$E_d = \sum_{j=1}^m G_{k,j} + P + \gamma_{1,1} Q_{k,1} + \sum_{i>1}^n \gamma_{2,i} Q_{k,i} \quad (5)$$

#### Frequent combination of actions

The simultaneity factors were consulted in the table 6.1 a) of the Spanish document “*Acciones en Puentes*” (Actions on Bridges), included in Appendix B.

## 3.2 Modeling

The approach viaduct model was simply obtained by replicating part of the deck of the bowstring bridge and changing the support conditions. For this reason, only the bowstring model is here described. The final model is presented in Figure 65.

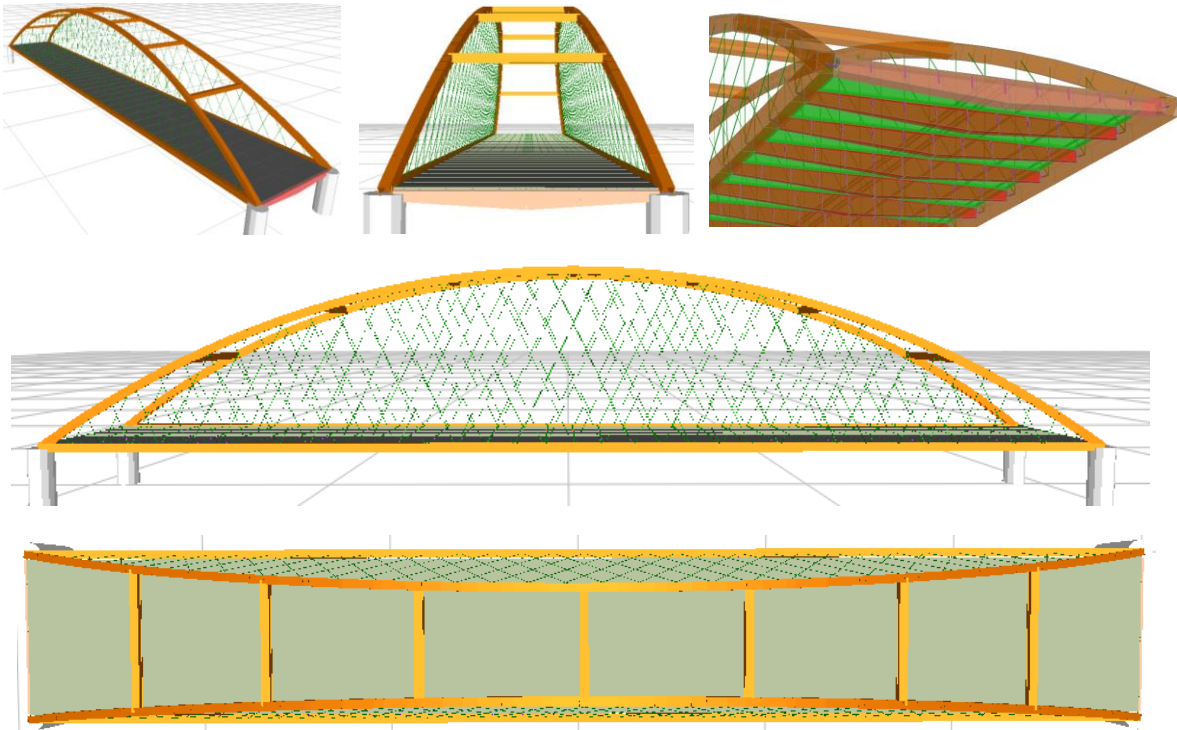


Figure 65 – Different views of the final model of the bowstring bridge.

### Chapter 3. Design Actions and Modeling

The composite deck had to be modeled with attention. Ties and ribs were modeled as frame elements on their center of gravity. Considering the slab to be horizontal on the model, which allows the lanes to be defined, the center of gravity of the rib and the slab at the middle section were both moved downwards, maintaining the same distance between them (Figure 66).

Ribs are connected to the center of gravity of the concrete deck element, in discrete joints using rigid elements. The space between these discrete joints is  $1/10$  of the ribs' length (Figure 67 and Figure 68).



Figure 66 – Rib, ties and slab sketch.

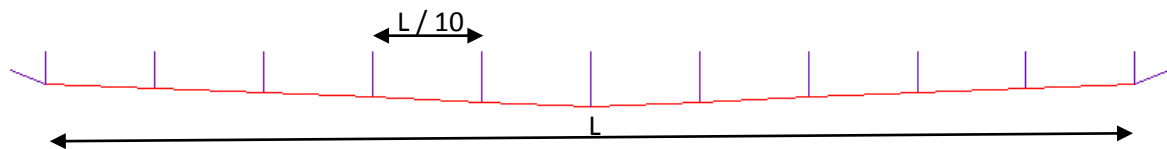


Figure 67 – Model of the rib with stiff elements. Rib frame element in red and stiff elements in purple.



Figure 68 – Extrude view of the rib as composite beam. Slab in green, steel beam in red, stiff elements in purple.

The first and last ribs – the end-cross-girders – with a bi-symmetrical box section have a different location of the center of gravity than the I ribs section and so their center of gravity is modeled slightly higher. All ribs are spaced 5 m between each other, and are connected at the tips, to the ties (Figure 69 and Figure 70).

Then, arches, hangers and bracing beams are first drawn in *AutoCAD* and then imported to SAP2000 model.



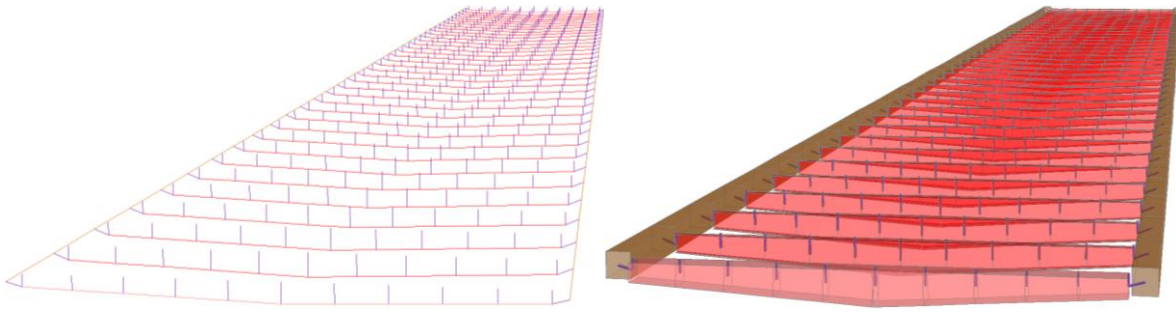


Figure 69 – Deck Model. Ribs and ties.

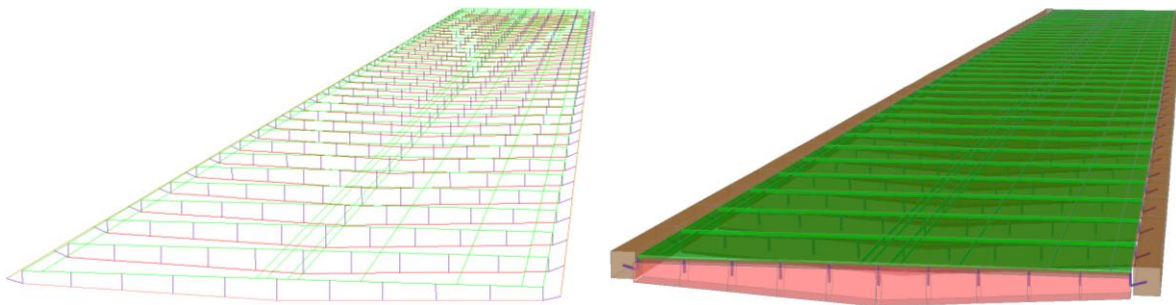


Figure 70 – Deck Model. Ribs, ties and slab.

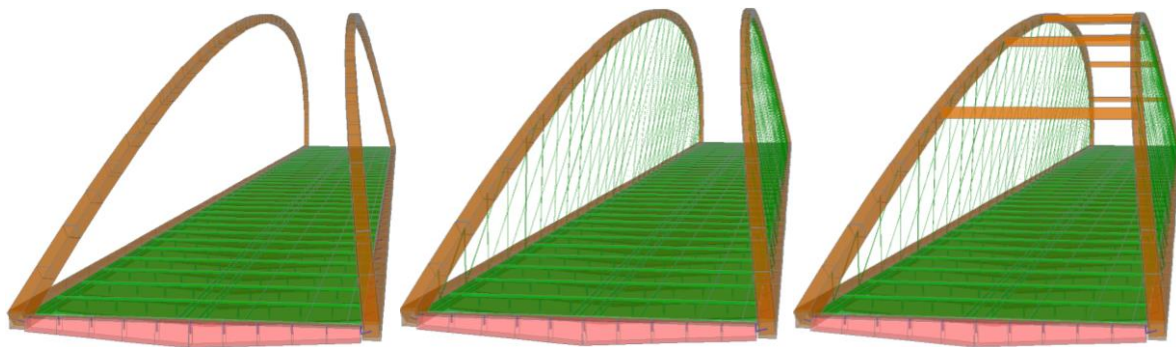


Figure 71 – Introduction of the arch, hangers and bracing beams to complete the model.

Finally, the support conditions are introduced in the model by releasing, accordingly, the shear forces, bending moments and torsional moments in the columns, at their end joint which connects to the tie. The lower joints of the columns are restrained to all movements and rotations since they are supposed to be rigidly connected to the foundation. Bowstring bridges are relatively tolerant to settlements and other ground movements or accelerations, although a bad

### Chapter 3. Design Actions and Modeling

terrain/foundation conditions could result in some additional stresses for a case where an unsymmetrical live load demands more one of the bridge columns than the other three.

The arches and the ties' sections are modeled with similar rectangular hollow sections to those defined previously. The hangers are released in both bending rotations in the ends, and released in torsion on one of the ends.

Different slab stiffnesses were modeled to contemplate the cracking and creep effects of the concrete slab, as well as the constructive process, as explained further in detail in Chapter 4. The reinforcement weight was considered by properly scaling the self-weight of the concrete slab.

Finally, it should be pointed out that the model has a limitation which must be referred: the connection between slab and ties. This connection is made at discrete points, where the ribs intersect the tie every 5 m, and not continuously, as in reality with the use of connectors. Therefore, the model is expected to predict higher concentrated bending moments and axial forces on the slab at these discrete points. These higher values need to be adjusted for design verifications by using average values between discrete points.

## 4. Structural Analysis

### 4.1 Overview

This chapter analyses the main structural elements that compose the bowstring span. The bridge is formed by the bowstring span and an approach span on each side. The structural solutions of these additional spans are relevant to the total structure visual impact and also to the constructive procedure, as explained. Therefore, these approach spans need also to be studied. The ribs are assumed to have similar stresses on both bridges so they are only studied in this chapter. As for the slab and longitudinal beams of the approach viaduct decks, the final results of the design procedure can be consulted in Appendix C. The columns were also analyzed; Results are presented for the approach viaduct in Appendix C and in Appendix D. Specifications for the expansion joints between decks are at the end of this chapter and also included in Appendix E.

### 4.2 Deck Slab Analysis

In the slab of the bowstring span the first important phenomenon to observe is the global bending moment of the deck - see the tie  $M_{3-3}$  diagrams of the bowstring bridge (Figure 95). However, the global moments are less important than in the approach viaduct deck as every transversal beam (rib) is considerably well supported by two hangers in each end.

The second important phenomenon is the tension that the slab will absorb from the tied-arch. Considering the constructive procedure, the slab will absorb only tension due to the SDL and Variable Loads as before that the precast slabs do not have stiff solid concrete connecting them and only the ties are there to resist the horizontal force. The same occurs with the transversal compressions induced by the composite behavior slab-rib. So, for the DL, the precast slabs are simply supported between ribs, spanning 4.6 m and therefore stresses will come from the bending moments obtained by:

$$m_{11} = \frac{pl^2}{8} = \frac{(0.25m \times 25kN/m^3 \times 1.08) \times 4.6^2}{8} = 18 \text{ kNm/m}$$

(\*) The load  $p = 0,25m \times 25kN/m^3 \times 1.08$  takes into account the adopted reinforcement bars weight which increase approximately by 8% the concrete weight.

(\*\*) Ribs are spaced 5 m between each other. Though, the span can be decreased to 4.6 m, which is still conservative, to account for the top flange minimum width of 400mm.

**Table 4 – Slab - DL – [simply supported slab]**

$f_{11}$	$f_{22}$	$m_{11}$	$m_{11-}$	$m_{22}$
0	0	18	0	0
$f_{11}, f_{22}$ (kN/m)		$m_{11}, m_{22}$ (kNm/m)		

Next, for the SDL action the bending moments and membrane axial forces are given in Table 5 and Figure 72.

**Table 5 – Slab - SDL**

$f_{11}$ (corner)	$f_{11}$	$f_{22}$ (1 <sup>st</sup> Rib)	$f_{22}$	$m_{11}$	$m_{11-}$	$m_{22}$
700	220	-250	-130	9	-12	6
$f_{11}, f_{22}$ (kN/m)		$m_{11}, m_{22}$ (kNm/m)				

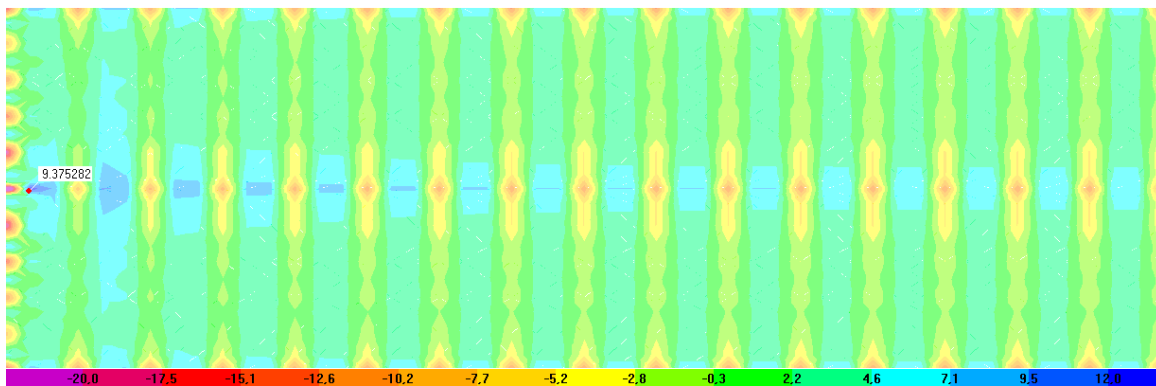


Figure 72 - Slab's  $m_{11}$  due to SDL (only left-half deck is shown).

The slab works under high tension values, not only for SDL but also when the other variable loads are present, so it will certainly crack. For this reason, the slab stiffness considered in the model is only 2.5 times the total rebar's stiffness. The value 2.5 intends to approximately contemplate the restriction offered by the concrete against the rebar strain, between cracks, normally named the tension stiffness effect.

The model does not consider a continuous connection between the slab and the tie so there are some meaningless  $m_{11}$  and  $m_{11-}$  in this zone that must not be taken into account. One reason for the first two 5 m spans to be the conditioning ones for the positive bending moment as to do with the deck's global bending which can be seen in the  $M_{3-3}$  of the tie in the next sub-chapter (Figure 95). It should be mentioned that noting the maximum stress value on the central reservation, and combine it with the maximum stress from the vehicles on another section, is a quite conservative procedure. Also, the negative moments are not really accurate since the model considers the interaction between the rib and the slab at discrete points only, over the stiff elements.

Furthermore, the flange width that supports the slab panels (800 mm at the ribs central section or 1000 mm at the end-cross-section) reduces even more the real local bending moments.

From the DL bending moments and the considerable global positive moment, the design of the slab results conditioned by a positive moment.

For the SDL's  $f_{11}$  the membrane axial forces induced in the slab are perfectly clear (Figure 73). They are applied by the arch legs at the extremities of the slab, and therefore the distribution is of tension stresses, from the end-edges to the center. In other words, the slab increasingly “helps” the tie to resist this horizontal force coming from the arch, as the shear forces coming from the tie to the slab propagate increasingly to its center.

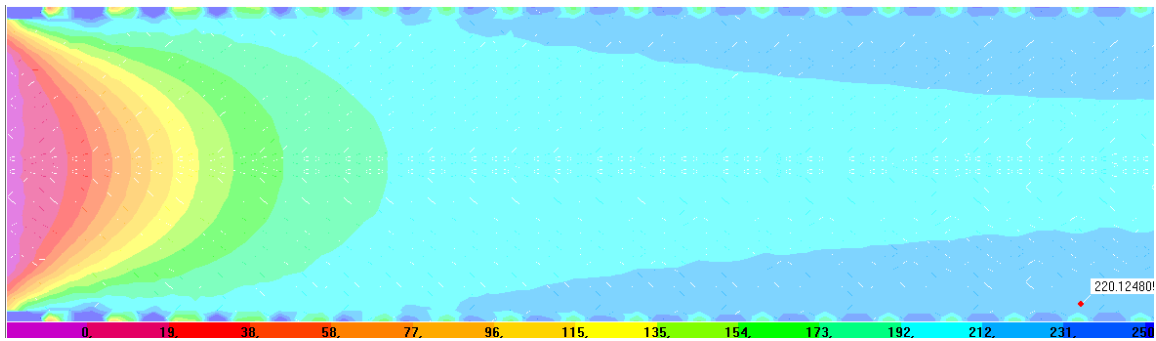


Figure 73 - Slab's  $f_{11}$  due to SDL (only left-half deck is shown).

The stresses on the slab due to the pre-stressing of hangers are quite insignificant and are not presented. They act in a specific non-critical area of the slab and induce small local bending moments. Though, in detail design this action should also be considered in slab design, as part of the hangers stressing is applied when concrete deck is structurally working.

When applying the live loads, the two different transversal positions of live load are tested. The most demanding one was the “UDL-All + TS(R31\_2R)” as it can be seen from Table 6 and Table 7 results.

**Table 6 – Slab – UDL(R1\_R)-All**

$f_{11}$ (corner)	$f_{11}$	$f_{22}$ (1 <sup>st</sup> rib)	$f_{22}$	$m_{11}$	$m_{11}$ -	$m_{22}$
1000	250	-340	-170	12	-12	9
$f_{11}, f_{22}$ (kN/m)			$m_{11}, m_{22}$ (kNm/m)			

**Table 7 – Slab - TS(R31\_2R)**

$f_{11}$ (corner)	$f_{11}$	$f_{22}$ (1 <sup>st</sup> rib)	$f_{22}$	$m_{11}$	$m_{11}$ -	$m_{22}$
200	140	-700	-350	101	-50	43
$f_{11}, f_{22}$ (kN/m)			$m_{11}, m_{22}$ (kNm/m)			

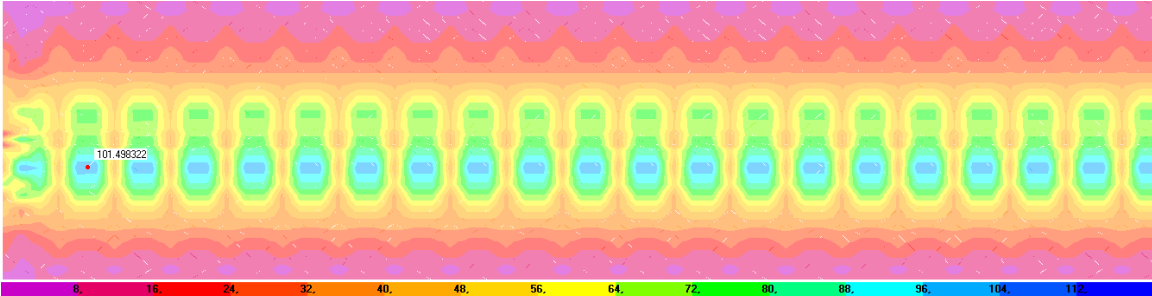


Figure 74 - Slab's  $m_{11}$  max envelope, due to TS(R31\_2R) (only left-half deck is shown).

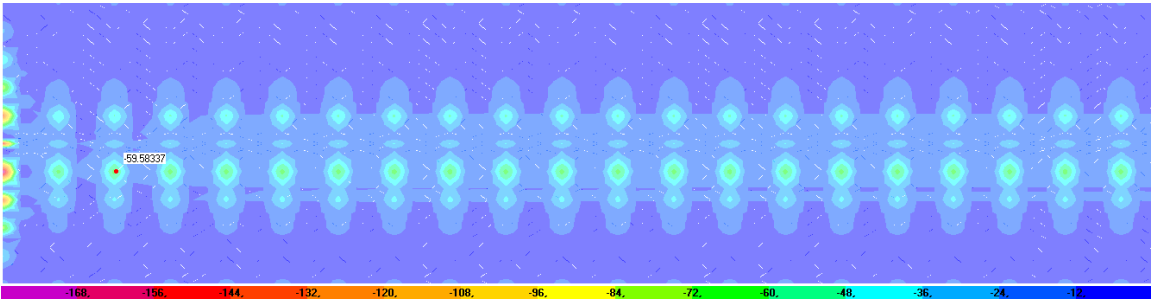


Figure 75 - Slab's  $m_{11}$  min envelope, due to TS(R31\_2R) (only left-half deck is shown).

The positive bending moments are more important than the negative ones for the Tandem System concentrated loads. This reflects that the bending stiffness of the slab is much more important than the torsional stiffness of all the ribs, except the boxed shape end-cross-girders, where the first 5 meters span have a lower value for the positive moments.

The negative bending moment over the 1<sup>st</sup> rib is not considered critical because of the reasons already given for the SDL and because this zone has practically no global tension stresses on the slab (as can be seen from Figure 73) so the design of the slab won't be conditioning at that section.

The wind action adds only a small effect on the longitudinal tension of the slab (Table 8 and Figure 76). The forces are directly related with the wind forces measured on the tie and its reasons are fully described there.

**Table 8 – Slab - Wind**

$f_{11}$ (corner)	$f_{11}$
0	180
(kN/m)	

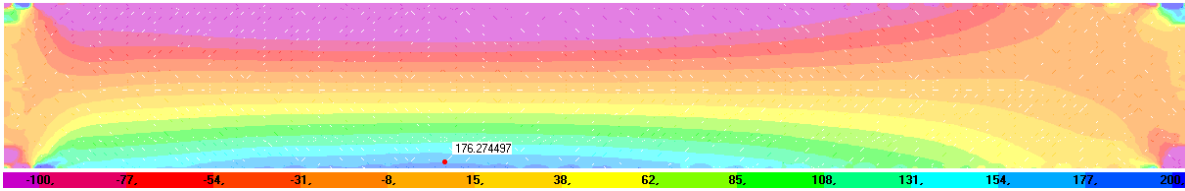


Figure 76 -  $f_{11}$  on the slab, due to wind load (all deck is shown).

The effects of temperature gradients are now presented. Like the wind, its effects are small and fully related with the interaction slab-ties, as explained in the next sub-chapter. The diagrams are shown to later compare with the tie forces. The relevant diagram for the design will be the positive temperature gradient, according with Table 9 and Figure 77 and Figure 78 results.

**Table 9 – Slab - Positive Uniform Temperature**

$f_{11}$ (corner) / 2	$f_{11}$ / 2
250	56
(kN/m)	

The stresses to take into account were divided by two, to approximately contemplate the creep effect on the concrete when subjected to thermic season gradients.

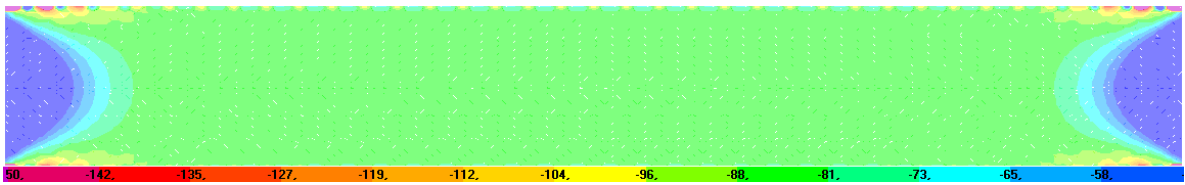


Figure 77 –  $f_{11}$  on the slab, due to negative uniform temperature (Deck:  $-22^{\circ}$ ; Arches and hangers:  $-29^{\circ}$ ).

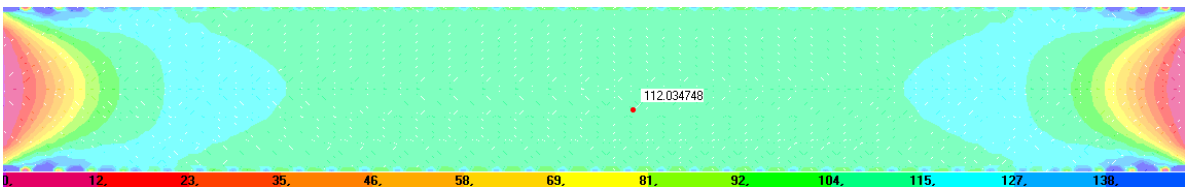


Figure 78 –  $f_{11}$  on the slab, due to positive uniform temperature (Deck:  $29^{\circ}$ ; Arches and hangers:  $41^{\circ}$ ).

## Chapter 4. Structural Analysis

Table 10 and Table 11 present ULS and SLS bending moments and membrane axial forces, at each direction.

**Table 10 – Slab - ULS**

<b>ULS = 1,35 × (DL + SDL + UDL + TS) + 0,6 × 1,5 × Wind + 0,6 × 1,5 × Temperature</b>					
$f_{11}$ (corner)	$f_{11}$	$f_{22}$ (1st Rib)	$f_{22}$	$m_{11}$	$m_{11}$
2790	1036	-1742	-878	189	-100
$f_{11}, f_{22}$ (kN/m)		$m_{11}, m_{22}$ (kNm/m)			

**Table 11 – Slab - SLS**

<b>SLS = 1 × (DL + SDL) + 0,4 × UDL + 0,75 × TS + 0 × Wind + 0,5 × Temperature</b>						
$f_{11}$ (corner)	$f_{11}$	$f_{22}$ (1 <sup>st</sup> rib)	$f_{22}$	$m_{11}$	$m_{11}$	$m_{22}$
1375	453	-911	-461	108	-54	42
$f_{11}, f_{22}$ (kN/m)		$m_{11}, m_{22}$ (kNm/m)				

For the conventional most loaded cross-section (with the critical stresses obtained from different slab sections), and making use of the software *Response2000*, it's simple to verify the rebar stress, in ULS, and to verify the crack width for the SLS. So, in the ULS:

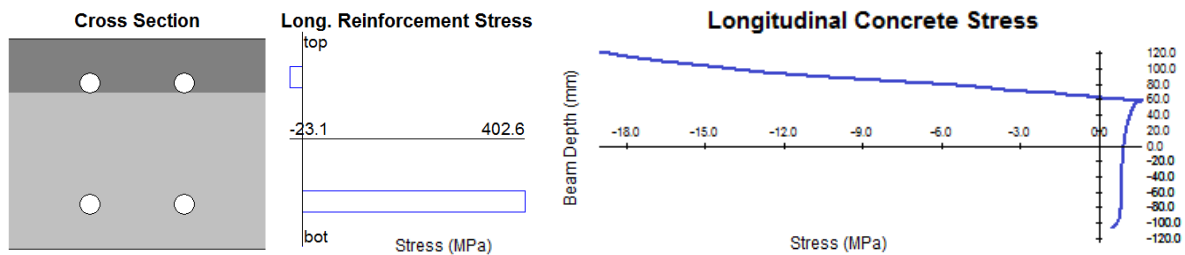


Figure 79 – Neutral axis location. Longitudinal reinforcement and concrete stress for the ULS verification ( $N_{ed}=1036$  kN/m ;  $M_{ed}=189$  kNm/m).

The neutral axis is located 60 mm from the top:

$$\frac{x_{Neutral\ Axis}}{h} = \frac{60mm}{250mm} = 0.24$$

The indicative value of 0.24 shows that the cross-section has a good ductility on collapse since reinforcement yields before the concrete fails.

(\*) A refined model, with a rigid local shell connecting each tie to the slab was used to study the transversal positive and negative slab bending moments, proving the results to be less critical than the longitudinal ones ( $|m_{22}^+| < |m_{22}^-|$  and  $m_{22}^-(ULS) = -164$ kNm/m).



And, still in the ULS, for support slab section:

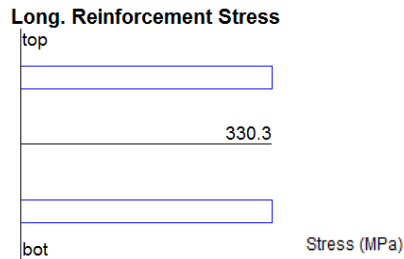


Figure 80 - Longitudinal reinforcement stress for the ULS verification. Support section with:  $N_{ed}=2790$  kN/m and  $M_{ed}=0$ .

The reinforcement stresses verify the security, for both analyzed sections:

$$\frac{f_{sd}}{f_{yd}} = \frac{403}{435} = 0.926 \leq 1.0$$

The slab shear stresses are less conditioning than the ones found in the slab of the approach viaducts, due to the support conditions of this last one. For this reason, shear resistance of the slab is verified only in Appendix C.1.

For the SLS, the cracking verification in the most loaded slab section is:

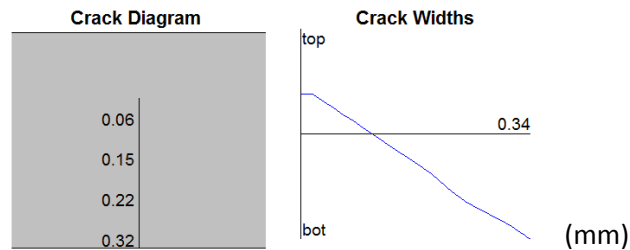


Figure 81 – Crack analysis of the slab for the SLS. Conventional section with  $N_{ed}=453$  kN/m and  $M_{ed}=108$  kNm/m.

And, for the support slab section:

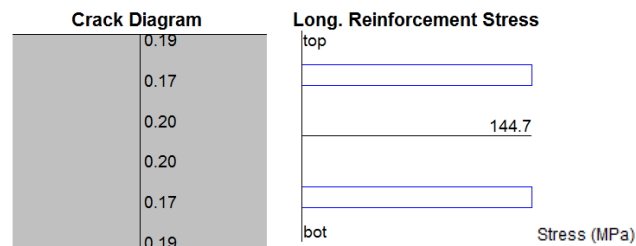


Figure 82 – Crack analysis of the slab for the SLS. Support slab section with  $N_{ed}=1375$  kN.

## Chapter 4. Structural Analysis

According to the *EN1992 1-1 7.3*, for the most exposure classes, and for a non-prestressed slab, the limit of the crack widths is 0.3 mm, and the maximum verified was 0.32 mm.

From this result it's important to remember that the conventional section used in verifications combines two different sections and the real section with the highest bending moment has a significant lower axial stress than the considered one. Furthermore, the slab will be fully shielded by a waterproofing cover, before settling the asphalt and all SDL. Concluding, the durability of the structure, according to the referred code, can be assured.

As for deflection, attending to the constructive procedures, it is quite difficult to predict it due to the dead loads, since the dimensions of the pre-slabs are not studied in this phase of the study. Anyway, the slab's deflection is calculated as a simply supported slab, for the DL, and for the following loads, using the FEM. Results are presented:

**Table 12 - Slab - SLS - Deflection**

	DL	SDL	UDL	TS	SLS - Total	L/1000
$\delta$ (mm)	1.1	0.3	0.7	2.1	3.3	5

The partial safety coefficients are applied only on the result "SLS-Total".

The estimated deflection from the DL is not conservative. But, due to the ribs top flange width, the real slab's span will be slightly lower, which reduces the total deflection bringing it to satisfactory limits.

### 4.3 Ribs Analysis

The transversal beams (ribs) should support slab panels during construction. Therefore, the composite section is only activated for SDL and live loads, as for the DL, only the steel section resists.

The resultant bending moments  $M_{33}$  have always a positive value (Figure 83). It's important to mention that the most demanding section is not the one at the center of the rib's span. That's due to the variation of the cross-section height along the span. Considering this variable section of the rib, the quotient "applying moments" vs "mechanical resistance" is more critical in a position about 5 m away from the center section, even though the section is class 4 and gets more instable

to the center section. The updated version *SAP2000 v15* “steel design/check” function, specifically used for the rib, can evaluate class 4 sections and confirms that the critical section is not the center section. On the other hand, the major shear forces occur at both ends of the rib.

To obtain the stresses due to DL, resisted only by the steel beam, a model with no stiffness for the concrete slab was used and the results are as presented in Figure 83 and Figure 84.

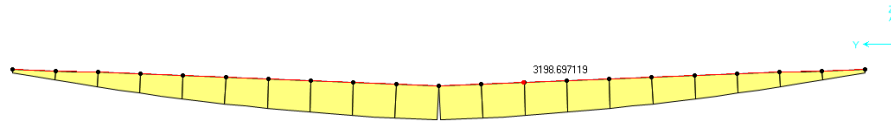


Figure 83 -  $M_{33}$  in rib's critical section for DL.  $M_{Ed}=3198\text{kN}$ .

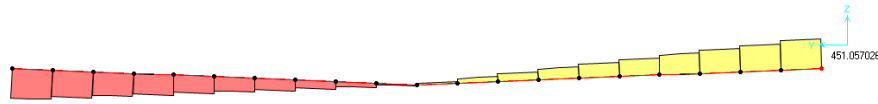


Figure 84 - Resultant  $V_{22}$  forces in rib for DL.  $V_{Ed}=451\text{kN}$ .

All other loads are applied on a composite beam slab model with the slab considered to be cracked. The live loads were transversely located close to the center of the rib, and results are showed in Figure 85 and Figure 86.

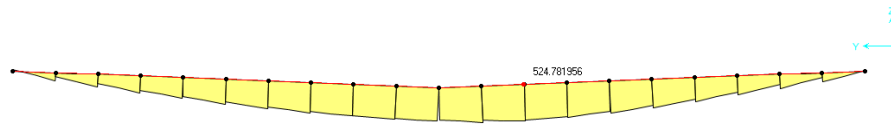


Figure 85 -  $M_{33}$  in rib's critical section for UDL(R1\_R).  $M_{Ed}=525\text{kNm}$ .

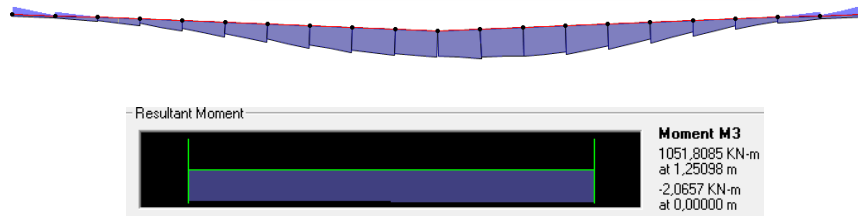


Figure 86 -  $M_{33}$  envelope in the rib for TS(R31\_2R).

When the composite behavior is activated, the axial forces on the steel beam correspond to tension, as expected.



Figure 87 – Resultant axial force in rib’s critical section for UDL(R1\_R).  $N_{Ed}=724\text{kN}$ .

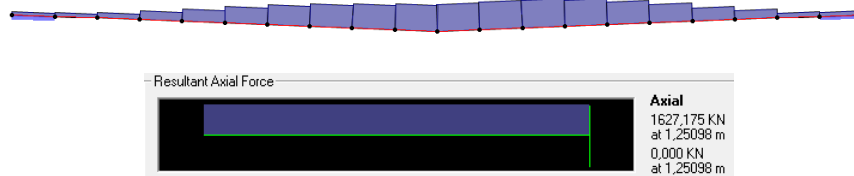


Figure 88 – Resultant axial force envelope in the rib for TS(R31\_2R).

The main resultant forces on the rib are summarized in Table 13.

**Table 13 - Ribs - Acting Forces and ULS**

	$M_{33}$	$M_{22}$	N	$V_{22}$	$V_{33}$	T	Slab Model
<b>DL</b>	3198		23	451			Unstiff
<b>SDL</b>	335		615	106			Normal
<b>UDL<sup>(1)</sup></b>	525	Not relevant	724	179	Not relevant	Not relevant	
<b>TS<sup>(2)</sup></b>	1052		1627	546			
<b>ULS<sup>(3)</sup></b>	6899		4035	1731			
	$M_{33}$ (kNm)			$N, V_{22}$ (kN)			

(1) UDL(R1\_R) was used for  $M_{33}$  and N, and UDL(1R\_R) for the  $V_{22}$ .

(2) TS(R31\_2R) was used for  $M_{33}$  and N, and TS(123R\_R) for the  $V_{22}$ .

(3)  $ULS = 1.35 \times (DL + SDL + UDL + TS)$

Wind, prestressing of the hangers and temperature gradients of the composite deck are assumed irrelevant for ULS security check. In terms of verification of the ULS, it was verified separately the normal stresses and the tangential stresses since the higher values do not occur in the same rib cross-section. Even when the rib has a composite behavior, the FEModel gives partial results for both the slab and the rib, so the rib security verifications from the given results are performed on the steel beam alone.

For the normal stresses, the analyzed section, close to the center section, is presented in Figure 89. Since section is from class 4, it is also presented the effective area of this cross-section, when the steel beam alone resists to the DL (Figure 90), and when the composite beam resists to SDL

and LL (Figure 91). For these last two loads, the top flange is assumed to be well connected and stabilized by the slab, so only the web is classified as class 4 there.

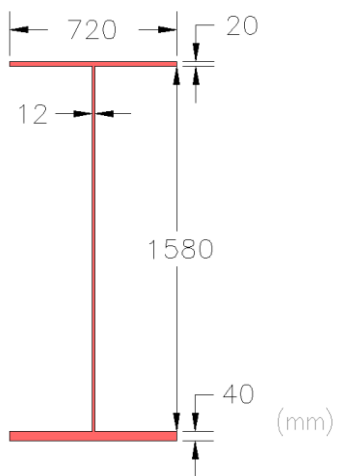


Figure 89 - Cross-section selected for the conditioning axial stresses.

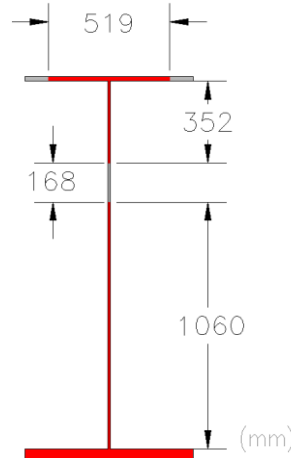


Figure 90 – Effective cross-section for DL axial stresses only.

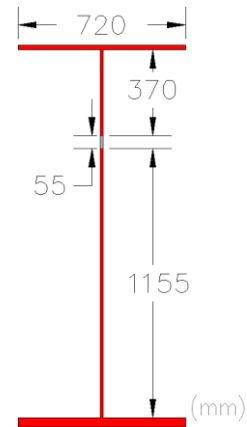


Figure 91 – Effective cross-section for SDL and LL axial stresses.

**Table 14 – Ribs – Cross-sections characteristics and ULS stresses**

Section of:	Figure 89	Figure 90	Figure 91	Units
<b>A</b>	0.0622	0.0561	0.0615	m <sup>2</sup>
<b>z<sub>g</sub> (from top)</b>	1.000	1.090	1.006	m
<b>I<sub>33</sub></b>	0.0298	0.0248	0.0296	m <sup>4</sup>
<b>W<sub>el 33,sup</sub></b>	0.0298	0.0228	0.0294	m <sup>3</sup>
<b>W<sub>el 33,inf</sub></b>	0.0466	0.0451	0.0467	m <sup>3</sup>
<b>N<sub>Ed</sub></b>	-	23	4012	kN
<b>M<sub>Ed 33</sub></b>	-	3198	3701	kNm
<b>σ<sub>sup</sub></b>	-	-140.1	-60.5	MPa
<b>σ<sub>inf</sub></b>	-	71.3	144.5	MPa
<b>f<sub>yd</sub></b>	355	355	355	MPa

The evaluation of the normal stresses from Table 14 present top and bottom stresses of 200.6 MPa and 215.8 MPa, lower than 355 MPa yielding limit.

As for the tangential stresses, verified at the end section of the rib (Figure 29), they are conservatively verified for the steel beam only. The maximum tangential stress, according to EN1993-1-1 6.2.6 is:

$$\tau_{Ed} = \frac{V_{Ed} \times S}{I_{33} \times t} = \frac{1731 \times 0.006763}{0.006064 \times 0.012} = 161 \text{ MPa} \leq 205 \text{ MPa} = \frac{355}{\sqrt{3} \times 1} = \frac{f_y}{\sqrt{3} \times \gamma_{M0}}$$

where:

$V_{Ed}$  – design value of the shear force

$I_{33}$  – moment of inertia of the cross section on the axis 3-3

$S$  – first moment of area about the centroid axis of that portion of the cross-section between the point at which the shear is required and the boundary of the cross-section

$t_{web}$  – web's thickness

As for the Serviceability Limit States, the Dead Loads were applied on the model with the concrete slab with no stiffness and the following loads on the stiff model, as the slab is already functioning when they apply (  $SLS = 1 \times (DL + OPL + HPP) + 0.4 \times UDL + 0.75 \times TS$  ).

**Table 15 - Ribs – SLS - Deflection**

	DL	SDL	UDL(R1_R)	TS(R32_1R)	Total
$\delta$ (m)	0.0399	0.0042	0.0025	0.0071	<b>0.0537</b>
Slab's stiffness	unstiff	normal	normal	normal	-

The conservative limit  $L/1000$  proposed in the European standard leads to a  $\delta_{max} = 0.0266$  m. A pragmatic and less conservative limit of  $L/500 = 0.0532$  m is virtually satisfied. The ribs should be constructed with a precamber deflection to withstand the dead loads, since for the remaining loads, the standard limit  $L/1000$  is satisfied. This way, the adopted constructive procedure, with no temporary rib supports, is perfectly possible.

## 4.4 Ties Analysis

Tie verifications must take into account the constructive procedure since all the steel weight of the structure and the concrete slab will firstly be supported only by the steel structure (i.e. ties, ribs, arch and hangers). To aid, some hangers must be stressed.

It is worth remembering that the model does not consider a continuous connection between the slab and the tie. This connection is only recognized where the ribs connect the tie, every 5 m. This

means that, for all vertical loads except Dead Loads, the portion of the weight that goes directly to the tie must be calculated manually to obtain the resultant local bending moment on the tie. This is only important on the bowstring bridge, where every 5 m the tie is supported by hangers. On the approach viaduct the concentrated loads every 5 m, due to the model deficiency, will have a similar effect as a distributed load. For the DL, due to the constructive procedure, all weight goes to the ribs.

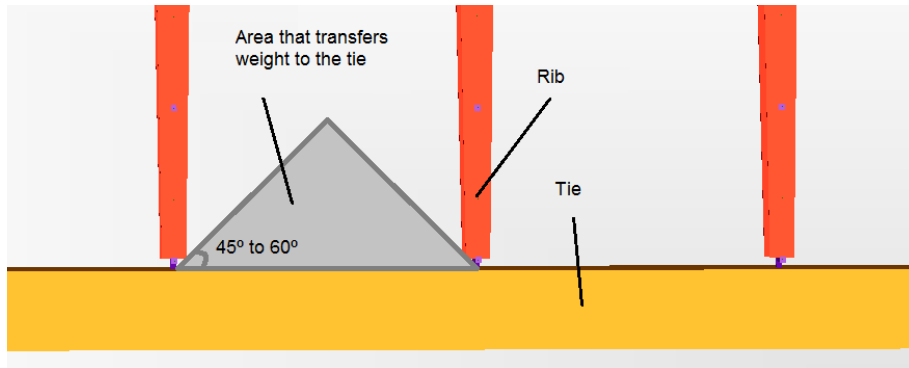


Figure 92 – Weight from vertical loads (except DL) being transferred directly to the tie.

The moments obtained for the 5 m span, for the SDL are approximately:

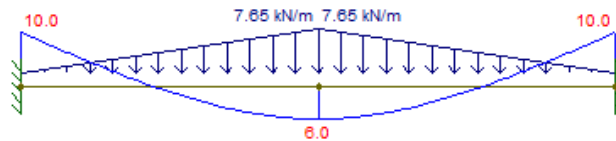


Figure 93 – SDL weight directly transferred to the tie.

The results are negligible when compared to the ones obtained from the loading coming from the ribs, so this procedure is not repeated for the live loads, which are at least 1 m away from the tie.

In the following figures, not only the tie is displayed but also the arch and hangers. Some of the following loads exhibit diagrams where some hangers are compressed for one of the loads, but when loads are considered together all hangers result in tension.

**Table 16 - DL - [non-stiff concrete slab]**

Tie Section	$N_{Ed}$	$V_{Ed\ 2-2}$	$M_{Ed\ 3-3}$	$V_{Ed\ 3-3}$	$M_{Ed\ 2-2}$	$T_{Ed}$
Center	17429	34	401.2	0	0	0
Corner	15130	494	1439	371	1149	1606
	$N_{Ed}, V_{Ed}$ (kN)		$M_{Ed}, T_{Ed}$ (kNm)			

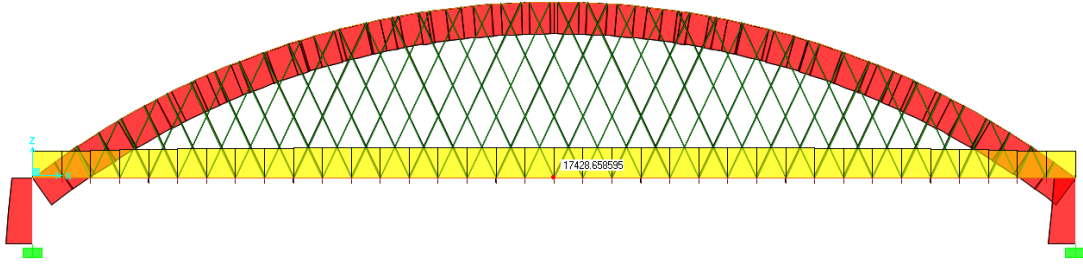


Figure 94 - Axial Force Diagram for all Dead Loads (concrete modeled without stiffness).

The global bending moment is outdone almost only by axial forces on the chords. This axial force could be initially estimated by the following approximate formula:

$$H = \frac{p \times l^2}{8 \times f}$$

This formula assumes an infinite axial rigidity, which turns to be a good approximation. For the total dead load ( $DL \approx 267.6 \text{ kN/m}$ ):

$$H(DL) = \frac{267.6 \times 180^2}{8 \times 30} = 36126 \text{ kN}$$

Which results in a  $36126/2 = 18063 \text{ kN}$  force in each tie.

The main bending moments are also displayed:

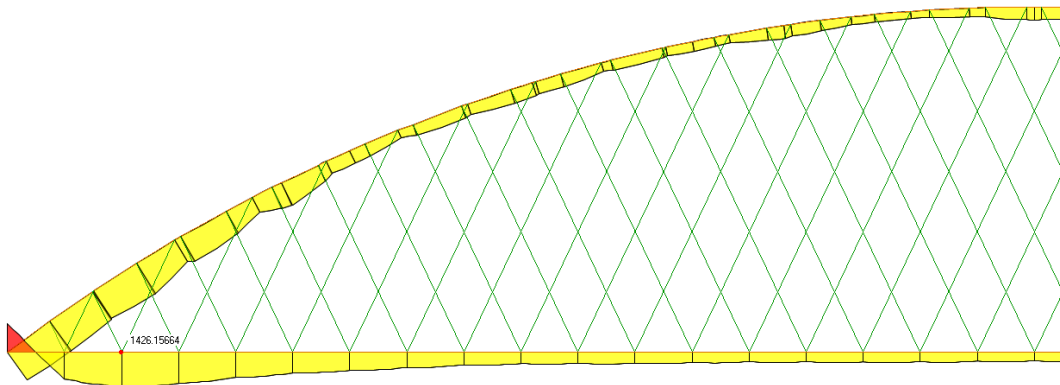


Figure 95-  $M_{3-3}$  diagram for DL (concrete modeled without stiffness).

The first observation of this diagram is that the bending moments are greater at the first few meters from the columns supports. This is a common behavior in tied arch bridges in general and



can be explained from the clamping that the arch offers to tie, restraining its bending rotation at the link between the two elements. In this zone, the hangers don't behave like a network yet, as, according to the definition, hangers don't cross each other at least twice, and the vertical distance between the arch and tie gets reduced rapidly, making the bending resistance of each chord more relevant here. This is one of the reasons *Per Tveit (2011)* recommends, as a possibility, to reduce the arch radius of curvature in this zone (other reasons are: more even axial forces and a shorter wind portal). Consequently, an improved hanger arrangement with this initial reduced curvature will be studied in Chapter 5, following *Per Tveit (2011)* advice:

*“A reduced radius of curvature near the ends of the arch can give less bending in the wind portal and a constant axial force in a longer portion of the arch.”*

Moreover, the slab and rib's weight, along with the fact that the rib's web and flanges are welded to the tie, induce a torsional request of the tie, which traduces in torsional stress if the tie is restrained to this rotation Figure 96.

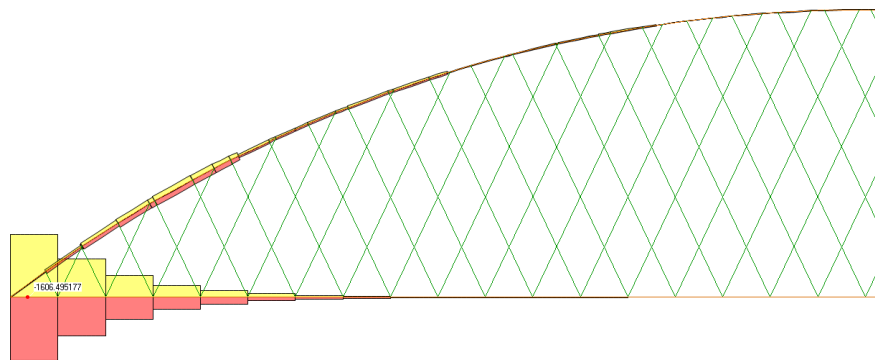


Figure 96 - Torsion diagram for all Dead Loads. Concrete modeled without stiffness.

From this torsional diagram, and knowing that the end-cross-girder, the arch and the tie are rigidly connected to each other, it is possible to confirm that at this section the tie is restrained to its torsional rotation.

For the following loads, the concrete slab is modeled with its cracked stiffness. Table 17 gives the tie efforts for the superimposed dead load (SDL), at mid span and link between the tie and the arch (corner).

**Table 17 - Ties - SDL**

Tie Section	$N_{Ed}$	$V_{Ed\ 2-2}$	$M_{Ed\ 3-3}$	$V_{Ed\ 3-3}$	$M_{Ed\ 2-2}$	$T_{Ed}$
Center	492	0	21	0	0	0
Corner	944	19	131	66	237	13
	$N_{Ed}, V_{Ed}$ (kN)		$M_{Ed}, T_{Ed}$ (kNm)			

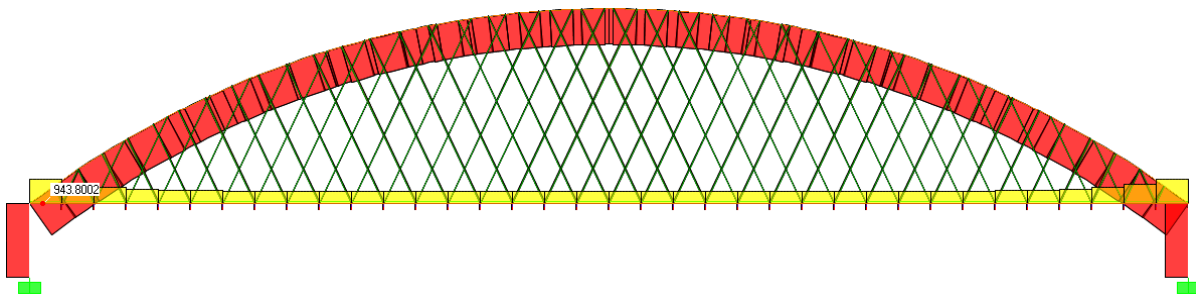


Figure 97 - Axial Force Diagram for SDL.

On this figure it can be understood the concrete contribution to the total deck axial force. This contribution increases to the center of the bridge as the interaction between the two materials is mobilized. Therefore, the axial prompt of the tie, at the center of the bridge, is reduced. This is also valid for the live loads.

The UDL were located transversely unsymmetrical (1R\_R) to request more one of the ties. It is interesting to note the bending moment distribution, whether the UDL is applied to all length of the bridge, or just half of it (Figure 98 and Figure 99).

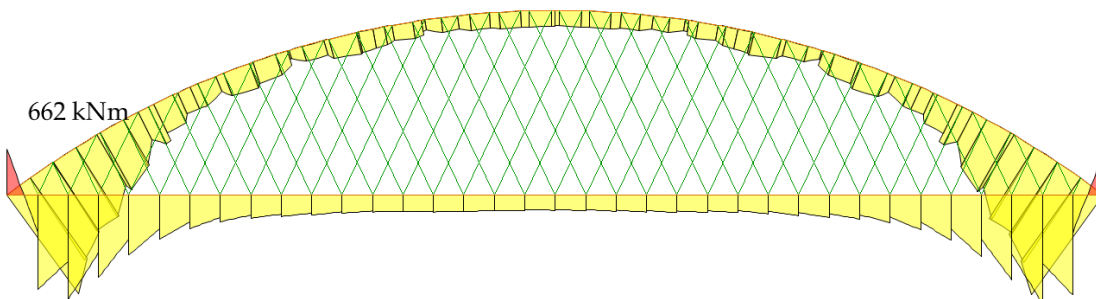


Figure 98 -  $M_{3-3}$  diagram on the most requested tie, for UDL(1R\_R)-All.

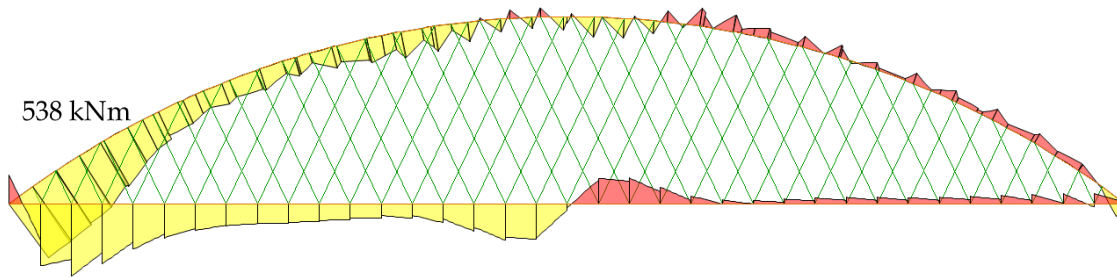


Figure 99 -  $M_{3-3}$  diagram on the most requested tie, for UDL(1R\_R)-Half.

The maximum values of  $M_{3-3}$  were obtained when the UDL acts in the entire bridge length. In fact, the only verification that seems more demanding by the UDL-Half, is the one regarding the hangers' relaxation.

When the 3 vehicles of the TS travel along the bridge, with the most unfavorable configuration – (123R\_R), the following envelope diagram is obtained:

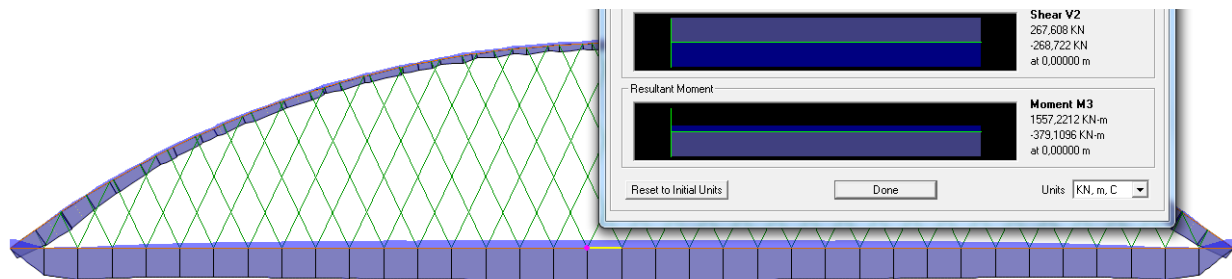


Figure 100 -  $M_{3-3}$  envelope for the TS(123R\_R) on the more loaded tie.

The UDL + TS resultant forces are resumed below:

**Table 18 – Ties - UDL(1R\_R) + TS(123R\_R)**

Tie Section	$N_{Ed}$	$V_{Ed\ 2-2}$	$M_{Ed\ 3-3}$	$V_{Ed\ 3-3}$	$M_{Ed\ 2-2}$	$T_{Ed}$
Center	2738	270	1644	75	216	466
Corner	4496	449	2100	326	1188	575
	$N_{Ed}, V_{Ed}$ (kN)		$M_{Ed}, T_{Ed}$ (kNm)			

The hanger pre-stress phase that presents interest to the verifications it's the 2<sup>nd</sup> one (the permanent one, according with the hanger's sub-chapter). The resultant bending moments on the tie, from these prestressed hangers are displayed in Table 19.

**Table 19 – Ties – HPP2**

Section	$N_{Ed}$	$V_{Ed\ 2-2}$	$M_{Ed\ 3-3}$	$V_{Ed\ 3-3}$	$M_{Ed\ 2-2}$	$T_{Ed}$
Center of Bridge	0	0	0	0	0	0
Corner of Bridge	717	-542	-1600	107	330	-36
$N_{Ed}, V_{Ed}$ (kN)			$M_{Ed}, T_{Ed}$ (kNm)			

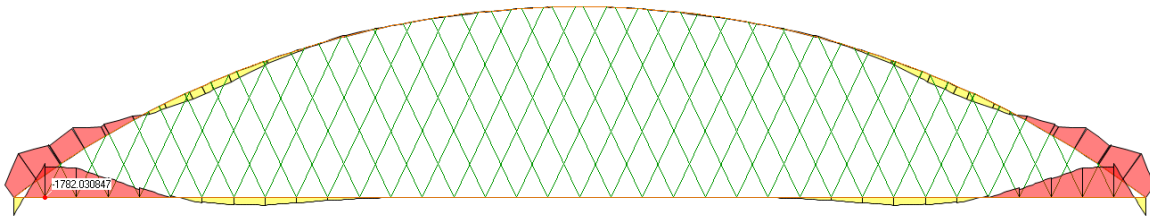


Figure 101 –  $M_{3-3}$  due to HPP2.

The wind effects on the bowstring bridge are presented in Table 20 and Figure 102 to Figure 105.

**Table 20 – Ties – Wind Action**

Tie Section	$N_{Ed}$	$V_{Ed\ 2-2}$	$M_{Ed\ 3-3}$	$V_{Ed\ 3-3}$	$M_{Ed\ 2-2}$	$T_{Ed}$
Center	1345	0	0	0	0	0
Corner	1485	0	0	765	3130	569
$N_{Ed}, V_{Ed}$ (kN)			$M_{Ed}, T_{Ed}$ (kNm)			

The most relevant results are the axial force and the  $M_{2-2}$  bending moments, when wind blows from North to South.

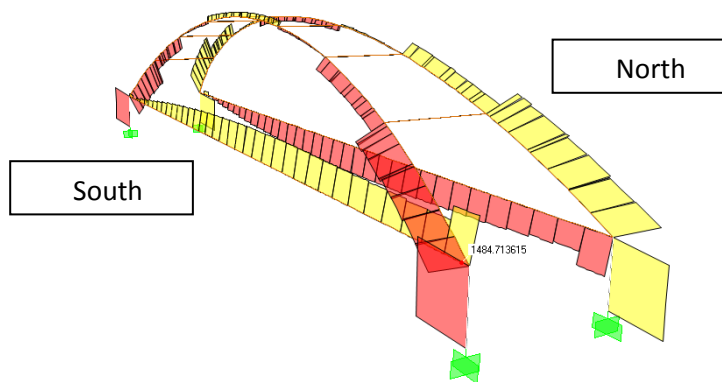


Figure 102 - Axial force under wind load.

There are 3 interesting effects that need to be explained to well understand this axial force diagram for wind loading:

1. Corners once again suffer from the effect of the non-mobilization of axial force by the slab.
2. The arches tendency to deform. The North arch is tensioned, making its correspondent tie compressed (Figure 103). Vice-versa for the south arch. The solidarity of displacements between the two arches is achieved through the bracing beams, which, distribute axial forces between arches.

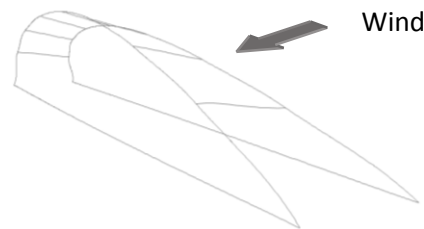


Figure 103 - Deformed shape when wind is applied.

3. Due to the external support conditions of the bridge deck and high bending inertia of the columns, from a top view, the bridge would have a tendency to deform like the following beam:



Figure 104 - Top view of the bridge's approximately deformed shape, when wind is applied.

At the left side of the bridge, the 2 corners of the ties have very low forces because the 3<sup>rd</sup> effect counter acts against the 2<sup>nd</sup> effect. At the mid-span, both 3<sup>rd</sup> and 2<sup>nd</sup> effects act together and therefore are summed. At the right corner, the 3<sup>rd</sup> effect disappears, the 2<sup>nd</sup> effect maintains and the 1<sup>st</sup> effect shows up.

The in-plane bending moment  $M_{2-2}$  is shown in Figure 105, revealing the importance of the bracing system to control these arch lateral moments.

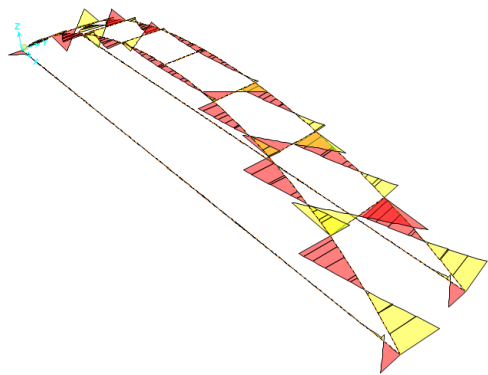


Figure 105 – In-plane bending moments  $M_{2-2}$  on the arches, when acting wind force.

As for the uniform temperature gradient, if the bridge deck was made of a single material, no stresses would occur since the structure is externally isostatic. A simple 2D model on *Ftool*, from Figure 106, confirms this assumption.

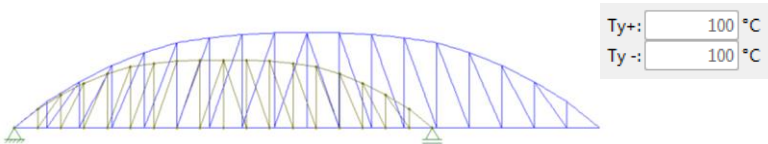


Figure 106 – Deformation of a 2D model created on *Ftool* software, subjected to positive uniform temperature (no stresses).

However, the deck is composite, using concrete and steel, and the arch and hangers are made of steel only. According to the *EN1991*, and as described in section 3.1.4 of this document, the correspondent temperatures are applied on the model, producing internal stress distributions of Figure 107.

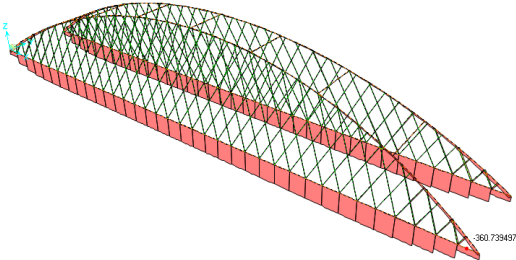


Figure 107 – Axial forces. Positive uniform temperature variation (Deck: 29°C ; Arch and hangers: 41°C).

When the arch wants to expand more than the deck, it tensions the deck and, in return, gets compressed. Although there are some tensile forces occurring at the corners of the ties, the final force there is still of compression. This compression occurs because the slab, with a smaller thermal expansion coefficient, will prevent the ties from expanding freely, and in turn, gets tensioned by them (remember Figure 78). The opposite stresses are registered for the negative temperature gradients.

These temperature gradients are occurring from season to season. For this reason the concrete creep plays an important role in reducing the resultant forces, as the elasticity modulus could be even more reduced. To stay on the conservative side, and as the concrete's stiffness was already modeled as cracked, the concrete creep wasn't taken into account for the tie verification. The negative uniform temperature variation will be the one who adds more severe efforts to the effects from previous described actions, being therefore given in Table 21.

**Table 21 – Ties - Negative Uniform Temperature Gradient**

Tie Section	$N_{Ed}$	$V_{Ed\ 2-2}$	$M_{Ed\ 3-3}$	$V_{Ed\ 3-3}$	$M_{Ed\ 2-2}$	$T_{Ed}$
Center	1050	0	40	0	0	0
Corner	285	30	170	-144	500	-38
	$N_{Ed}, V_{Ed}$ (kN)			$M_{Ed}, T_{Ed}$ (kNm)		

Using all the efforts from the different actions the ULS combination is resumed in Table 22.

**Table 22 – Ties – Forces in the ULS**

<b>ULS = 1,35 × (DL + SDL + UDL + TS) + 1,0 × HS2 + 0,6 × 1,5 × Wind + 0,6 × 1,5 × Temperature</b>						
Tie Section	$N_{Ed}$	$V_{Ed\ 2-2}$	$M_{Ed\ 3-3}$	$V_{Ed\ 3-3}$	$M_{Ed\ 2-2}$	$T_{Ed}$
Center	31552	410	2885	101	292	629
Corner	32956	838	3944	1892	7783	3550
	$N_{Ed}, V_{Ed}$ (kN)			$M_{Ed}, T_{Ed}$ (kNm)		

The section of the corner of the bridge is the most demanding one for the ULS verification, being presented for this section the normal and tangential stresses at ULS.

**Table 23 – Ties – Corner Cross-Section Elastic Verification**

Stress	$N_{Ed}$	$V_{Ed\ 2-2}$	$M_{Ed\ 3-3}$	$V_{Ed\ 3-3}$	$M_{Ed\ 2-2}$	$T_{Ed}$	Total	Limit
$\sigma_{x,Ed}$ (MPa)	203.2	-	57.7	-	131.1	-	392.0	420
$\tau_{Ed}$ (MPa)	-	7.5	-	18.0	-	33.2	58.7	242
Elastic interaction of tangential and normal stresses							0.930	≤ 1.0

## Chapter 4. Structural Analysis

Note that the tangential stresses have little importance even when they sum the effects of the obtained torsional moments. Therefore they are evaluated using the simplification of a tie section as a bi-symmetrical rectangular tube, as illustrated in Figure 108.

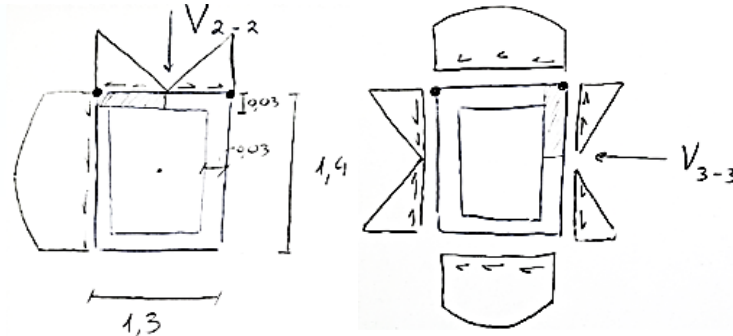


Figure 108 – Ties tangential stress distributions.

The interaction between tangential and longitudinal stresses is made according to Von-Mises criterion presented in *EN1993-1-1 6.2.1 (5)*, and proves that ULS of resistance of the tie is verified.

$$\left(\frac{\sigma_{x,Ed}}{f_y/\gamma_{M0}}\right)^2 + 3 \times \left(\frac{\tau_{Ed}}{f_y/\gamma_{M0}}\right)^2 = \left(\frac{392.0}{420}\right)^2 + 3 \times \left(\frac{58.7}{420}\right)^2 = 0.930 \leq 1.0$$

As for the service limit state (SLS), by controlling deflection, vibration is indirectly controlled as well. The conservative limit defined in the European standard is considered  $L/1000$ , where  $L$  is the span in (m). A frequent SLS combination is used for the deflection verification:

$$\text{SLS} = 1 \times (\text{DL} + \text{OPL} + \text{HPP}) + 0.4 \times \text{UDL} + 0.75 \times \text{TS} + 0.5 \times \text{Temperature}$$

To evaluate the real deflection due to hangers' prestress, attending to the construction procedures and to both models created, one with unstiff concrete, another with stiff concrete, the following evaluation must be done:

$$\delta_{\text{HPP(Total)}} = \text{HPP1 (unstiff concrete)} + [\text{HPP2 (stiff concrete)} - \text{HPP1 (stiff concrete)}]$$

The live load combination more demanding for the ties deformation is naturally the “UDL-All + TS(123R\_R)”. Deflection for each load action and a combined value are presented in Table 24.



**Table 24 - Service Limit State - Deflection**

Load	$\delta$ (m)	Model Used
DL	0.0696	Unstiff Slab Model
SDL	0.0108	Stiff Slab Model
HPP1 <sub>(partial)</sub>	0.0025	Unstiff Slab Model
HPP1 <sub>(partial)</sub>	0.0022	Stiff Slab Model
HPP2 <sub>(partial)</sub>	0.0038	Stiff Slab Model
HPP <sub>(total)</sub>	0.0041	-
UDL(1R_R)	0.0453	Stiff Slab Model
TS(123R_R)	0.0155	Stiff Slab Model
Temperature	0.02	Stiff Slab Model

$$\delta_{total} = 0.0696 + 0.01080 + 0.0041 + 0.4 \times 0.0453 + 0.75 \times 0.0155 + 0.5 \times 0.02 = 0.1243 \text{ m}$$

$$\frac{L}{1000} = \frac{180\text{m}}{1000} = 0.18\text{m} \geq 0.124\text{m}$$

The deflection estimated, and therefore the vibration, are verified within the limits of the Service Limit State, even without considering the need of a ties precamber which can easily be used.

## 4.5 Arches Analysis

From all the results presented for the tie it is also possible to see the arch axial forces and moments, and it is possible to foresee that the determinant cross-section will be somewhere close to the beginning of the arch. Therefore, only this part of the arch is verified, with, again, the conservative approach of considering the highest bending moments and axial forces in the first few meters of the arch, occurring in the same cross-section. The main forces acting in the arch for the DL are resumed in Table 25.

**Table 25 – Arch - DL- [non-stiff concrete slab]**

N <sub>Ed</sub>	V <sub>Ed 2-2</sub>	M <sub>Ed 3-3</sub>	V <sub>Ed 3-3</sub>	M <sub>Ed 2-2</sub>	T <sub>Ed</sub>
-18948	-143	1514	151	1352	125
N <sub>ed</sub> , V <sub>ed</sub> (kN)			M <sub>ed</sub> , T <sub>ed</sub> (kNm)		

## Chapter 4. Structural Analysis

The following Figure 109 confirms again that the arch constrains the tie to torsional rotation and the end-cross-girder to flexion. It's also visible the bracing beams function on holding the arches. These two effects result in an in-plane distribution of bending moments for the DL of Figure 109.

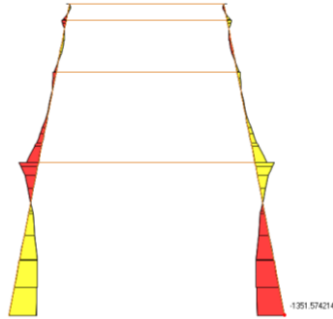


Figure 109 – In-plane bending moment  $M_{2-2}$  diagram for Dead Loads. View of both arches and bracing beams.

As in the other structural elements' verifications, the following loads were obtained in a model, considering the concrete slab as being cracked, namely SDL (Table 26), hangers stress (Table 27), live loads (Table 28), wind action (Table 29) and temperature gradients (Table 30).

**Table 26 – Arch - SDL**

$N_{Ed}$	$V_{Ed\ 2-2}$	$M_{Ed\ 3-3}$	$V_{Ed\ 3-3}$	$M_{Ed\ 2-2}$	$T_{Ed}$
-4750	-49	525	22	145	72
$N_{Ed}, V_{Ed}$ (kN)			$M_{Ed}, T_{Ed}$ (kNm)		

**Table 27 – Arch - HPP2**

$N_{Ed}$	$V_{Ed\ 2-2}$	$M_{Ed\ 3-3}$	$V_{Ed\ 3-3}$	$M_{Ed\ 2-2}$	$T_{Ed}$
-1288	-116	-1728	-59	183	60
$N_{Ed}, V_{Ed}$ (kN)			$M_{Ed}, T_{Ed}$ (kNm)		

**Table 28 – Arch - UDL-All + TS(123R\_R)**

$N_{Ed}$	$V_{Ed\ 2-2}$	$M_{Ed\ 3-3}$	$V_{Ed\ 3-3}$	$M_{Ed\ 2-2}$	$T_{Ed}$
-7736	-153	1452	45	843	300
$N_{Ed}, V_{Ed}$ (kN)			$M_{Ed}, T_{Ed}$ (kNm)		

**Table 29 – Arch - Wind**

N <sub>Ed</sub>	V <sub>Ed 2-2</sub>	M <sub>Ed 3-3</sub>	V <sub>Ed 3-3</sub>	M <sub>Ed 2-2</sub>	T <sub>Ed</sub>
-1153	114	1329	443	5987	676
N <sub>Ed</sub> , V <sub>Ed</sub> (kN)			M <sub>Ed</sub> , T <sub>Ed</sub> (kNm)		

**Table 30 – Arch - Positive Uniform Temperature Gradient**

N <sub>Ed</sub>	V <sub>Ed 2-2</sub>	M <sub>Ed 3-3</sub>	V <sub>Ed 3-3</sub>	M <sub>Ed 2-2</sub>	T <sub>Ed</sub>
-183	-77	305	-17	283	58
N <sub>Ed</sub> , V <sub>Ed</sub> (kN)			M <sub>Ed</sub> , T <sub>Ed</sub> (kNm)		

The Ultimate Limit State that is the most conditioning is the same as the tie. Effort results of ULS and stresses are presented in Table 31 and Table 32.

**Table 31 – Arch – Forces in the ULS**

<b>ULS = 1,35 × (DL + SDL + UDL + TS) + 1,0 × HS2 + 0,6 × 1,5 × Wind + 0,6 × 1,5 × Temperature</b>					
N <sub>Ed</sub>	V <sub>Ed 2-2</sub>	M <sub>Ed 3-3</sub>	V <sub>Ed 3-3</sub>	M <sub>Ed 2-2</sub>	T <sub>Ed</sub>
-44926	-548	4455	619	8985	1392
N <sub>Ed</sub> , V <sub>Ed</sub> (kN)			M <sub>Ed</sub> , T <sub>Ed</sub> (kNm)		

**Table 32 – Arch - Corner Cross Section Elastic Verification**

Stress	N <sub>Ed</sub>	V <sub>Ed 2-2</sub>	M <sub>Ed 3-3</sub>	V <sub>Ed 3-3</sub>	M <sub>Ed 2-2</sub>	T <sub>Ed</sub>	Total	Limit
σ <sub>x,Ed</sub> (MPa)	-220.6	-	52.0	-	132.6	-	405.1	420
τ <sub>Ed</sub> (MPa)	-	-3.8		5.2		11.0	20.1	242
Elastic interaction of tangential and normal stresses							0.937	≤ 1.0

However the buckling analysis should also be performed, as described in Chapter 5. Using the result of  $\chi = 0.790$  from Chapter 5, the design buckling resistance result is obtained by:

$$N_{b,Rd} = \frac{\chi \times A \times f_y}{1.0} = 0.790 \times 85554 = 67588 \text{ kN} \geq N_{ed} = 44926 \text{ kN}$$

As the arch section has a box shape, it is not susceptible to torsional deformations. The interaction factors are therefore calculated making use of the *Table B.1* of the *EN1993-1-1*.

While the instability occurs with an out-of-plane movement for the all observed buckling modes (first 30 modes observed for: i) load in all span and ii) load in half span), in-plane movements are simultaneously visible in every single buckling mode, since the arches are inclined at 79° and

cannot buckle outwards without some vertical movement. Therefore instability in both axis of the arch cannot be easily separated, and thus using a conservative approach,  $\lambda_y$  is assumed to be equal to  $\lambda_z$ , and both values  $\chi_y$  and  $\chi_z$  are equal too.

The estimative of the values of  $C_{m_y}$  and  $C_{m_z}$  are based on the main bending moment diagrams outline and clearly presented in Figure 110.

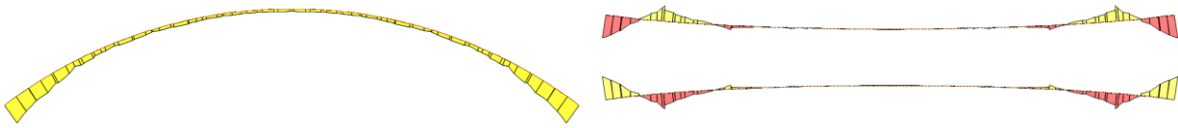


Figure 110 – Bending moments  $M_{3-3}$  (on the left) and  $M_{2-2}$  (on the right) of the arch when applied a vertical uniform load over the entire span (conditioning load distribution, from Chapter 5).

For  $C_{m_z}$ , the variation of the  $M_{2-2}$  is much more accentuated then for  $M_{3-3}$ . Conservatively, the factors are according with Table 33.

**Table 33 – Arch - Moment, Reduction and Interaction Factors, according to EN1993-1-1 6.3**

$\Psi (C_{m_y})$	$\Psi (C_{m_z})$	$C_{m_y}$	$C_{m_z}$	$\bar{\lambda}_y$	$\bar{\lambda}_z$	$\chi_y$	$\chi_z$	$\chi_{LT}$	$K_{yy}$	$K_{zy}$	$K_{zz}$	$K_{yz}$
0.5	-0.5	0.8	0.4	0.811	0.811	0.790	0.790	1.0	1.059	0.847	0.529	0.529

The final verification according to the EN1993 6.3.3 (4), should be performed using equations (6a) and (6b). Both equations verify the condition  $\leq 1$  (eq. (6c) and (6d)) and therefore the safety conditions are verified.

$$\frac{N_{Ed}}{\frac{X_y \times N_{Rk}}{\gamma_{M1}}} + k_{yy} \times \frac{M_{y,Ed} + \Delta M_{y,Ed}}{X_{LT} \times \frac{M_{y,Rk}}{\gamma_{M1}}} + k_{yz} \times \frac{M_{z,Ed} + \Delta M_{z,Ed}}{\frac{M_{z,Rk}}{\gamma_{M1}}} \leq 1 \quad (6a)$$

$$\frac{N_{Ed}}{\frac{X_z \times N_{Rk}}{\gamma_{M1}}} + k_{zy} \times \frac{M_{y,Ed} + \Delta M_{y,Ed}}{X_{LT} \times \frac{M_{y,Rk}}{\gamma_{M1}}} + k_{zz} \times \frac{M_{z,Ed} + \Delta M_{z,Ed}}{\frac{M_{z,Rk}}{\gamma_{M1}}} \leq 1 \quad (6b)$$

$$\frac{44926}{0.790 \times 85554} + 1.059 \times \frac{4455}{36000} + 0.529 \times \frac{8985}{28462} = 0.963 \leq 1.0 \quad (6c)$$

$$\frac{44926}{0.790 \times 85554} + 0.847 \times \frac{4455}{36000} + 0.529 \times \frac{8985}{28462} = 0.937 \leq 1.0 \quad (6d)$$

## 4.6 Hangers Analysis

To verify the hanger's safety, several analyses must be made:

1. Hangers' axial force in the ULS, limited to 84.5%<sup>(\*)</sup> of the ultimate resistance.
2. Hangers' characteristic axial force, limited to 50% of the ultimate resistance.
3. Relaxation of hangers, for any position of the variable loads and during the construction stages.
4. Fatigue analysis for SLS conditions.

First, on the relaxation issue, and taking into consideration the constructive procedure, the hangers will support different loads, during the different construction stages and in service Table 34.

**Table 34 - Hangers' Supported Loads**

In service	Supported Load
1	DL (Steel)
2	DL (Steel + Concrete)
3	DL + SDL
4	DL + SDL + Live Loads

To prevent the hangers to relax during these stages, some hangers must be prestressed and it must be studied i) when the prestress should be applied, and ii) the prestress needed at each stage.

For this study, some assumptions are made:

- Concrete's variable stiffness along its life cycle won't affect significantly the installed hanger forces;
- Time effects like steel relaxation in the hangers won't be considered.

Firstly, an influence matrix was built which shows what happens to the first 8 hangers, when each one of those hangers is prestressed separately. It was not found necessary that the matrix contemplated all hangers.

<sup>(\*)</sup>Tension Rod Type 860, S460N, 80mm diameter,  $N_{R,d} = 1953,8$  kN, according to EC3, from PFEIFER Cable Structures.

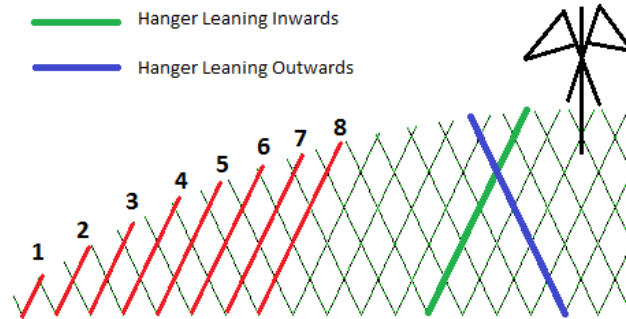


Figure 111- Hanger's numeration.

With this numeration and making use of symmetry of the bridge, there will be for example 4 hangers with number 1, two in each arch. "H1" will be the notation for hanger number 1.

These 8 hangers were chosen for the influence matrix because they will be the ones who tend more to get into compression due to permanent loads. In fact, the dead loads produce important compressions in the first few hangers leaning inwards. This is because, in this zone, the hangers don't cross each other twice and they do not behave like a network. They do, instead, work very much like a truss beam. A simple truss beam model illustrates the similarities between Figure 111 and Figure 112.

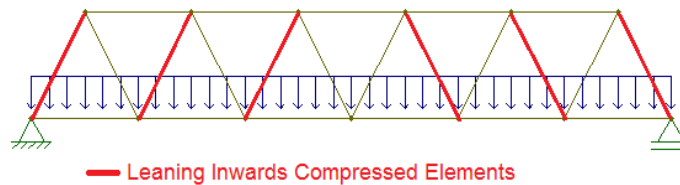


Figure 112 – Model of a truss beam (the leaning inwards diagonals are compressed).

As in the truss beam, these leaning inwards hangers, the closer they are to the end of the arch, the more compressed they tend to be for the dead loads. To prevent hanger's compression, tension stress is applied to them, making all the immediate adjacent hangers, leaning inwards and outwards, compress. Fortunately, the hangers leaning outwards are naturally very loaded in tension from the dead loads. The force distribution in the hangers for Steel Dead Loads is presented in Figure 113. Except for the variable loads, only half of the hangers of one of the arches are shown because double symmetry is valid.

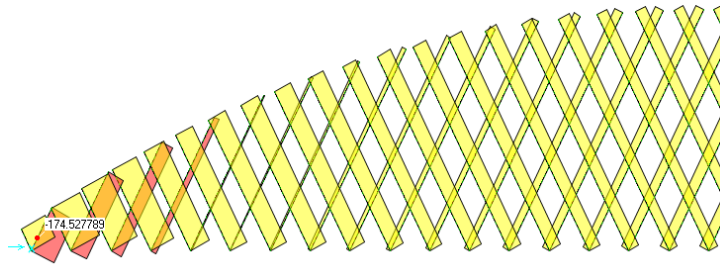


Figure 113 - Hangers axial force due to Steel DL.

Prestress of the hangers can be modeled in *SAP2000* as a negative temperature variation, a deformation or a strain. Strains were used. The referred influence matrix is presented, both for an unstiff concrete model and for the normal cracked stiffness concrete model in Table 35 and Table 36.

**Table 35 – Hangers Influence Matrix [kN] – [No concrete slab on the model]**

		Applying -0.0001 strain to:							
		H1	H2	H3	H4	H5	H6	H7	H8
Reaction:	H1	84.4	-15.10	-4.4	-0.1	0.6	0.2	-0.1	-0.2
	H2	-8.3	74.8	-22.3	-8.1	-0.8	1	0.7	0.1
	H3	-1.7	-16.1	70.7	-25.2	-10.1	-1.4	1.4	1.2
	H4	0	-4.7	-20.4	69.8	-25.9	-11.2	-2	1.6
	H5	0.2	-0.4	-7.1	-22.3	70.2	-25.8	-11.8	-2.6
	H6	0	0.5	-0.8	-8.6	-23.1	71	-25.5	-12.3
	H7	0	0.3	0.8	-1.4	-9.7	-23.4	71.8	-25.1
	H8	0	0	0.6	1	-2	-10.5	-23.5	72.4

**Table 36 – Hangers Influence Matrix [kN] – [Cracked stiffness concrete]**

		Applying -0.0001 strain to:							
		H1	H2	H3	H4	H5	H6	H7	H8
Reaction:	H1	85.2	-14.20	-4.2	-0.2	0.5	0.1	-0.1	-0.2
	H2	-7.8	76.3	-21.2	-7.9	-1	0.8	0.6	0.1
	H3	-1.7	-15.4	72.1	-24.4	-10.1	-1.7	1.1	1.1
	H4	0	-4.7	-19.7	71	-25.3	-11.3	-2.3	1.3
	H5	0.1	-0.5	-7.1	-21.8	71.1	-25.3	-11.9	-2.9
	H6	0	0.4	-1.1	-8.7	-22.6	71.8	-25	-12.3
	H7	0	0.2	0.7	-1.6	-9.8	-23	72.5	-24.7
	H8	0	0	0.6	0.8	-2.3	-10.6	-23.1	73.1

The minor difference between matrix values proves that the slab stiffness influence on the hangers' behavior is not important.

The diagonal of the matrix has naturally the highest positive values and the adjacent hangers of the tensioned hanger are always compressed. As the sum of the forces on each column is positive (the tension of a hanger is not only balanced by other leaning inwards adjacent hangers compression, but also by other elements deformation, like the bending of the arch or the compression of the leaning outwards hangers) it is always possible to find a combination that solves the relaxation problem for these 8 hangers. At the end of this process it's necessary to evaluate if the leaning outwards' hangers are still all in tension.

With this influence matrix, one can find the right prestress to apply to verify relaxation for the different constructive stages, on these 8 hangers. However it is important to define a combination of prestress that verifies relaxation for a large number of construction stages simultaneously, avoiding numerous prestress procedures during construction. Successfully, the Hanger Prestress Phase number 1 (HPP1) verifies simultaneously three constructive stages (CS):

**CS1** - DL (Steel) - in a model without the concrete slab.

**CS2** - DL - both steel and concrete – in a model with an unstiff concrete slab.

**CS3** - DL + SDL - both verified, as a (good) approximation, in the normal cracked stiffness model.

Using the first influence matrix (model without the concrete slab), the first 2 referred situations are checked. In other words, the minimum ( $N_{min}$ ) axial force on each hanger, during these 2 stages of construction, remains positive, although very low, according with Table 37 results.

**Table 37 - Hangers Prestress Phase 1**

	$\epsilon$ (Strain)	Prestress (kN)	$N_{Ed}$ (CS1) (kN)	$N_{Ed}$ (CS2) (kN)	$N_{min}$ (kN)
H1	-0.000680	482.1	-175	-408	74.1
H2	-0.000500	202.2	-116	-195	7.2
H3	-0.000399	82.0	-81	-60	1.0
H4	-0.000330	44.0	-42	38	2.0
H5	-0.000240	13.2	-10	106	3.2
H6	-0.000160	2.4	1	137	3.4
H7	-0.000090	-3.6	5	157	1.4
H8	-0.000030	-15.3	16	177	0.7



The column “ε (Strain)” was obtained iteratively on *Excel* until all  $N_{min}$  resulted in tension and represents the actual strain (prestress) that is applied in the HPP1.

The column “Prestress” represents the resultant forces on the hangers from the prestress combination defined in the column “ε (Strain)”. It is automatically filled, from the referred interaction matrix and from the strain applied. For example, the value 482.1 kN in the H1 is obtained by:

$$\sum \left[ \frac{\varepsilon(Hi) \times M_{1i}}{-0.0001} \right] = \frac{-0.000680}{-0.0001} \times 84.4 + \frac{-0.000500}{-0.0001} \times (-15.1) + \frac{-0.000399}{-0.0001} \times (-4.4) + \dots = 482.1 \text{ kN}$$

$\varepsilon(Hi)$  – Strain applied on hanger i.

$M_{ij}$  - terms of the influence matrix.

“-0.0001” – standard strain, applied to obtain the influence matrix.

For the CS3 action, the second influence matrix was used. Iterating an equal “ε (Strain)” in both matrixes, the 3 construction stages were possible to verify, resulting in HPP1. The CS3 relaxation-free check is shown:

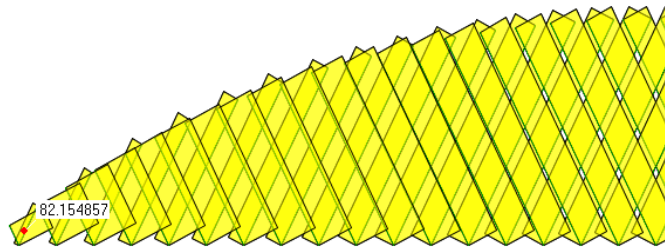


Figure 114 – Axial forces on the hangers, for “DL+SDL”. Cracked concrete stiffness (approximation).

Next, there is one last complex load case to be used to verify hangers – the live loads. For this reason, a new prestress phase must be introduced - HPP2 – to withstand these new stresses. This HPP2 must verify relaxation simultaneously for:

**CS3** - DL+SDL (permanent in-service situation)

**CS4** - DL+SDL+LL (extreme in-service situation)

Once more the small importance of the variable stiffness of the concrete slab, from construction, is neglected. Thus, using the influence matrix of the normal cracked stiffness concrete model, the HPP2 is obtained by Table 38.

**Table 38 - Hangers Prestress Phase 2**

	ε (Strain)	Prestress (kN)	N <sub>Ed</sub> (CS3) (kN)	N <sub>Ed</sub> (CS4) (kN)	N <sub>min</sub> (kN)
H1	-0.00130	932.9	-411	Variable with the LL	521.9
H2	-0.00100	442.8	-105		337.8
H3	-0.00080	211.6	56		267.6
H4	-0.00060	95.3	153		248.3
H5	-0.00040	30.6	212		242.6
H6	-0.00020	-28.8	233		204.2
H7	-0.00010	-14.7	247		232.3
H8	-0.00003	-43.9	262		218.1

The “ε (Strain)” is the total strain to be applied, and not the increment from phase 1. For the CS3, permanent in-service conditions, all hangers are tensioned. As for the CS4, N<sub>Ed</sub> has different values for different loads, different load distributions and different load combinations. In this study, the axial force diagrams will be presented for two different combinations of loads.

Logically also to get the most demanding load situation for the hangers, all live loads distributions applied are the ones transversely closer to the tie.

The first combination to verify relaxation is:

$$N_{Ed} = DL + SDL + HPP2 + 1.35 \times [UDL(Half) + TS(123R_R)]$$

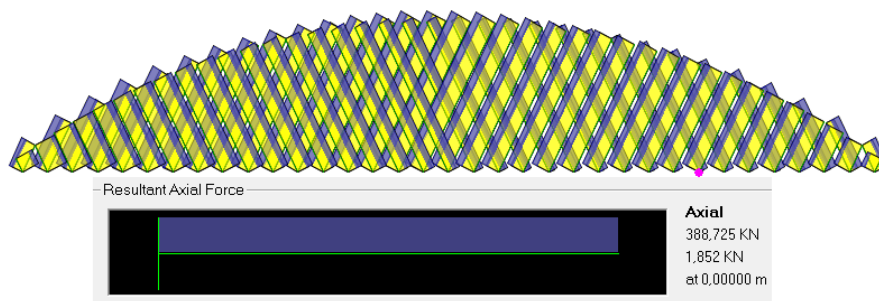


Figure 115 - Hanger forces for “DL + SDL + HPP2 + 1.35\*[UDL(Half) + TS(123R\_R)]”. Traction forces only. Detail of the 8<sup>th</sup> leaning inwards hanger, counting from the right.

**Note:** According to *Per Tveit(2011)*, the relaxation is a verification that has no tragic consequences for most cases, especially if unverified by small values of compression. *Per Tveit* even declares that nowadays, making good use of the recent software’s available and nonlinear analysis, some arch bridges are calculated with some relaxed hangers, with no particular consequences. Despite these considerations, the adopted slope verifies no relaxation occurs even for scaled live loads.

The yellow color represents tension force. The blue/purple color represents the force variation from the TS envelope. These results of near relaxation indicate that the pre-design of the hanger's slope is correct and accurate. For the combination with the UDL applied in the entire span, as expected, no relaxations occur.

The other ultimate limit states of the hangers will now be assessed. Since it is not easy to predict which one will be the conditioning hanger, the stresses from the different loads are again combined and scaled directly in *SAP2000*. The first ULS combination is:

$$ULS_1 = 1.35 \times [DL + SDL + UDL(Half) + TS(123R_R)] + HPP2$$

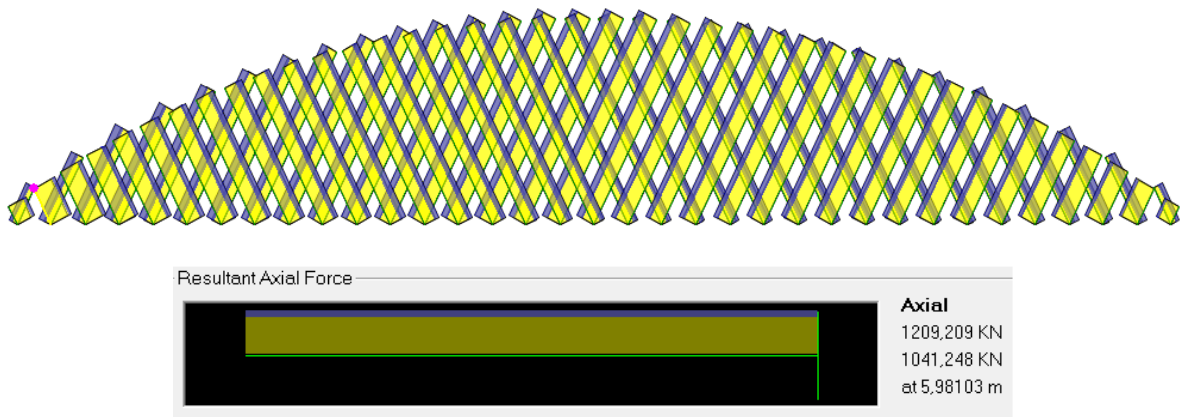


Figure 116 – Axial force on hangers for ULS: 1.35\*[DL+SDL+UDL(Half)+TS(123R\_R)] + HPP2. Detail of the 2<sup>nd</sup>, from the left, leaning outwards hanger.  $N_{Ed,Max}=1209$  kN.

The second one, which differs only on the UDL, is:

$$ULS_2 = 1.35 \times [DL + SDL + UDL(All) + TS(123R_R)] + HPP2$$

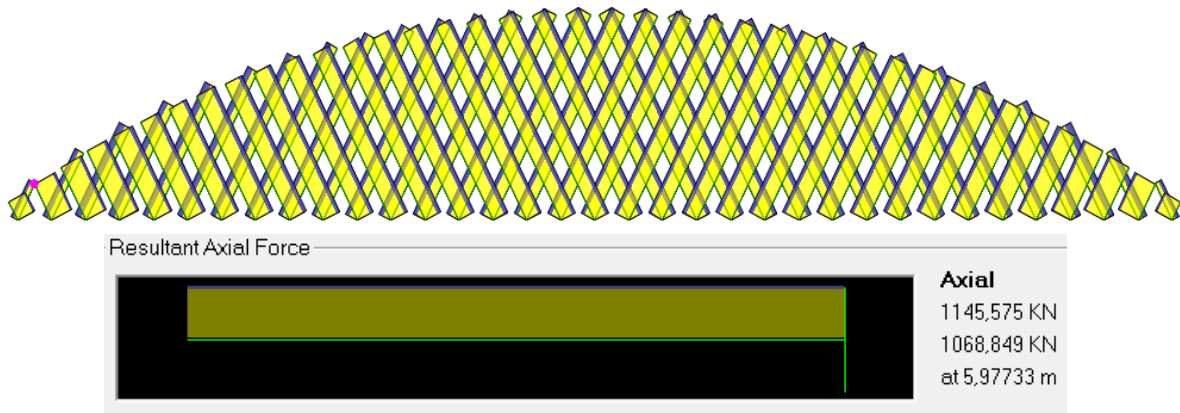


Figure 117 - Axial force on hangers for ULS: 1.35\*[DL+SDL+UDL(All)+TS(123R\_R)] + HPP2. Detail of the 2<sup>nd</sup>, from left, leaning outwards hanger.  $N_{Ed,Max}=1146$  kN.

## Chapter 4. Structural Analysis

The first combination is the critical one. The ULS verification is made:

$$\frac{N_{Ed}}{N_{Rd}} = \frac{1209}{1953.8} = 0.619 \leq 1.0$$

The characteristic axial stress limit should also be checked. Characteristic axial stress will result from all dead, live and prestress loads, non-scaled. The conditioning load combination and axial stress distribution is presented:

$$DL + SDL + HPP2 + UDL(All) + TS(123R\_R)$$

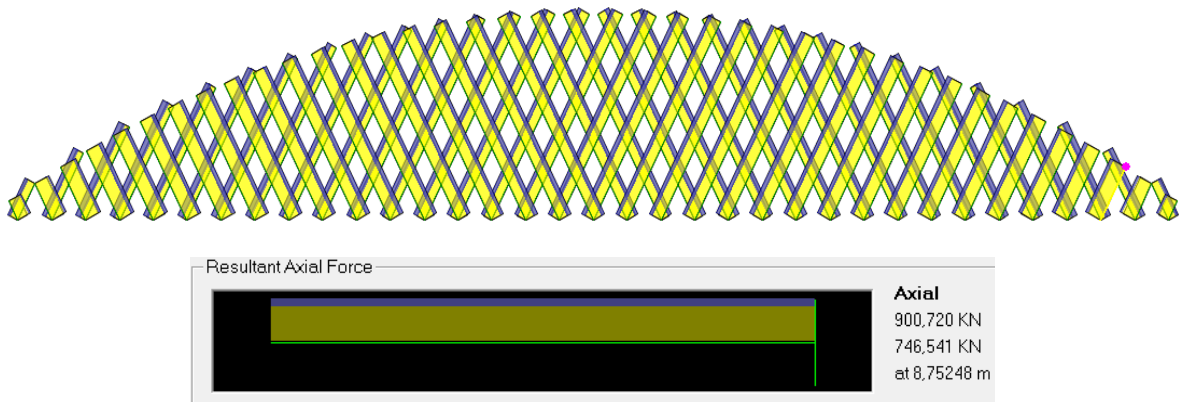


Figure 118 - Axial Force on hangers for ULS: (Dead+SDL+UDL 1R\_R All+TS 123R\_R+ HPP2)\*1.0. Detail of the 3<sup>rd</sup>, from the right, leaning outwards hanger.

The verification, according to *EN1993-1-11* 7.2 is that the characteristic axial force doesn't exceed 50% of the hanger's resistance.

$$\frac{N_{Ed,characteristic}}{0.5 \times N_{Rd}} = \frac{901}{0.5 \times 1953.8} = 0.922 \leq 1.0$$

The verification is fulfilled. Finally, the fatigue issue is approached. For this verification it was simulated the bridge crossing of Load Model 3 over the bridge, a vehicle defined in *EN1991 Part-2* 4.6.4, with the following geometric characteristics:

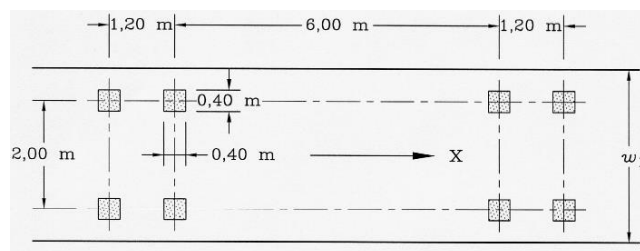


Figure 119 – LM3 for fatigue verification, according to *EN1991 Part-2*.

Each one of the four axis weights 120kN. When analyzed, the axial force envelope on the hangers results in the results presented in Figure 120, when LM3 crosses the bridge close to one of the arches.

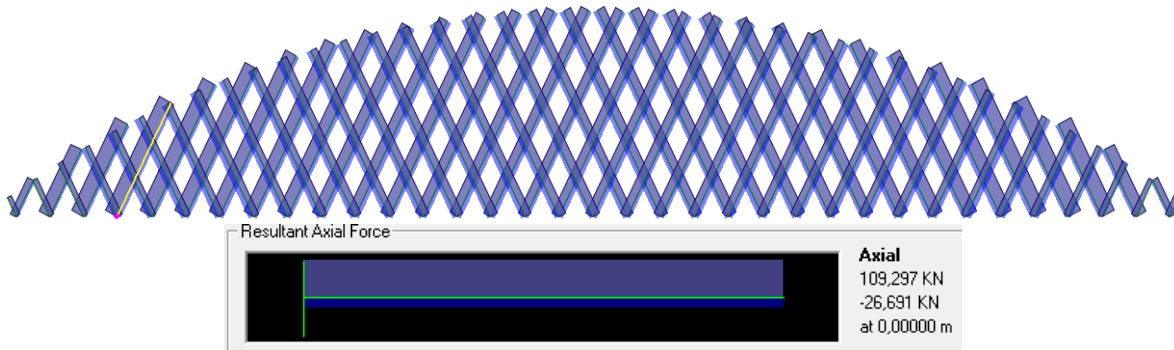


Figure 120 – Hanger’s axial force’s envelope, when subjected to the fatigue load model.

The maximum force and stress variation is obtained in the 4<sup>th</sup> hanger leaning inwards:

$$\Delta N_{max} = 109.3 - (-26.7) = 136 \text{ kN}$$

$$\Delta \sigma_{max} = \frac{\Delta N_{max}}{Area} = \frac{136\,000 \text{ [N]}}{0.005027 \text{ [m}^2\text{]}} \times 10^{-6} = 27 \text{ MPa}$$

According to *EN1993-1-9*, and using a conservative coefficient  $\gamma_{Mf} = 1.35$ , for severe damage consequences of the collapse of one hanger (which it is not very realistic for a bowstring arch with a network suspension system) leads to a limit of  $\Delta \sigma_{max} = 78 \text{ MPa}$ , more than double than the  $\Delta \sigma_{max}$  obtained. Therefore hangers’ fatigue is also verified.

## 4.7 Expansion Joints

The approach bridge decks and the bowstring bridge deck are separated by expansion joints. Horizontal displacements of both these decks, over the same column, must be carefully predicted. These displacement limits are the only ones considered in this design as an *Ultimate Limit State* verification, as all bridge decks must be allowed to expand freely.

## Chapter 4. Structural Analysis

The two main factors that contribute to the horizontal displacements of the structure are the temperature gradients on both bridges, and the deformation of the tensioned Bowstring bridge deck. Earthquake action is very low in this region and the estimated displacements are not representative.

Taking into consideration the constructive procedure, when the bowstring steel structure arrives to its final position it is already deformed due to its own dead load, so only the dead load from the concrete slab is taken into account, in a model with a non-stiff slab. This stiffness greatly affects the results. All other subsequent loads are applied on a model with a cracked stiffness slab for obtaining more realistic displacements.

**Table 39 – Decks Horizontal Displacements (m)**

Cause	Approach viaduct	Bowstring bridge
$\Delta_{\text{Temperature}^+}$	0.0267	0.0559
$\Delta_{\text{Temperature}^-}$	-0.0202	-0.0424
DL(Concrete)	-	0.0562 <sup>(*)</sup>
SDL	-	0.0095 <sup>(*)</sup>
UDL	-	0.0115
TS	-	0.0013
Wind	-	0.0037

From these results the maximum scaled displacement, on the approach viaduct, is:

$$\Delta_{max}^{Access\ B.} = 1.5 \times (0.0267 + 0.0202) = 0.0704\ m$$

And the maximum scaled displacement on the bowstring span is:

$$\begin{aligned} \delta_{max}^{Bowstring} &= 1.35 \times (0.0562 + 0.0095 + 0.0115 + 0.0013) + 0.6 \times 1.5 \\ &\times (0.0559 + 0.0037) = 0.1596\ m \end{aligned}$$

$$\delta_{min}^{Bowstring\ B.} = 1.5 \times (-0.0424) = -0.0636\ m$$

$$\Delta_{max}^{Bowstring\ B.} = 0.1596 + 0.0636 = 0.2232\ m$$

(\*) Even these values could be neglected in expansion joints specifications since it is natural that both the concrete slab and the SDL are applied before expansion joints are put in place.

The structural joint must allow a total displacement of:

$$\Delta_{Total} = 0.0704 + 0.2232 = 0.294 \text{ m}$$

The adopted expansion joint allows a 300 mm movement and can be seen in *Appendix E*. The displacement values obtained are perfectly possible over the adopted columns, with a 3 m diameter.





## 5. Hanger Arrangements and Arch Instability Investigations

### 5.1 Overview

In this chapter different hangers' arrangements are investigated, namely: "Vertical", "Nielsen", "Network" and "Optimized Network", as illustrated in Figure 121.

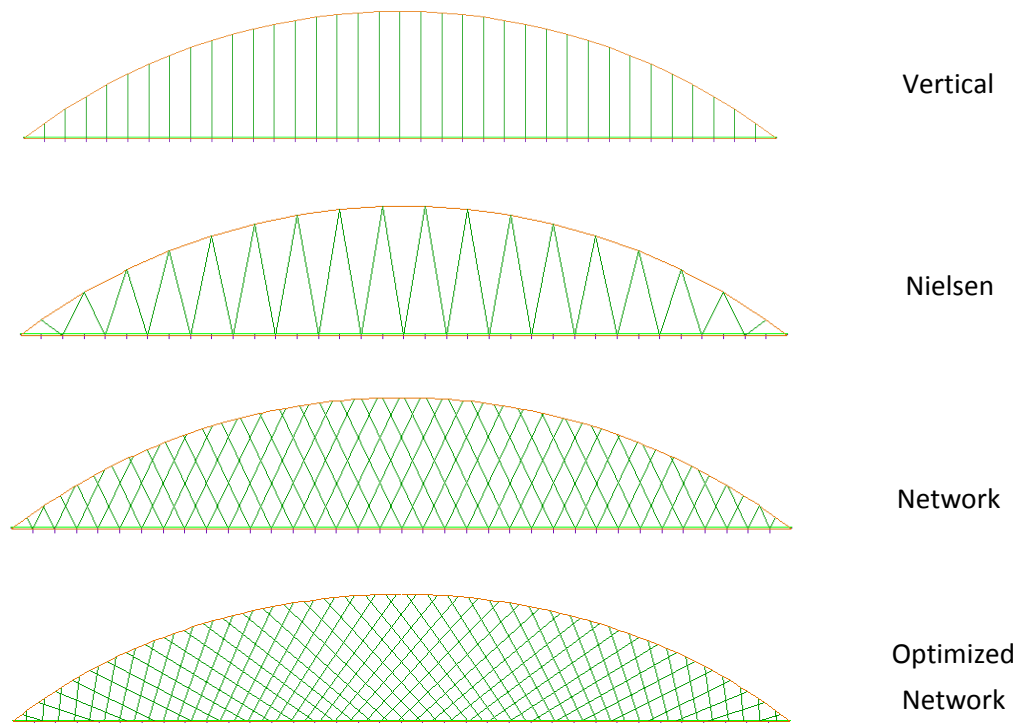


Figure 121 – Different hanger arrangements models investigated.

Four models with the same materials, deck and arch cross sections were adopted. Only the hangers have different cross-section's areas, defined as inversely proportional to the number of hangers, for a more proper comparison. The steel S460N was assumed in all hangers of the four models (Table 40).

The Optimized Network arrangement results from establishing equally distant nodes on the arch and varying the slope of the hangers according to *Brunn & Schanack (2003)* recommendations, which result from their extensive work on the subject.

**Table 40 – Hangers Characteristics on the Different Models**

Arrangement:	Vertical	Nielsen	Network	Opt. Network	
Nº of hangers	35	34	70	80	-
Cross-section diameter	0.1132	0.1148	0.0800	0.0748	m
Cross-section area	0.01010	0.01040	0.00503	0.00439	m <sup>2</sup>
$f_{yd}$	460	460	460	460	MPa
$N_{Rd}$	4646	4784	2312	2021	kN

Finally it is intended to investigate the influence of the hangers' arrangement on the stability. Furthermore, an investigation of the different methods of assessing instability using a FEModel, the European standards procedure, or a simplified method proposed by *Outtier et al. (2010)*, is presented using the four solution of hangers arrangements previously introduced.

## 5.2 Hanger Arrangements' Investigations

To analyze all models, two Load Distributions (LD) were defined: i) "LD-All" with the load applied in the entire span, and ii) "LD-Half" loading the left half of the span. The value of the applied load matches with the Load Model 4 preconized in *EN1991 Part 2 4.3.5*, so the blue color of the following schemes corresponds to a  $5\text{kN/m}^2$  vertical uniform distributed load.

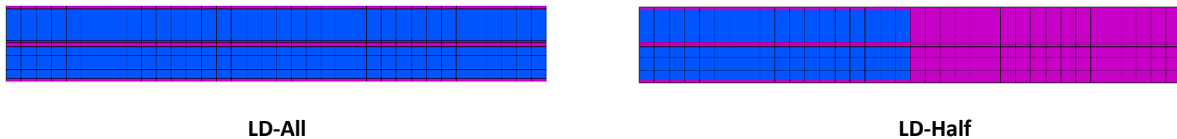


Figure 122 – Representation of both Load Distributions to be applied.

The results of the main forces and displacements, for all hanger arrangements are displayed in Table 41.

**Table 41 – Main forces and displacements on the different hanger arrangements.**

Arrangement	LD:	Vertical		Nielsen		Network		Opt. Network		Units
		All	Half	All	Half	All	Half	All	Half	
Arch	$M_{33,max}$	1631	-12203	937	916	848	688	996	817	kNm
	$N_{max}$	-8492	-4513	-7767	-5633	-7664	-5576	-7811	-5635	kN
	$M_{33,max}$	-1563	-10955	934	1114	732	737	607	656	kNm
Tie	$N_{max}$	5339	9721	4931	3653	4967	3677	4738	3517	kN
	$\delta_{max}$	132.1	860.2	62.2	77.7	56.8	38	65.1	38.3	mm

The normal forces and bending moments diagrams were obtained in *SAP2000* and can be found in Figure 123 and Figure 124. To better visualize the results, some charts are illustrated next.

Chapter 5. Hanger Arrangements and Arch Instability Investigations

Load Distribution - ALL

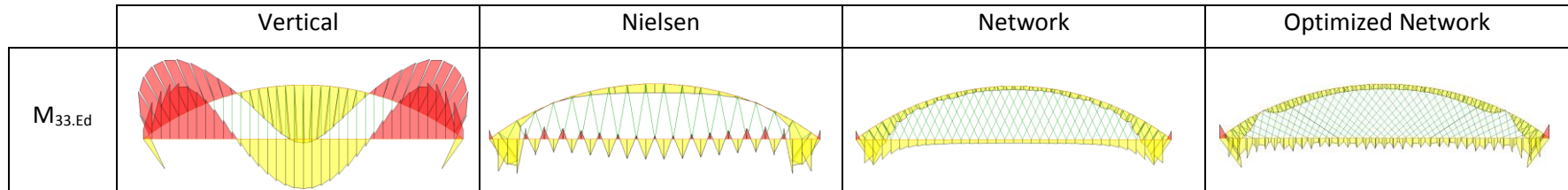


Diagram Scale Factor = 0.02

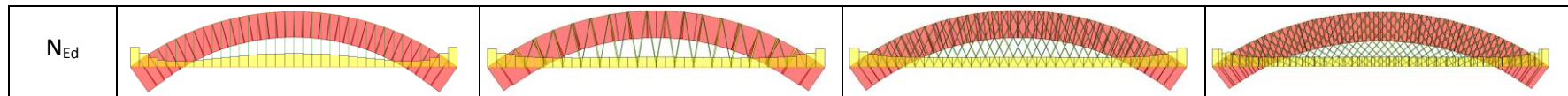


Diagram Scale Factor = 0.002

Load Distribution - Half

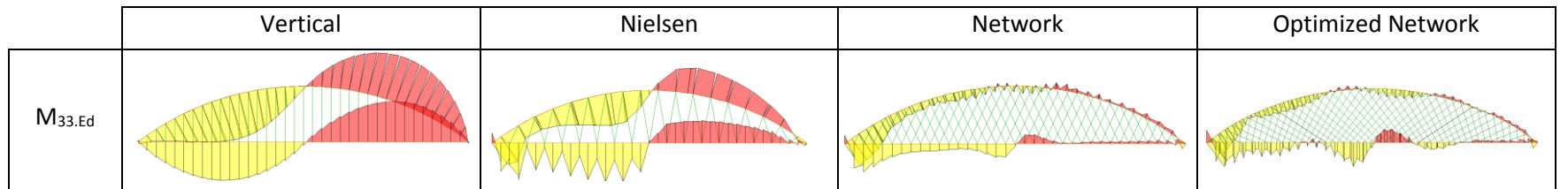


Diagram Scale Factor = 0.002

< ----- Diagram Scale Factor = 0.02 ----- >

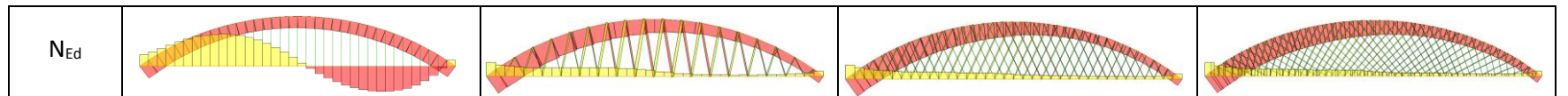


Diagram Scale Factor = 0.002

Figure 123 – Normal forces and bending moments diagrams for the Live Load LM4 on all or half deck span.



Figure 124 – Highest axial forces and bending moments in the arch and ties for the Live Load LM4 applied on all or half deck span.

## Chapter 5. Hanger Arrangements and Arch Instability Investigations

From the presented results, several important notes arise:

- Vertical arrangement is tremendously vulnerable to half-span loading. It balances unsymmetrical loads by bending both of the arch and the tie, since hangers do not connect different sections of the bridge. The same issue is observed with respect to deflections. The bending moments on the arch for LD-Half reach 17.7 times the value of the bending moments on the Network Arch for the same load!
- The distance between nodes of hanger attach on the arch did not influence the results.
- A higher number of hangers fairly decrease the bending moments on the ties.
- The adopted solution – Network Arch – has the best results on the arch and on deflections of the deck and arch.
- The Optimized Network arch has the best results on the tie.
- With about the same number of hangers as the Vertical, the Nielsen arrangement behaves, apparently, impressively well, in respect to the main axial forces and bending moments.

And, some notes can be made in respect to the axial forces and bending moments diagrams:

- The Network solution has an evenly low  $M_{33,Ed}$  in most of the span length (except at the corners), in contrast to the optimized network solution, making it possibly economic to adopt different tie sections along the arch span.
- In the Optimized Network solution the hangers do not anchorage at the same section as the ribs, which causes the observed bending moments' diagrams, and some extra shear forces.
- The Optimal Network has an incredibly even axial force diagram for the arches (only 4% axial force variation from the spring to the top of the arch in the LD-All), as anticipated by *Brunn & Schanack (2003)*. However, this was not enough to obtain a lower limit of the maximum axial force of the Network arrangement.
- The Vertical model has an important compression force on the tie, for LD-Half, which may induce instability, in particular, during an unsymmetrical casting of concrete.

The next step is to evaluate the hangers behavior. First, on the axial forces obtained, an optimal arrangement solution accomplishes two goals:

1. Low maximum axial force - Since models differ on the number of hangers, the way to better access this is to measure  $N_{max} / N_{Rd}$ .  $N_{Rd}$  is proportional to the area, which was defined inversely proportional to the number of hangers;

- Even axial forces (low  $N_{\text{variance}}$ ) - This prevents oversized hangers or/and different solutions for different hangers.

The axial force results on the hangers are presented in Table 42.

**Table 42 – Hanger axial forces for different hanger arrangements**

Arrangement:	Vertical		Nielsen		Network		Opt. Network		Units	
	LD:	All	Half	All	Half	All	Half	All		Half
$N_{\text{min}}$		215	58	46	-889	-118	-168	14	-65	kN
$N_{\text{max}}$		344	222	584	1114	283	304	248	211	kN
$N_{\text{average}}$		277	138	289	144	144	72	154	77	kN
$N_{\text{Rd}}$		4646		4784		2312		2021		kN
$\frac{N_{\text{max}}}{N_{\text{Rd}}}$		7.4%	4.8%	12.2%	23.3%	12.2%	13.1%	12.3%	10.4%	-
$N_{\text{variance}}$		24.4%	60.6%	102.3%	671.5%	96.4%	322.2%	60.9%	174.0%	-

The axial force amplitude variation between hangers -  $N_{\text{variance}}$  – is simply assessed as:

$$N_{\text{variance}} = \frac{N_{\text{max}} - N_{\text{average}}}{N_{\text{average}}}$$

And the following charts illustrate the different percentage results between models:

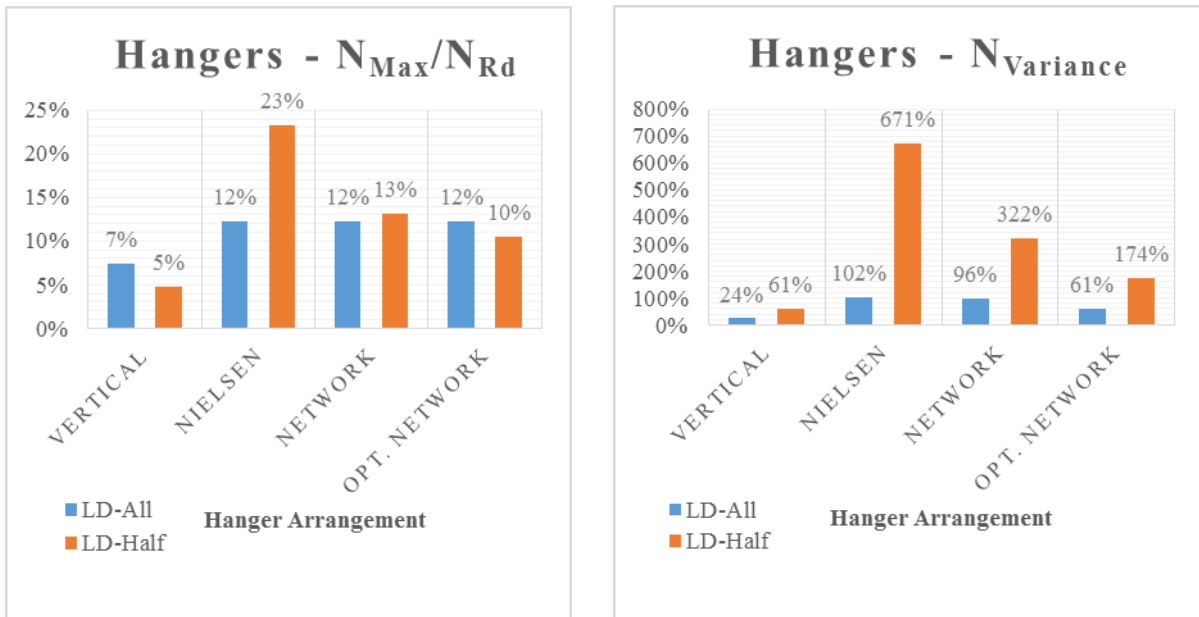


Figure 125 – Hangers  $N_{\text{max}} / N_{\text{Rd}}$  and axial force amplitude variation.

From these results it can be seen that:

- Nielsen arrangement is by far the most unfavorable in this hanger forces analysis, in contrast to the previous fairly good results. The  $N_{\min} = -889$  kN indicates an alarming compression value and the truss-beam like behavior (see Figure 112) proves to have a very serious consequence on the hangers relaxation. In fact, it was observed that this compression force alone exceeds the tension forces from the permanent loads. Moreover, an even higher  $N_{\max}$  leads to the very penalizing results observed.
- To compensate, and undoubtedly related to the disturbing results obtained previously on the arch and ties efforts distributions, the Vertical arrangement shows the best results here, with very low hangers force variations.
- The Optimized Network arrangement, which proved previously not to be better than the Network, finally reveals its benefits, from having virtually no compressed hangers and a considerably well distributed axial force between hangers.

Next, investigating the fatigue issue, the LM3 from *EN1991-2 4.6.4* was again used to assess the stress variations on the hangers of the different arrangements. The results from its circulation close to one arch are summarized in Table 43. The results show that none of the hanger arrangements presents problems with respect to fatigue verification.

**Table 43 - Fatigue assessment between arrangements**

Arrangement:	Vertical	Nielsen	Network	Opt. Network	Units
$\Delta N_{\max}$	77.8	292.8	136	103.4	kN
$\Delta \sigma_{\max}$	7.7	28.2	27.1	23.5	MPa

Finally, with respect to the relaxation issue, all models were subjected to the same ULS combination of loads. The observed number of compressed hangers, on each arch, is presented in Table 44.

$$DL + SDL + 1.35 \times [UDL(Half) + TS(123R_R)]$$

**Table 44 – Relaxed hangers on the different arrangements**

	Vertical	Nielsen	Network	Opt. Network
Nº of relaxed hangers	0	10	6(*)	1
% of relaxed hangers	0.0%	29.4%	8.6%	1.3%

(\*) If HPP2 is added to the combination on the Network arrangement, no compressed hangers appear, as seen in section 4.6.



Although in this bridge solution none of the arrangements has problems checking fatigue, these last results differences are an extent of the analysis and commentaries already made.

On the Nielsen arrangement compressed hangers are removed, as seen in Figure 126, for the LD-Half, to illustrate the consequences when compression forces exceed tension forces in the hangers:

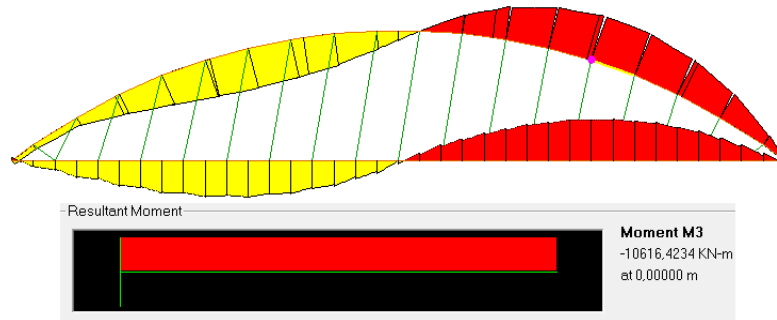


Figure 126 – Nielsen arrangement, when LD-Half is applied and compressed hangers are iteratively removed.  $M_{33,Max} = -10616$  kNm.

A bending moment of -10616 kNm was obtained, contrasting with the previously obtained 688 kNm using also the compressed hangers. The final conclusions are therefore clear:

- For unsymmetrical loads, the bending moments on the arch of the Vertical arrangement solution increase 17.7 times more than the ones of the network arch! This is the main reason why Network arches are presented here as an interesting solution when live loads are important. This huge demand of the arch bending resistance seriously compromises the structure cost and aesthetics.
- The Nielsen arrangement has severe relaxation problems. For unsymmetrical loads it gets many of its hangers relaxed, as shown in Figure 126. This considerably affects the apparently good distribution of forces and moments' results presented in Table 41, since hangers cannot mobilize compression forces. For this reason, when there is a live load in the imminence of relaxing hangers, the effects of incrementing that live load on the structure are very much like the ones in the Vertical Model. So, accordingly to a higher or lower relevance of the live loads, the Nielsen arrangement behaves respectively, more closely to the Vertical Model or more closely to the Network models.
- The Network proved to have the lowest forces and moments on the arches, and, in respect to the ties, when compared to the Optimized Network, the slightly higher maximum values can be compensated by the possibility of adopting two different cross-sections along the

span (one at the corners, another at the remaining span length). Its disadvantages to the Optimized Network, regarding the hangers, can be partially compensated by applying appropriate prestress, as defined in section 4.6.

- The Optimized Network exposed its benefits mainly in the hangers' results.
- Within the same arrangement, it was verified that the more axial stiffness the hangers have, the more uneven forces result.
- The higher the number of hangers, the lower bending moments on the ties.
- While a higher number of hangers may lengthen the construction procedure, hangers with a bigger cross-section might need additional means and equipment to be put in place and prestressed.
- Aesthetics about these different arrangements will be up to each designer to evaluate, although it is clear that network types of suspension led to very slender and elegant overall bowstring decks.

## 5.3 Arch Instability Analysis

### 5.3.1 Load cases and sequence of application

The buckling resistance of the arches is much dependent of the load distribution. To evaluate this issue, five different load distributions were applied. The value of the applied load again matches with the Load Model 4 preconized in *EN1991 Part 2 4.3.5*. The blue color of the following schemes corresponds to a  $5\text{kN/m}^2$  vertical uniform distributed load, this time with five different patterns:

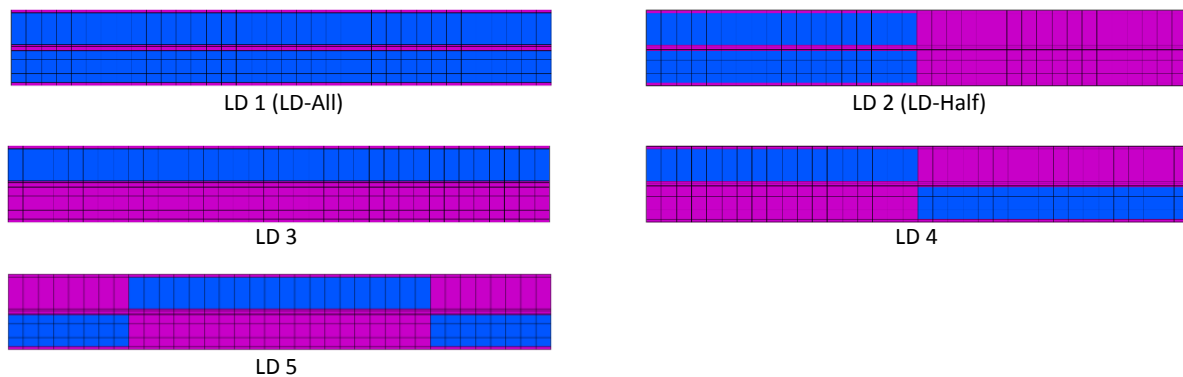


Figure 127 – Load Distributions applied in this section, to assess the arch instability.

Dead loads are pretty well distributed on the whole span, while live loads can assume many different positions. It will be seen further on this chapter that a high live load value may, in some load patterns, evoke relaxation of hangers or buckling of the deck, consequently decreasing the bridge's stiffness and buckling stability. For this reason, loads increase in order to reach the buckling load, must be carefully chosen. There are three different reasonable scenarios to analyze buckling with the FEModel:

- a)  $DL + \lambda LL$  – dead loads are applied, but only live loads are increased until buckling failure.
- b)  $\lambda (DL+LL)$  – both dead and live loads are increased until buckling failure.
- c)  $\lambda LL$  – only live loads are applied and increased until buckling failure.

First, it should be remembered that, setting aside wind and not considering other loads that are less critical on this topic, and only at ULS, bridge design loads are roughly expected to be close to  $1.35(DL+LL)$ . On the other hand, live loads have a more variable nature and are naturally more prone to take higher values than expected, comparing to the more predictable bridge's dead loads. Thus:

- Method a) is on the safe side. It contemplates DL and multiplies LL. For even a more precise analysis, DL and SDL should be separately analyzed, the DL with an unstiff concrete model, and the SDL with the normal stiff concrete model, to account for the construction procedure. Concrete stiffness doesn't affect significantly the stresses on the arch, but it does affect the stresses on the slab and ties, which in turn can change the buckling mode (a buckling of the deck occurs for LD2 on Vertical and Nielsen Models). Though, since *SAP2000 v14.2* has linear buckling analysis limitations, method a) is not performed. Initial load conditions (DL), not being increased on the buckling analysis, cannot be computed.
- Method b) is probably the closest to reality, but, reminding live loads variable nature in the real scenario, it is unsure if this method will present safe results, since no problematic events (relaxation and buckling of the deck), derived from high live loads, are evoked this way.
- Method c), by exclusion of both previous methods, will be the one performed in this study. The results may not be, in principle, as realistic as the ones obtained in previous scenarios but surely they are on the safe side.

Note: "DL" are mentioned here, exceptionally, as all dead loads, including SDL – Superimposed Dead Loads.

### 5.3.2 Critical loads and buckling modes

The results of the stability analysis, using method c), are resumed in Table 45.

**Table 45 – Instability Analysis Results**

Hangers arrangement	Load Distrib:	1	2	3	4	5
Vertical	$\lambda$	12.219	22.007	24.218	24.303	24.385
	$N_{Ed}$ [kN]	8492	4513	6200	5578	5111
	$N_{FE,el}$ [kN]	103761	99316	150152	135562	124630
Nielson	$\lambda$	16.890	28.186	33.613	31.599	32.842
	$N_{Ed}$ [kN]	7769	5162	5682	5062	4637
	$N_{FE,el}$ [kN]	131215	145498	190989	159954	152288
Network	$\lambda$	16.964	26.090	33.765	33.901	33.901
	$N_{Ed}$ [kN]	7677	5576	5604	4644	4636
	$N_{FE,el}$ [kN]	130231	145478	189221	157435	157164
Optimized Network	$\lambda$	16.303	26.224	32.457	32.586	32.573
	$N_{Ed}$ [kN]	7811	5635	5696	4675	4982
	$N_{FE,el}$ [kN]	127343	147775	184872	152338	162277

where:

$\lambda$  = number of times that the LM4 must be multiplied to cause buckling on the arch = buckling factor.

$N_{Ed}$  = max. compression force on the arch when LM4 is applied.

$N_{FE,el} = \lambda \times N_{Ed}$  = max. compression force on the arch in the imminence of buckling.

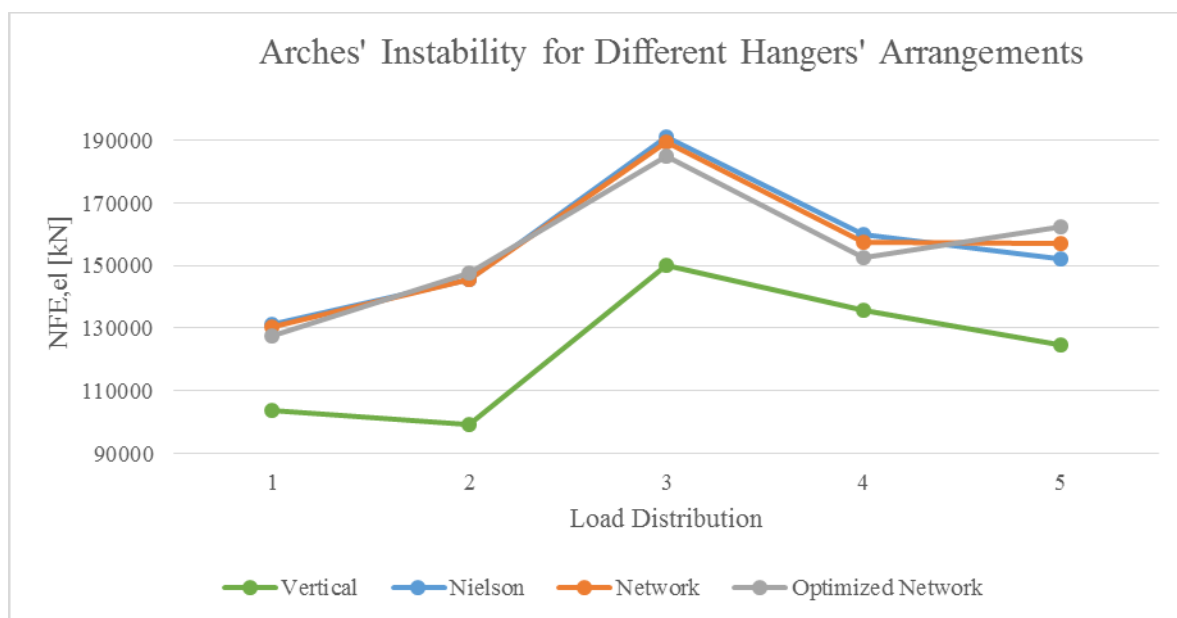


Figure 129 – Comparison of the stability analysis results.

In-plane buckling and out-of-plane buckling are two concepts often referred to in this chapter. They correspond to two different scenarios of buckling modes as illustrated in Figure 130 and Figure 131.

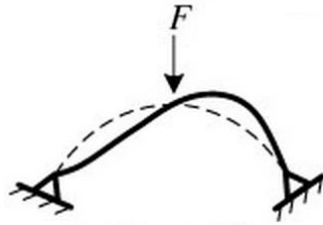


Figure 130 – In-plane buckling mode.

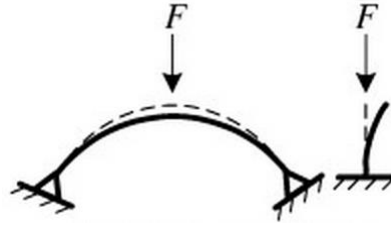


Figure 131 – Out-of-plane buckling mode.

For the four models and all load distributions, the obtained buckling shape is primarily out-of-plane and as observed in Figure 132.

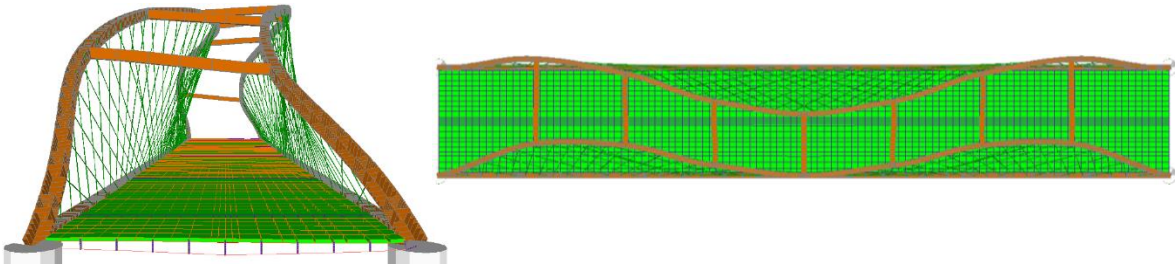


Figure 132 Optimized Network Model. Buckling shape for LD1.  $\lambda=16.30$ .

As for the LD2, the Vertical and Nielsen models behave differently from all others and slightly from each other. First, for both Network models, the instability for the Load Distribution 2 (LD2) occurs like presented in Figure 133, and with the stresses distributions of Figure 134.

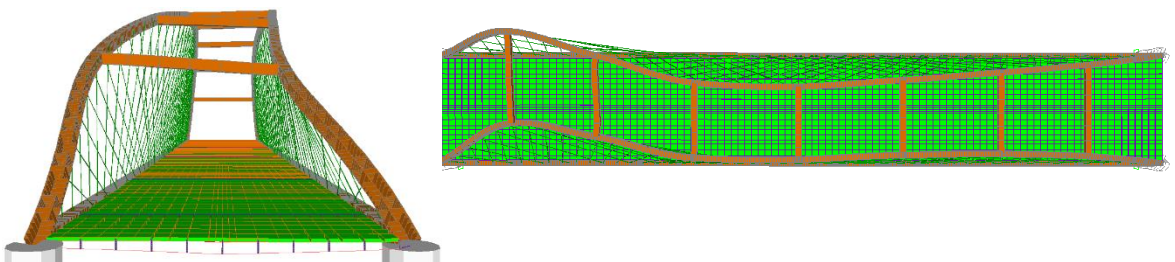


Figure 133 Optimized Network Model. Buckling shape for LD2. (Load applied on left half of the span).  $\lambda=26.22$ .

A detailed view of the hangers' axial stress reveals that, for this LD2, compression occurs in several hangers:

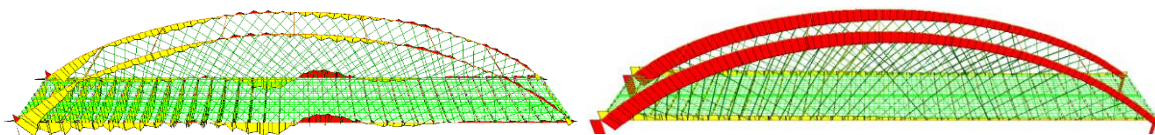


Figure 134 – Bending moments 3-3 and axial force diagrams, on Optimized Network Model, for the LD2. (Load applied on left half of the span).

## Chapter 5. Hanger Arrangements and Arch Instability Investigations

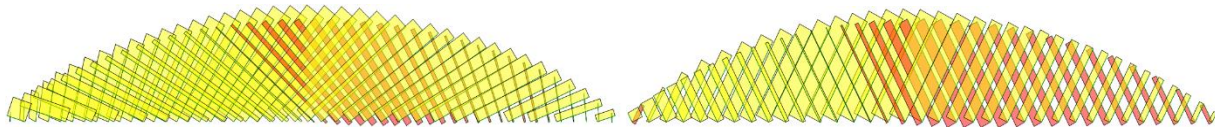


Figure 135 – Hangers' axial force on the Optimized Network Model (Left) and on the Network Model (Right) for the LD2. (Load applied on left half of the span).  $N_{\min} = -168$  kN (Network Model).

In fact, all load distributions relax some of the hangers in the Network Model, even LD1 as seen in previous chapters, while for the Optimized Network Arch, only LD2 produces relaxation in some hangers.

Network Model gives the most compressed hanger, for LD2, with a 168kN compression force. An approximately 345kN tension force is also applied to these hangers from all permanent loads. Thus, a live load 2 times higher than the predicted in LM4 would have to be applied in order to occur relaxation of hangers. However, the buckling analysis gives buckling factors much higher than 2.

On the one hand, a simple analysis can be made in *SAP2000* admitting compressed hangers. This way, the “Compressed Hangers  $\lambda$ ” buckling factor obtained doesn't take into account relaxation of hangers. On the other hand, a multi-step analysis where relaxation of hangers is taken into account would return a more “Real  $\lambda$ ”, in the real meaning of  $\lambda$  – number of times the live load can be multiplied until buckling occurs. Since relaxed hangers reduce structure's stiffness and may rush instability, this number decreases. Finally, another buckling factor “No Compressed Hangers  $\lambda$ ” can be obtained where all compressed hangers are removed and a simple analysis is then performed. The darker lines in the graph of Figure 136 illustrate these statements.

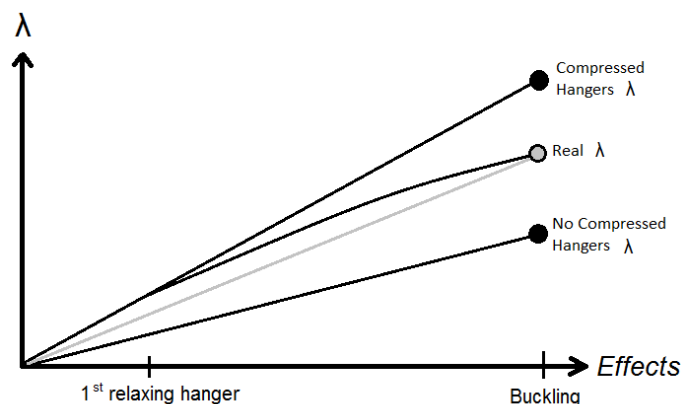


Figure 136 – Compressed Hangers  $\lambda$  - Buckling factor given by *SAP2000* without taking into account relaxation. Real  $\lambda$  – Buckling factor given by a multi-step analysis where hangers cannot mobilize compression. No Compressed Hangers  $\lambda$  – Buckling factor given by *SAP2000* with a model where compressed hangers were previously removed.

The “Effects”, on the horizontal axis, are a qualitative measure. They can be either interpreted as stresses or deflections.

Note that “Real  $\lambda$ ” designation is not accurate as it only takes into account the relaxation of hangers. It assumes linear behavior of all materials until buckling occurs, which is not true, and it also does not take into account directly the geometrical initial imperfections nor residual stresses. These residual stresses, according to the study *Outtier (2007)*, have little influence and can be neglected. But geometrical initial imperfections have consequences on the subsequent “Effects” (i.e. stresses and/or deflections), as can be seen in schemes of Figure 137. These initial imperfections are the main reason to adopt a reduction factor for the relevant buckling mode lower than 1 when the elastic critical force “ $N_{cr}$ ” is, as in the present case, many times greater than the design resistance of the cross-section for uniform compression.

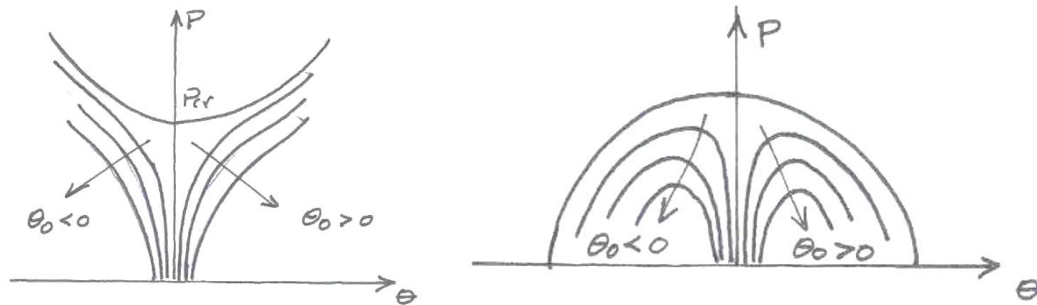


Figure 137 – Geometrical initial imperfections ( $\Theta_0$ ) and their consequences on the displacement ( $\Theta$ ) when loading ( $P$ ) acts.

Actually as it can be seen from Figure 137, these imperfections influence the behavior of the arch from the beginning of loading and decrease its buckling resistance. That is why these will be, roughly, taken into account (along with the residual stresses), from the curves and process described in *Section 6.3* of the *EN1993-1-1*. This influence on the arch’s behavior is also dependent on the arch’s slenderness. Non-dimensional slenderness of beams with values around 0.8 are the most sensitive to geometric imperfections. Thus, buckling reduction factor depends only on both geometrical initial imperfections and slenderness.

Note that the stiffness and, consequently, the slenderness of the arch are in some way related to the slope of the lines of the graph of Figure 136. The lighter curved line translates the loss of stiffness when hangers start to relax, which in turn decreases the critical load value and slenderness. When the critical load is inputted to the referred method of the *Eurocode* to obtain non-dimensional slenderness, a supposedly constant slenderness, until buckling failure, is assumed by the method.

## Chapter 5. Hanger Arrangements and Arch Instability Investigations

For example, if “*Real λ*” was adopted in the calculations, the method would “assume” that the arch behaved like the grey (lighter) line in Figure 136. It then becomes apparent that adopting the “*Real λ*” can be penalizing since the arch will most likely work under live loads smaller than 2 times the LM4 loading, where relaxation does not occur. Consequently, even more penalizing is to analyze the model with no compressed hangers.

An assessment was carried out to understand if the influence of the geometrical imperfections should be considered on the stiffer model, by adopting the “*Compressed hangers λ*”. The arch’s maximum axial force, when the exact load that causes the first hanger to relax is applied, is:

$$N_{DL} + N_{SDL} + 2 \times N_{LM4-LD2} = -34850 \text{ kN}$$

with:

$N_{DL}$  – Arch axial force due to Dead Loads.

$N_{SDL}$  – Arch axial force due to Superimposed Dead Loads.

$N_{LM4-LD2}$  – Arch axial force due to the Load Model 4, with the Load Distribution 2.

The cross-section’s plastic resistance of the arch is:

$$N_{pl,Rd} = -85554 \text{ kN}$$

The design buckling resistance of the arch, calculated with the “*Compressed hangers λ*”, admitting the LD2 as the conditioning one and using “curve a” of the Eurocode, as explained further in this chapter, would result in:

$$N_{b,Rd} = 0.814 \times (-85554) \text{ kN} = -69648 \text{ kN}$$

Theoretically, there is a combination of loads that could cause the relaxation of hangers so the correct design buckling resistance of the arch, for this LD2, would be somewhere between -34850 kN and -69648 kN, depending on how serious or negligible, respectively, the relaxation effect is to the arch stability.

Interestingly, the difference between “*Compressed hangers λ*” and “*Real λ*” is actually small. The arch loses some of its in-plane support when hangers relax, but as it can be observed, the out-of-plane buckling is the conditioning one. To prove this, a Network Model where compressed hangers were iteratively removed, followed by a linear analysis, allowed to obtain the “No Compressed Hangers λ”, and, comparing to the “Compressed Hangers λ”, the arch only got its buckling factor reduced from 26.09 to 25.80 (Figure 138 and Figure 139).



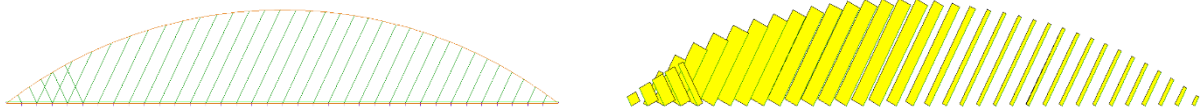


Figure 138 – Network Model and its hangers' axial forces for the LD2, after iteratively removing compressed hangers.

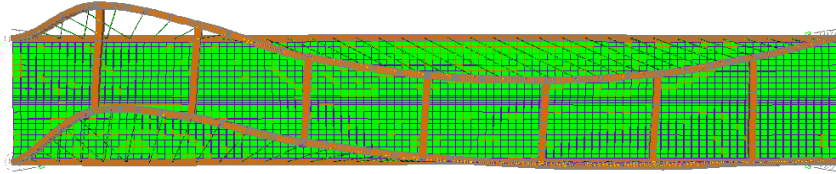


Figure 139 – Buckling mode of the Network Model after being removed all compressed hangers. Very similar to the previously seen Compressed Hangers Model buckling mode.

Concluding, with such a small difference, relaxing hangers have a very little influence on the structure stiffness, and, the buckling resistance, for LD2, is very close to the -69648 kN. Based on these results and comparing to the design buckling resistance given from LD1, with the slightly lower value of  $N_{b,Rd} = -67557\text{kN}$ , it is determined that LD1 is the conditioning loading. These results are in agreement with *Per Tveit (2011)* that states:

*“Even if some hangers relax, moderate live load on part of the span gives smaller maximum stresses in the arch than the same live load on the whole span. This is because the partial live load gives smaller axial force in the arch.”*

Next, it is also very interesting to notice that for the Vertical and Nielsen Models, with the LD2, the buckling shapes contain both the buckling of the ties and arches, as shown in Figure 140.

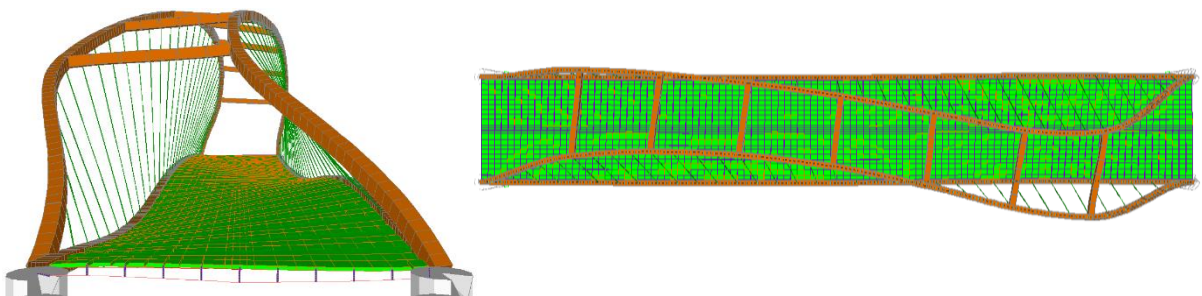


Figure 140 - Vertical Hangers' Model. Buckled shape for LD2 (Load applied on left half of the span).  $\lambda=22.01$ .

This is a direct consequence of the stresses distributions for LD2 loading shown in Figure 142 and Figure 141.

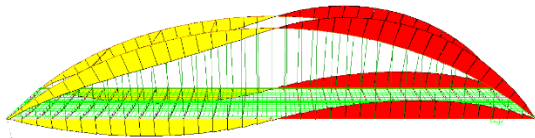


Figure 142 – Bending moment 3-3 Diagram on Vertical Hangers' Model, for the LD 2 (Load applied on left half of the span).

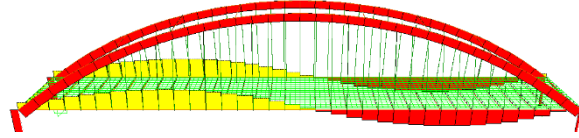


Figure 141 - Axial Force Diagram on Vertical Hangers' Model, for the LD 2 (Load applied on the left half of the span).

It can be seen that part of the ties are compressed due to the negative bending moment on the right half of the deck and due to the longitudinal composite behavior of the deck. This composite behavior causes the concrete to tension and the tie to compress, when the deck bends (on the undeformed shape, the concrete slab and the tie are connected and the centroid of the slab is about 0.5 m higher than the center of the steel tie, resembling a large longitudinal composite beam).

On the other hand, since tension stresses on the tie from all permanent loads are approximately 4 times the compression stresses from the live loads, the ties, in reality, will always stay tensioned and the sense of this instability analysis approach can again be questioned.

All buckling factors' values obtained by the present method c) ( $\lambda$  LL), are somewhere between 12 and 34. So, even if method a) was used ( $DL + \lambda$  LL), the dead loads contribution wouldn't be critical for the buckling results. Finally, the most important result is that the buckling loads of the stability analysis for the LD1 and LD2, in this Vertical Model, are similar. Admitting that LD1 and DL produce a similar response on the bridge, it is the same as saying that ( $\lambda$  DL) and ( $\lambda$  LL) have similar results, and so, method b) -  $\lambda$  (DL+LL), probably the closest to reality, and method c) – ( $\lambda$  LL) – would present even more similar results. Conclusion is that the LD1 results from this analysis are very close to reality. Remembering that the results between LD1 and LD2 have really close values, then, when taking into account this deck buckling issue for high live load values, although it is on the safe side, it will not affect significantly the final buckling model results, whether conditioned by LD1 or LD2.

For the Nielson Model, serious relaxation occurs for unsymmetrical loading distributions (as seen previously, for live loads only, the LD2 would give almost 900kN compression forces in some hangers, which are not compensated by the approximately 600kN tension forces given from all permanent loads). Compressed hangers were, also here, iteratively removed from the model until no hangers were compressed. This was also repeated for LD4 and LD5 as these produced some relaxations as well. LD4 and LD5 are relatively far from being conditioning so compressed hangers there were simply removed, to ensure safe results. For the LD2, the resultant buckling mode, after removing compressed hangers, is included in Figure 143.

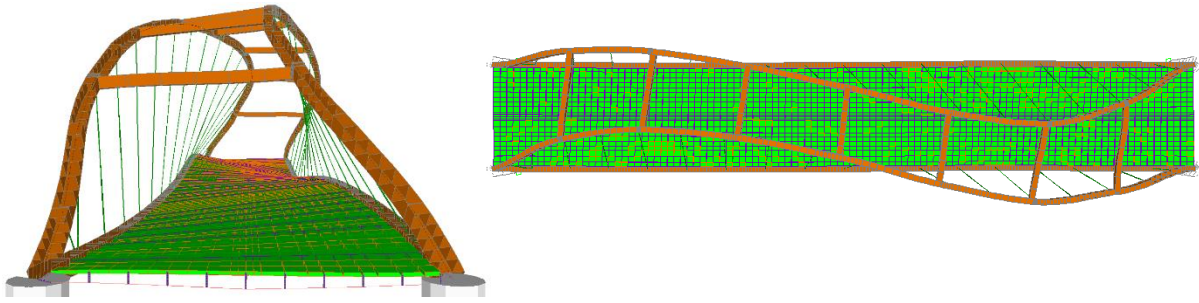


Figure 143 – Nielsen Hangers Arrangement Model. Compressed hangers removed. Buckled Shape for LD2 (Load applied on the left half of the span).  $\lambda=28.19$ .

The resultant bending moments and axial forces diagrams have a similar outline as the Vertical Model. Yet, the values of the bending moments and axial forces, are respectively 20% lower and 10% higher on the Nielsen Model. The difference is explained by a slightly stiffer Nielsen Model, which will conduct more loads axially through the arch than the Vertical Model.

Despite Nielsen's dramatically different forces between hangers and even with compressed hangers removed, as it regards to instability, it behaves remarkably well, with results close to both Network Models. It may be interesting to compare the bending moments in all models, for the conditioning load distribution for almost all cases, which is LD1 (LD-All) (Figure 144). This explains the main differences between the Vertical, and all other models' results on instability. The scale factor was defined equally in all diagrams for a directly visual comparison.

These results are quite in agreement with *Per Tveit (2011)* conclusions:

*"In a normal network arch the decisive load cases are maximum load on the whole span. For these load cases equidistant nodes along the arch give the smallest buckling lengths in the arch and the smallest bending moments due to curvature of the arch."*

But, not exactly in agreement *Per Tveit's conclusions*, the large distance between arch nodes in the Nielsen Model didn't affect its buckling resistance, nor did the optimized network model see significant improvements here. For the same reason that the relaxing hangers, on the Network Model, didn't affect significantly the critical load's value, the author thinks that this statement is less valid for bridges with inclined arches where out-of-plane buckling occurs more prominently than the in-plane plane buckling, as the present case.

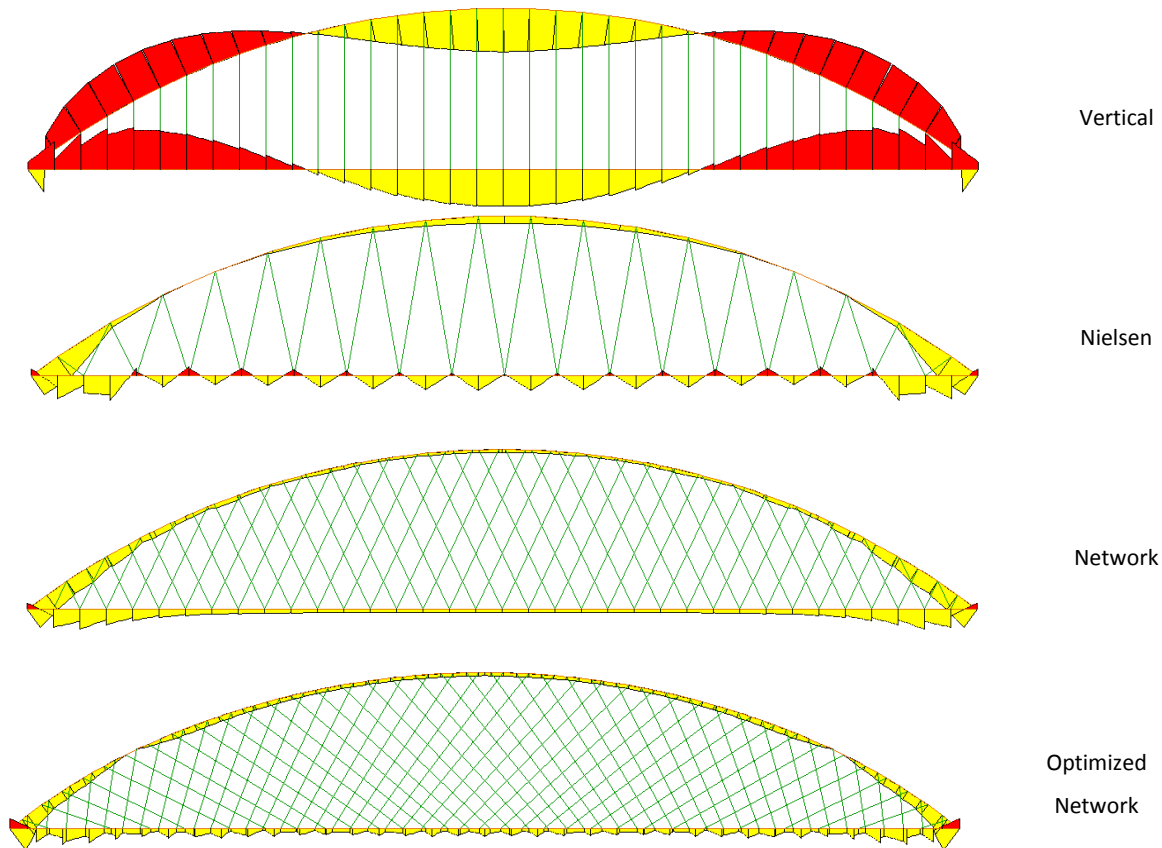


Figure 144 - Comparison between bending moment 3-3 diagrams, due to LD1. (All diagrams have the same scale factor).

Network arrangements are known for increasing stability in cases where in-plane buckling is dominant and conditioning, and inclusively studies have been made to quantify this increase on in-plane stability – [Schanack F. (2008)]. Though, as Valenzuela (2010) states:

*“When analyzing inclined network arch bridges, an integrated methodology for the simplified analysis of in plane and out of plane buckling of the arch need to be developed, follows the proposal’s equations of Schanack. This new methodology must consider not only how the hanger’s arrangement influence the strength of the whole mechanism, but also the arch-hanger interaction in a complete FEM 3D model.”*

The inclination of the arches, along with the tridimensional bracing beams linking the two arches, makes extremely difficult to occur a pure in-plane buckling. Actually, a pure in-plane buckling with a few number (less than the number of bracing beams) of waves is virtually impossible since it would

activate the bracing beams axial stiffness, without laterally bending the arch. Additionally, the arch has a higher in-plane bending inertia than the out-of-plane bending inertia.

All assumptions adopted until this point, considering linear analysis, contributed to approximation of the buckling loads. Only a nonlinear analysis could in fact simulate the true behavior of the arch bridge for this stability study, where also plasticity of materials should be considered, giving, this way, realistic results of the bridge stresses and deflections, for the different load distributions applied.

About that, some studies investigated these aspects. First it was said previously that residual stresses can be neglected. It seems also geometrical imperfections have little influence on results, since *Valenzuela (2010)* studied another steel network arch bridge, and finally quotes:

*“For the network arches, nonlinear analysis considering the assignment of geometrical imperfections showed that the magnitude of bending moments along the arch increases only 1% in the second order analysis. Thus, when considering network arrangement, increases in bending moments by second order effects are not significant.”*

Finally, according to *De Backer (2009)*, nonlinear geometrical analysis would give an increased buckling factor as these consider the change in the direction of action of the hanger’s force when the arches’ out-of-plane deformation happens. This again shows that a linear stability analysis leads to results on the safe side. Nevertheless, a nonlinear analysis is a much more complex approach, hardly handled by *SAP2000 v14.2*, and it is outside the scope of this study.

### 5.3.3 Other forms of evaluating the arch critical load

*“Imperfections of arch bridges are smaller than can be expected for straight members”* - *De Backer (2009)*. This statement reveals that the buckling curves found in the *Eurocode 3* for straight members can be overly safe, when directly applied to the verifications of arch members. According with the *EC3*, the arch normalized slenderness  $\bar{\lambda}$  must first be calculated by eq. 7.

$$\bar{\lambda} = \sqrt{\frac{A \times f_y}{N_{cr}}} \quad (7)$$

with:

## Chapter 5. Hanger Arrangements and Arch Instability Investigations

A - Area of the arch cross-section

$f_y$  – Yield strength of the used steel

and,  $N_{cr}$ , the critical elastic normal force of the arch, is obtained as follows:

$$N_{cr} = \left(\frac{\pi}{\beta l}\right)^2 \times EI_z$$

with:

$l$  – Bridge span

$EI_z$  – Out-of-plane bending stiffness of the arch

$\beta$  – Buckling length factor

The buckling factor is first obtained for “Out-of-plane buckling of arches with wind bracing and end portals”, according with the annex D3.4 of the EN1993-2. The parameters required in the process are:

$h$  (length of the arch between the spring and the first wind bracing) = 35 m

$h_r$  (average of all hangers' length) = 21.57 m

$h/h_r = 1.62$

$I$  ( $I_z$  of the arch) = 0.0471 m<sup>4</sup>

$I_0$  ( $I_y$  of the bracing beam) = 0.0417 m<sup>4</sup>

$b$  (deck's width) = 26 m

$$\eta = \frac{I \times b}{I_0 \times h} = \frac{0.0471 \times 26.6}{0.0417 \times 35} = 0.858$$

With the given parameters, from *table D.1* of the EC3, the buckling length factor results in  $\beta=0.62$  and  $N_{cr}$  is obtained by:

$$N_{cr} = \left(\frac{\pi}{0.62 \times 35}\right)^2 \times 210 \times 10^6 \times 0.0471 = 207310 \text{ kN}$$

This result is approximately the double of the  $N_{cr}$  obtained through FEM analysis for the Vertical Model. The apparent reason for this result is that this method considers an effective wind-bracing after the first arch-cross-girder, since it only considers the instability in the wind portal arch frames (Figure 145). This is far from reality as these bracing beams are far apart and work also in bending.

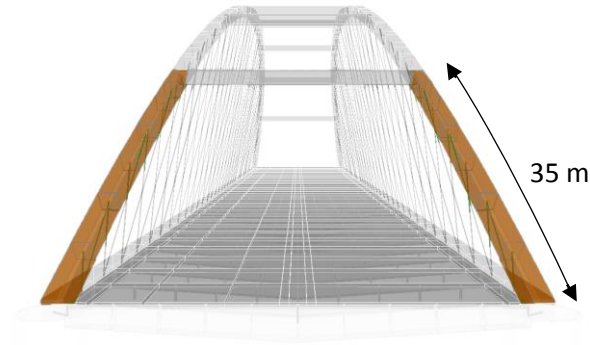


Figure 145 – Wind portal arch frames (darker and colored).

This result gave an idea of the buckling resistance of this bridge if a more efficient, possibly less aesthetic, wind-bracing was used (always within the assumption that in-plane buckling wouldn't become critical). Actually a wind-bracing made of rigid elements was added to the FEModel to confirm the *Eurocode's* prediction (Figure 146).

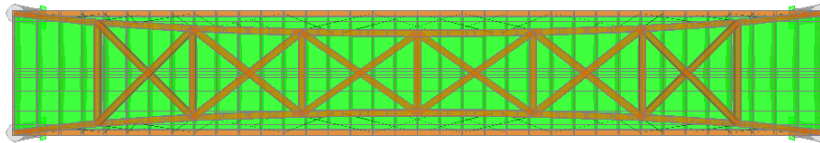


Figure 146 – FE Network Model, with effective wind-bracing frames. These frames were modeled with a rigid material.

And the buckling shape, as illustrated next for the conditioning LD1, gave a buckling factor result of  $\lambda = 29.5$  and a maximum axial compression force on the arch of  $N_{Ed} = -7670$  kN, which results in a  $N_{FE,el} = 226265$  kN (Figure 147). This is a very similar, slightly higher, result than the given from the *Eurocode* ( $N_{cr} = 207310$  kN) and may have to do with *Eurocode's* several approximations, or simply due to the imprecision on reading the *table D.1* of the code, which gives  $\beta$  - buckling length factor.

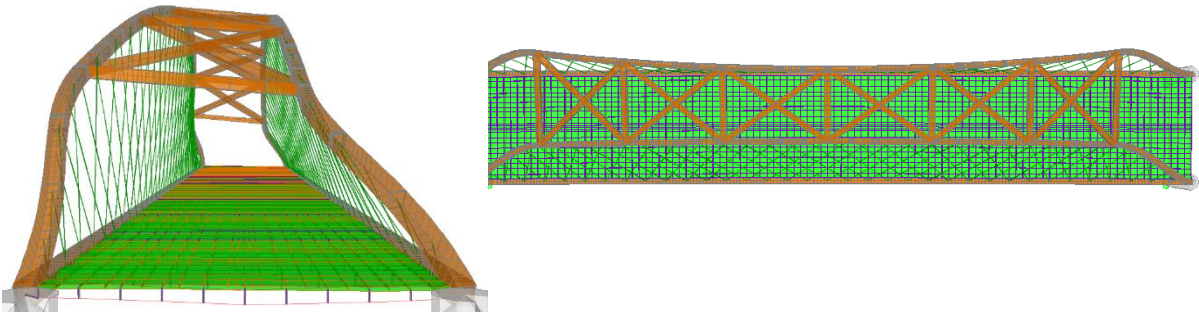


Figure 147 - FE Network Model, with effective wind-bracing frames. First buckling mode for LD1.  $\lambda=29,51$ .

## Chapter 5. Hanger Arrangements and Arch Instability Investigations

From this result it is clear that more effective bracings beams highly increase stability. To adopt them, in the final solution, is a matter of balancing the arch resistance's increment, with aesthetics. In the present solution, reduction factors around 0.8 were satisfactory enough and no improvement on the bracing and loss of esthetical value were required. Anyway, a good example of this effective bracing system is shown in Figure 148.



Figure 148 – Example of an efficient bracing system. Waikato River Network Arch Bridge.

But also of interest is to proceed according to “Out of plane buckling factors for free standing arches” *EC3* procedure, which naturally gives a load bound of the real value.

Having a constant inertia on the arch, a rise of 0.163 times the span, and with all load transmitted by hangers to the arch, one obtains, according to *EN1993-2 D.3.3*:

$$\beta_1=0.613 \quad ; \quad \beta_2=0.650 \quad ; \quad \beta = \beta_1 \times \beta_2 = 0.613 \times 0.650 = 0.398$$

Therefore:

$$N_{cr} = \left( \frac{\pi}{0.398 \times 180} \right)^2 \times 210 \times 10^6 \times 0.0471 = 19021 \text{ kN}$$

This result obtained by this *Eurocode* procedure is the equivalent of analyzing the stability of the bowstring bridge of Figure 149, without wind-bracing.

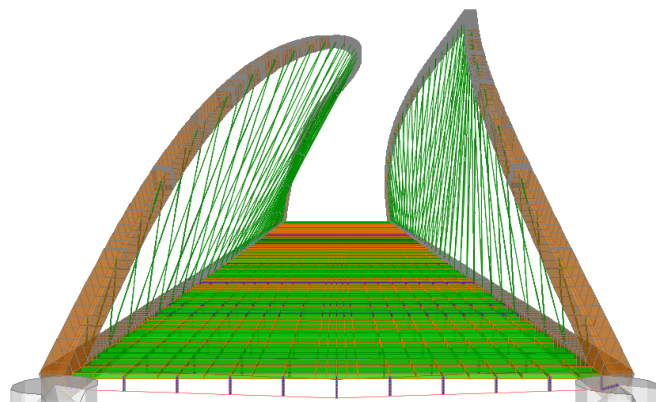


Figure 149 – Network Model without wind-bracing. LD1 buckling analysis.  $\lambda=3,27$ .



And for this equivalent bridge, the FEM analysis gave:  $\lambda=3.266$  ;  $N_{Ed} = -7668$  kN ;  $N_{FE,el} = 25044$  kN. Again, very much coincident with the *Eurocode's* result and slightly less conservative.

The immediate conclusion is that the difference between these two *Eurocode's* procedures: “Out of plane buckling of arches with wind bracing and end portals” and “Out of plane buckling of free standing arches”, is simply too big for them to provide satisfying results and conclusions. They can only be considered as defining an upper and lower boundary of the real critical load of the actual structure.

A proposed method to obtain a more accurate buckling factor  $\beta$  by Belgian researchers – *Outtier et al. (2010)*, can be a solution. This method was achieved based on a database of more than 50 steel tied arch bridges spanning from 45 to 200 m. A linear and a detailed nonlinear elastic-plastic analysis was performed on these bridges with differences on the size of the arch box section, on the type of bearing system, on the load type, hanger configuration and also on the amplitude and size of the assumed imperfections. Then a comparison was made between nonlinear results (more accurate) and results from the linear analysis, complemented with *EN1993-1-1* curves and procedure to attend to imperfections and residual stresses. This comparison resulted in two proposed procedures, from these researchers:

1. The first one is to perform a linear analysis on the FEModel and then adjust the influence of imperfections and residual stresses with “curve a” of the *EN1993-1-1 Section 6.3*, since it was verified that this curve was the most suitable one for steel tied-arch bridges, having a welded box section as the arch cross-section and with span lengths of 50 to 200 m.
2. The second is to determine the  $N_{cr}$  according to the *EN1993-2 Annex D.3*, but with an alternative buckling length factor -  $\beta_{alt}$  - as described next.

The  $\beta_{alt}$ , proposed by *Outtier et al. (2010)* was defined as a function of the out-of-plane bending inertia of the arch –  $I_z$  - and the arch's span –  $l$ :

$$\beta_{alt} = \beta_A + I_z \times (\beta_B - l \times \beta_C)$$

Its parameters  $\beta_A$ ,  $\beta_B$  and  $\beta_C$  were numerically obtained by adjusting the  $\beta_{alt}$  result to real values of  $\beta$  obtained with the nonlinear elastic-plastic analysis for the 50 bridges examples. At the end, the “adjustment” was remarkably good, and when later accounting for imperfections and residual

## Chapter 5. Hanger Arrangements and Arch Instability Investigations

stresses with “curve a”, an even more accurate and safe reduction factor  $X_{alt}$  was achieved, when compared to the real reduction factor that came with nonlinear analysis.

With the obtained parameters, valid for rise/span ratios between 0.15 and 0.20, the alternative buckling length factor is:

$$\beta_{alt} = 0,255 + I_z \times (16,939 - 1 \times 0,114) \quad (8)$$

Which, by introducing the designed arch bridge data, results in:

$$\beta_{alt} = 0,255 + 0,0471 \times (16,939 - 180 \times 0,114) = 0,0863 \quad (9)$$

Therefore:

$$N_{cr} = \left( \frac{\pi}{0,0863 \times 180} \right)^2 \times 210 \times 10^6 \times 0,0471 = 404551 \text{ kN} \quad (10)$$

This result is unexpectedly high and some considerations can be made. First, it should be referred that a crucial cause for the results of the buckling length factor is the lateral clamping of the arch springs. A higher  $I_z$  on the arch is associated with a weaker lateral clamping since, in the spring, the cross-sections which the arch connects to, in particular the end cross-girders that are usually conditioned by the transversal bending, get relatively smaller and therefore offer less clamping to the arch so, a weaker clamping results, and  $\beta$  increases. Observing carefully this simplified alternative method it is first noticeable that the  $\beta_{alt}$  resulted lower than its factor  $\beta_A$ , which means that the second member of the expression to obtain  $\beta_{alt}$  (that takes into account the bending inertia and span length of the arch) has a negative value. In fact, for spans greater than 150 m, this addend results negative, and the inertia contributes negatively to the buckling length factor. Additionally, by introducing in the formula a slightly higher value  $I_z$ , for the same 180 m span,  $\beta$  results negative, which is unconceivable. Thanks to one of the researcher’s consideration on this issue, it was confirmed that this was not intended to occur. Even though the proposed formula initially was envisaged for bridges spanning until 200 m, the proposed alternative buckling length factor starts losing its sense for bridges spanning over 150 to 160 m. Finally, the beta-factors are dimensionless, whereas  $I_z$  has the dimension of  $m^4$ . The formula should somehow be improved by introducing  $I_z$  as a dimensionless parameter. Concluding, it is worthwhile trying to improve the formula and to extend

its validity domain in the future since it offers a pretty straightforward and easy procedure to obtain the critical buckling load of a bowstring arch bridge.

### 5.3.4 Discussion of the results

The results obtained by the FEModel linear analysis, adjusted as prescribed by *Outtier et al (2010)* (using curve a), are finally presented in Table 46, for the 4 hangers' arrangements:

**Table 46 – Design buckling resistance comparison for the 4 hangers' geometries.**

	$N_{cr}$	$\lambda$	$\alpha$	$\chi$	$N_{b,rd}$
Vertical	99316	0.928	0.21	0.715	61186
Nielsen	131215	0.807		0.791	67708
Network	130231	0.811		0.790	67557
Opt. Network	127343	0.820		0.784	67098

These final results, of the Network Model, were adopted for the design of the network arch bridge solution presented in this study.

The vertical model has a significantly (10%) lower buckling resistance compared to the other hangers arrangements, so again the advantages of a network arrangement are clear.

However, an important conclusion on this chapter is that hangers' arrangements don't significantly affect directly the stability of the arch. This is because the dominant buckling modes on the present bridge have a predominant out-of-plane deformation, little affected by the hangers' arrangement. "*The hangers give the arch good support in the plane of the arch.*" – *Tveit. P (2011)*. Nevertheless, hangers' arrangements do have a serious and critical influence on the stress distribution of the entire bridge. The different distributions of axial forces and bending moments between models will greatly influence the stability of the arch, and that traduces into the differences obtained between models' results.

From the performed comparison between methods used for assessing stability it is possible to conclude that a linear analysis on a FEModel gives values, not only on the safe side, but also gives a reasonable idea of the real buckling stability and behavior of the arch. Though, here, common sense must be used to evaluate the possibly problematic events occurring under the extremely high live

## Chapter 5. Hanger Arrangements and Arch Instability Investigations

loads or to even decide on which loads to increase until buckling failure. Nonlinear analysis gives even more accurate results but may need extra man-hours, a powerful software and good background knowledge to be performed, which can be a drawback in the design process. As for an option without a FEModel, using only the *Eurocode's* guidance, results may vary quite a lot, which turns to be potentially dangerous issue or, taking the "lower boundary", very uneconomical.

In the author's opinion, for out-of-plane conditioned tied-arch bridges *Eurocode* may be carefully used in the two situations analyzed and successfully compared: i) when no bracing beams exist, or ii) when the bracing beams form a really stiff structure. It is however clear that an integrated methodology for the simplified analysis of in-plane and out-of-plane buckling of the arch still needs to be developed.

## 6. Conclusions and Future Developments

### 6.1 General Conclusions

The conclusions of this study are mainly focused on the performance of the Network arch bridge.

The design performed allowed substantial material savings when compared to many other tied arch bridge solutions. Then, both Network arrangements analyzed evidenced clear structural advantages over the Vertical arrangement, for the most relevant results analyzed, i.e. forces and bending moments distributions on the arch and on the ties, global deflections and overall stability. Even though, only the half-span load case truly shown the large advantages for the Network arrangements, the full span load case also presented clear advantages for them. In fact, the Vertical hangers' arrangement only presented benefits for the hangers' forces, as a consequence of over requesting the bending stiffness of the chords. Additionally, using the Nielsen hangers' arrangement, if significant unsymmetrical live loads occur, the relaxation of hangers will cause serious consequences making this solution to behave dangerously similarly to the Vertical model. Since the Nielsen arrangement has no advantages to offer for the hangers' forces, unless its hangers are resistant to compression, it results with no relevant benefits over the Network arrangements. It is clear that large arch spans enhance all these results and differences between arrangements.

With respect to arch buckling, with the inclination of the arches and with the presence of the bracing beams it is extremely unlikely to occur a pure in-plane buckling. The inclination of the arches also reduces the wind portal frames and the bracing beams length, resulting in a more stable solution than another one with "vertical" arches.

Regarding aesthetics, a higher number of hangers may in fact result into a more transparent structure, due to the arch and tie cross-section savings, and also due to hanger's smaller cross-sections.

The pre-design of the hanger's arrangement, facilitated by *Per Tveit (2011)* and *Brunn & Schanack (2003)*, proved to be remarkably accurate on the benefits it predicted, which should be an extra encouragement for engineers who design Network bridges for the first time.

Finally, this study hopes to have demonstrated that Network arch bridges can be competitive and structurally efficient when compared to other tied-arch bridges. The minor number of existing

examples, amongst with the confirmed advantages of this structure, by several researchers' work and some built examples, suggests that engineers should make a greater commitment to the understanding and eventual designing of Network arch bridges. They should be a more often adopted bridge solution, for structural efficiency, for competitive gains, and for aesthetical reasons.

## 6.2 Future Developments

Possible improvements and future developments to the study presented here, are as follows:

- Could be studied a ties cross-section changing from the corners to the remaining length of the span.
- A composite slab should be attempted using a steel sheet as a formwork to possibly reducing marginally the slab's thickness. Even though the ribs of the steel plate, oriented longitudinally, could compromise some of the transversal composite behavior of the ribs, the gains from the point of view of construction may be relevant. Also, for the pre-slab solution adopted, some results were against the security in respect to the unknown dimensions of the pre-slab, assumed with an equal bending inertia as the final slab.
- The ribs variable cross-section could be slightly optimized in the detailed design.
- Other load length ratios could be attempted to test relaxation.
- A nonlinear instability analysis could be performed to confirm the predicted buckling results.
- A better arch curvature, close the arch springs, other than the advised 80% of the main curvature by *Brunn & Schanack (2003)*, could be envisaged, since the bending moments' results suggest there must be a better curvature to decrease the moments at the spring.

## References

**Brunn & Schanack (2003)** - Benjamin Brunn & Frank Schanack - Calculation of a double track railway network arch bridge applying the European standards - Dresden University of Technology, Department of Civil Engineering, Institute for Structures and Materials, Chair of Steel Structures.

**De Backer (2009)** - De Backer, A. Outtier & Ph. Van Bogaert - The effect of using beam buckling curves on the stability of steel arch bridges H. - Bridge Research Group, Civil Engineering Department, Universiteit Gent, Gent, Belgium.

**EN1990** - European Committee for Standardization (CEN), "Eurocode 0 – Basis of structural design", April 2002

**EN1991-2** - European Committee for Standardization (CEN), "Eurocode 1 – Actions on structures – Part 2: Traffic loads on bridges", September 2003

**EN1991-1-4** - European Committee for Standardization (CEN), "Eurocódigo 1 – Acções em estruturas – Part 1-4: Acções gerais. Acções do vento", 2010

**EN1991-1-5** - European Committee for Standardization (CEN), "Eurocódigo 1 – Acções em estruturas – Part 1-5: Acções gerais. Acções térmicas", 2009

**EN1992-1-1** - European Committee for Standardization (CEN), "Eurocode 2 – Design of concrete structures – Part 1-1: General rules and rules for buildings", December 2004

**EN1993-1-1** - European Committee for Standardization (CEN), "Eurocode 3 – Design of steel structures – Part 1-1: General rules and rules for buildings", December 2003

**EN1993-1-9** - European Committee for Standardization (CEN), "Eurocódigo 3 – Projecto de estruturas de aço – Parte 1-9: Fadiga", 2010

**EN1993-1-11** - European Committee for Standardization (CEN), "Eurocode 3 – Design of steel structures – Part 1-11: Design of structures with tension components", October 2006

**EN1993-2** - European Committee for Standardization (CEN), "Eurocode 3 – Design of steel structures – Part 2: Steel Bridges", October 2006

## References and Appendixes

**EN1998-1** - European Committee for Standardization (CEN), “Eurocode 3 – Design of structures for earthquake resistance – Part 1: General rules, seismic actions and rules for buildings”, December 2004

**Gonçalves, P. (2012)** - Pedro Pereira Clemente Andrade Gonçalves - Estudo Prévio de um Tabuleiro em Arco Superior do tipo Bowstring - Tese de Mestrado, Instituto Superior Técnico.

**Outtier (2007)** - Amelie Outtier - Assessment of the out-of-plane imperfections of a steel tied arch bridge - Ghent University, Civil Engineering Department, Belgium. ARCH’07 – 5th International Conference on Arch Bridges.

**Outtier et al. (2010)** - Amelie Outtier, Hans De Backer, Ken Schotte, Dries Stael, Philippe Van Bogaert - Design methods for buckling of steel tied arch bridges - 34th International Symposium On Bridge And Structural Engineering, Venice.

**Per Tveit (2011)** - The Network Arch. Findings on network arches during 54 years. Available at:

[http://home.uia.no/pert/index.php/The\\_Network\\_Arch](http://home.uia.no/pert/index.php/The_Network_Arch) [10/09/2013]

**Schanack F. (2008)** - Frank Schanack - “Network Arch Bridge” Ph D Thesis, Universidad de Cantabria, ACHE, Santander, España.

**Valenzuela (2010)** - Matías A. Valenzuela, Franco R. Rojas, Ángel C. Aparicio - Finite-element nonlinear geometric analysis for a proposal steel arch bridge over the Llobregat River in Barcelona - 6th International Conference on Arch Bridges.

### **Bridges:**

**Pentele Bridge (2006)** - M8 Dunaújváros Danube-bridge, Hungary:

<http://en.hid.hu/references/view/pentele-bridge-7> [10/9/2013]

**Lake Champlain Bridge (2011)** – The new bridge connecting Vermont to New York State:

<http://www.bridgeweb.com/MemberPages/Article.aspx?typeid=3&id=2549> [10/9/2013]

**Fort Pitt Bridge (1959)** – Monongahela River, City of Pittsburgh:

<http://www.brooklineconnection.com/history/Facts/FtPittBridge.html> [10/09/2013]



# Appendixes

## References and Appendixes

## Appendix A – Bowstring Bridge Characteristics and Loads

**Table A.1 - Bowstring bridge main characteristics**

Arch span	180	m
Arch curved length	193.13	m
$t_{\text{concrete slab}}$	0.25	m
$b_{\text{concrete slab}}(\text{width})$	25.08	m
$b_{\text{cover}}(\text{width})$	21.96	m
$t_{\text{cover}}$	0.07	m
Rib's length	25.08	m
Number of ribs	35	-
f (arch height)	30	m
Start angle (arch)	37.758	degrees
N <sup>o</sup> hangers	140	-
Average hanger length	23.80	m

**Table A.2 – Materials adopted for each element**

	Tie	Arch	Rib	Hanger	Slab	
Material	-	S420	S420	S355	S460N	C40/50
$f_{yd}$	MPa	420	420	355	-	26.7

**Table A.3 - Material's Unit Weight -  $\gamma$**

Concrete	25	kN/m <sup>3</sup>
Asphalt cover	25	kN/m <sup>3</sup>
Light Concrete ( <i>UniLeve D1.0</i> )	13	kN/m <sup>3</sup>
Steel	77	kN/m <sup>3</sup>

**Table A.4 - Dead Loads**

Reinforced Concrete Slab		Volume (m <sup>3</sup> /m)	Weight (kN/m)	Total Weight (kN)
250 mm thick slab		6.269	156.73	28211
250 mm thick slab + reinforcement		6.269	169.53	30515
Steel Elements (Element units)		Area (m <sup>2</sup> )	Weight (kN/beam)	Total Weight (kN)
Arches (2)		0.2037	-	6077
Ties (2)		0.1622	-	4496
Hangers (140)		0.005027	-	1290
Ribs (35)	center section	0.0689	-	-
	end section	0.0353	-	-
	average section	0.0521	100.6	3521
End cross girders (2)	center section	0.1488	-	-
	end section	0.1168	-	-
	average section	0.1328	256.4	513
	Bracing beams (7)	average length	0.1856	249.8
Total Steel Dead Load		-	-	17645

**Table A.5 - Superimposed Dead Loads**

SDL	kN/m <sup>2</sup>	kN/m
Two central concrete blocks	-	16.51
Asphalt cover	1.75	38.44
Two light concrete sidewalks	-	4.9582
Two railing systems	-	4
Two lighting systems	-	1.1
Total SDL		65.01

**Table A.6 - Live Loads**

UDL	12960	kN	72	kN/m
TS	1200	kN	-	kN/m
Live Loads <sub>total</sub>	14160	kN	(72+)	kN/m

**Table A.7 – Resume of the *Bowstring* bridge main vertical loads**

DL <sub>concrete</sub>	169.5	kN/m	30515	kN
DL <sub>steel</sub>	98.0	kN/m	17645	kN
DL <sub>(total)</sub>	267.6	kN/m	48160	kN
SDL	65.0	kN/m	11701	kN
DL + SDL	332.6	kN/m	59861	kN
UDL	72	kN/m	12960	kN
TS	-	kN/m	1200	kN
DL+SDL+UDL+TS	404.6	kN/m	74021	kN
1.35*(DL+SDL+UDL+TS)	546.2	kN/m	99928	kN

## References and Appendixes

## Appendix B – Combination of Actions $\Psi$ Factors

Bases para la combinación de acciones  
Valores representativos

TABLA 6.1-a FACTORES DE SIMULTANEIDAD  $\psi$

ACCIÓN		$\psi_0$	$\psi_1$	$\psi_2$	
Sobrecarga de uso	Vehículos pesados	0,75	0,75	0	
	gr 1, Cargas verticales	Sobrecarga uniforme	0,4	0,4	0 / 0,2 <sup>(1)</sup>
		Carga en aceras	0,4	0,4	0
		gr 2, Fuerzas horizontales	0	0	0
	gr 3, Peatones	0	0	0	
	gr 4, Aglomeraciones	0	0	0	
	Sobrecarga de uso en pasarelas	0,4	0,4	0	
Viento	$F_{wk}$	En situación persistente	0,6	0,2	0
		En construcción	0,8	0	0
		En pasarelas	0,3	0,2	0
Acción térmica	$T_k$	0,6	0,6	0,5	
Nieve	$Q_{Sn,k}$	0,8	0	0	
Acción del agua	$W_k$	Empuje hidrostático	1,0	1,0	1,0
		Empuje hidrodinámico	1,0	1,0	1,0
Sobrecargas de construcción	$Q_c$	1,0	0	1,0	

(1) El factor de simultaneidad  $\psi_2$  correspondiente a la sobrecarga uniforme se tomará igual a 0, salvo en el caso de la combinación de acciones en situación sísmica (apartado 6.3.1.3), para la cual se tomará igual a 0,2.

## References and Appendixes



## Appendix C - Approach Viaduct Structural Verifications

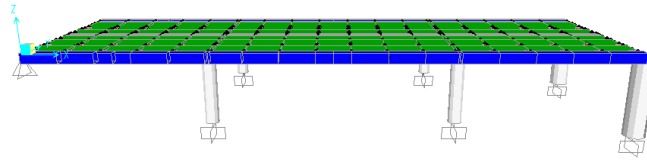


Figure 150 – Left approach viaduct model.

### C.1 Deck Slab

The main differences from this slab to the one in the bowstring span, is the global bending moment, affected by the different support conditions, and the un-existing tension from the arch's functioning. In this bridge deck, the resultant stresses were also obtained for an un-cracked stiffness slab model.

The global and local deflections of these approach viaducts' slab are profoundly related the longitudinal bending behavior and can be seen next, where the local deflection result from the 5 m slab span between ribs.

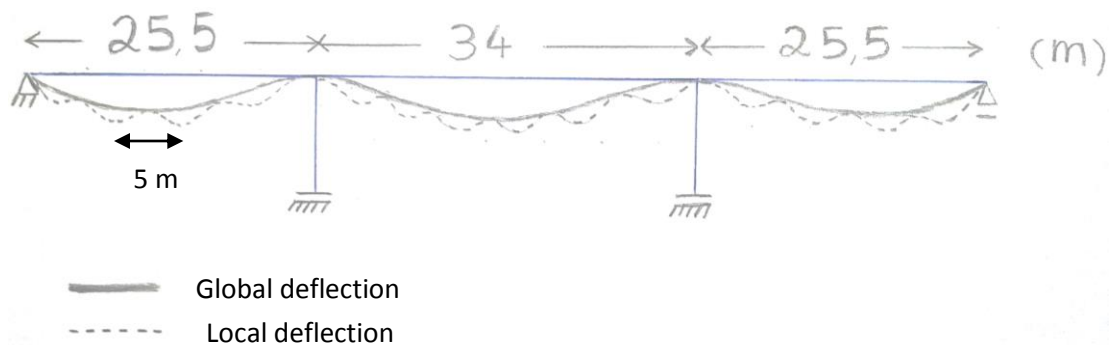


Figure 151 - Global and Local deflections.

Considering the constructive procedures, which induces the use of simply supported pre-slabs, the summary of the relevant stress results are displayed in the next page.

## References and Appendixes

**Slab - Stress Results**

	$m_{11}^+$	$m_{11}^-$	$V_{max}$
DL	180	0	17
SDL	8	-11	20
UDL <sup>(1)</sup>	13	-16	20
TS <sup>(2)</sup>	90	-45	95
ULS <sup>(3)</sup>	174	-97	205
SLS <sup>(4)</sup>	99	51	120
<hr/>			
	$m_{11}$ (kNm/m)	$v_{max}$ (kN/m)	

$$(1) \text{ UDL}(R1\_R) - m_{11}. \text{ UDL}(1R\_R) - v_{max}$$

$$(2) \text{ TS}(R31\_2R) - m_{11}. \text{ TS}(123R\_R) - v_{max}$$

$$(3) \text{ ULS} = 1.35 \times (\text{DL} + \text{SDL} + \text{UDL} + \text{TS})$$

$$(4) \text{ SLS} = 1 \times (\text{DL} + \text{SDL}) + 0.4 \times \text{UDL} + 0.75 \times \text{TS}$$

The tension and compression longitudinal forces on the slab, from the longitudinal composite behavior of the tie when bending, are negligible, comparing to those on the bowstring, and do not occur at the same section of the maximum bending moments do so they were not considered together.

The slab of the bowstring resists to slightly higher bending moments, combined with tension forces, so this slab of the approach viaducts won't be conditioned by these moments.

The shear forces are more relevant in this viaduct deck than in the bowstring bridge deck and are difficult to obtain accurately due to the model's deficiency on the tie-slab interaction. This deficiency causes the model to return very incongruent concentrated values. The conditioning zone is close to the columns and average values were adopted. The shear resistance verification follows the *Eurocode 2* formulation:

$$V_{Rd,c} = [C_{Rd,c} k (100 \rho_l f_{ck})^{\frac{1}{3}} + k_1 \sigma_{cp}] b_w d$$

Where for the present case:

$$C_{Rd,c} = \frac{0.18}{\gamma_c} = \frac{0.18}{1.5} = 0.12$$

$$d = 197.5 \text{ mm}$$

$$k = 1 + \sqrt{\frac{200}{d}} = 2.0 \leq 2.0$$

$$\rho_l = \frac{39.27 \times 10^{-4}}{1 \times 0.1975} = 0.0199$$

$$f_{ck} = 40 \text{ MPa}$$

Thus, the slab shear resistance, without proper reinforcement for the shear effort effects is obtained by:

$$V_{Rd,c} = 0.12 \times 2(100 \times 0.0199 \times 40)^{\frac{1}{3}} \times 1000 \times 197.5 \times 10^{-3} = 204.2 \text{ kN}$$

$$V_{Rd,c} = 204.2 \sim 205 = V_{Ed}$$

The shear resistance and the design value of the applied shear force have similar values. The security is not verified by a small difference. This deserves two important considerations, i) an appropriate tie-slab interaction in the model is crucial to well evaluate this problem, and also ii) the rib-slab interaction, done in the model at discrete points, crucially affects the results. If a future detailed local analysis of this problem doesn't assure the necessary resistance, two immediate interesting solutions can be adopted:

1. Deliberately produce a settlement on the central columns, decreasing some permanent global moments and global shear stresses in these zones (although the concrete creep reduces some of this effect);
2. Change, from the light concrete solution on the sidewalks, to a thicker reinforced concrete slab in this area. Both ribs and longitudinal beams have conditions to lodge this little extra weight;
3. Consider a proper reinforcement for resisting the shear efforts.

Concluding, the same slab solution of the bowstring span can be used on the approach viaduct decks.

## C.2 Longitudinal Beams

Scaffolding is used during the deck construction to aid the positioning and welding of the steel structure of the approach spans. However, this scaffolding is assumed to have no contribute to the ties resistance, during construction. For that reason, the ties will resist alone to the dead loads (a non-stiff concrete slab is modeled), and only for the superimposed dead loads and live loads the longitudinal composite behavior of the tie-slab is activated (a stiff concrete slab is modeled).

## References and Appendixes

The summary of the resultant forces, at the most demanding section (above the central columns), is presented in the table of next page.

	$M_{33}^+$	$M_{33}^-$	$N^-$	$V_{22}$	$V_{33}$	$M_{22}$	T	Slab Model
DL	5766	-10027	0	-2001	0	0	-250	Unstiff
SDL	1290	-2300	-360	-530	25	176	-36	Stiff
UDL <sup>(1)</sup>	2429	-3869	-654	-825	49	31	70	Stiff
TS <sup>(2)</sup>	4100	-2626	-502	-797	148	300	538	Stiff
ULS	18340	-25410	-2047	-5607	300	684	435	Stiff
Units	kNm	kNm	kN	kN	kN	kNm	kNm	

(1) UDL(1R\_R)

(2) TS(123R\_R)

However, another ULS needs to be verified: the launching of the arch over the approach deck already built.

	$M_{33}^+$	$V_{22}$
DL(Steel)	1406	0
Arch Concentrated Load <sup>(1)</sup>	25001	2206
ULS	35649	2978
Units	kNm	kN

(1) Concentrated load in each longitudinal beam at the conditioning section: 4411 kN (4411kN results from the bowstring steel structure weight 17645kN, divided by four supports).

This ULS (Constructive Process) is the most demanding combination due to the high value of the bending moment applied. This special request of the longitudinal beam resistance, and the deflections observed for all loads influenced the choice of a thicker solution for the cross section than the one in the bowstring span. The external dimensions of the element are kept the same for aesthetic reasons.

Nevertheless, the elastic resistance of these beams is still verified since:

$$M_{Ed,33} \leq M_{eL,Rd\ 33} \Leftrightarrow 35649\ kNm \leq 37501\ kNm$$

The design shear force applied ( $V_{Ed} = 2978$  kN) is much lower than the design shear resistance ( $V_{c,Rd}=25480$  kN). As for the SLS, the deflections, and indirectly the vibrations, are verified for all the loads applied:

**Longitudinal Beam – SLS – Deflections**

	DL	SDL	UDL	TS	Total	L/500
$\delta$ (m)	0.0327	0.0071	0.0078	0.0161	0.064	0.068
Model	Unstiff	Stiff	Stiff	Stiff	-	-

The limit of L/500 is accomplished and again the highest value results from the DL as expected, although a precamber deformation should be introduced to eliminate the permanent vertical deformations. The live load deflections do not constitute an issue since the stiff concrete increases very much the bending stiffness of the deck. The longitudinal deck deflection is verified.

There is a possibility of adopting the same cross-section here as in the bowstring bridge if temporary steel columns are used to support the longitudinal beams at mid-span sections during the launching of steel arch and after, during the execution of the concrete slab.

### C.3 Columns

The most stressed columns are the two close to the abutment, which restrain the deck transversal movement. The resultant forces are displayed:

**Approach Viaduct Conditioning Column – Normal Forces and bending moments**

	DL	SDL	UDL(1R_R)	TS(123R_R)	Earthquake	Wind	Total
$N_{Ed}$ (kN)	-4416	-945	-1514	-963	-	-	-7838
$M_{Ed,22}$ (kNm)	-	-	-	-	271	838	1109

As it can be seen the most demanding action is the wind. Nevertheless, the circular columns with 2 m diameter for aesthetical reasons are extremely oversized for these actions so only the minimum reinforcement defined in *EN1992-1-1* should be applied. The aesthetical concern is to decrease the contrast to the wider main columns that also support the bowstring bridge.

## References and Appendixes

## Appendix D – Bowstring Arch Main Columns Verifications

Four main columns, two in each end of the bowstring span support simultaneously the approach deck and the bowstring bridge deck. The most stressed column is the one that restrains all the bowstring bridge displacements, and its forces, with the following design effects at the bottom cross section are displayed.

Main Column – ULS - Forces at the bottom cross-section					
	Approach Viaduct	Bowstring	Column	Total	Units
$N_{Ed,min}$	1395	14965	1997	18357	kN
$M_{Ed,22}$	838	34230	-	35096	kNm
$M_{Ed,33}$	0	9105	-	28278	kNm

Bending moments  $M_{22}$  and  $M_{33}$  are both caused by the wind action and are already scaled by a factor of 1.5 at ULS. The axial forces aren't scaled since their effects are beneficial to the design check. The earthquake was not conditioning in the design.

The  $M_{33}$ , which is in the same direction as the bridge, is particularly high. This is due to the support conditions in both columns which prevent the left side of the bowstring bridge to rotate freely. The bending stiffness of each column is so great that it can compare to the horizontal bending stiffness of the deck, making it to partially behave as illustrated in Figure 104 of the ties sub-chapter, when wind acts. This results in high “longitudinal” bending moments in the columns. The bending induced in the column by the eccentric axial forces from each bridge support over the column can be largely eliminated by the correct positioning of the support plates of each bridge, and no second order eccentricities are to be expected for these low slenderness columns. Columns are circular massive concrete section, 3 m diameter and with 55 rebars disposed circularly with a 25 mm diameter (Figure 152).

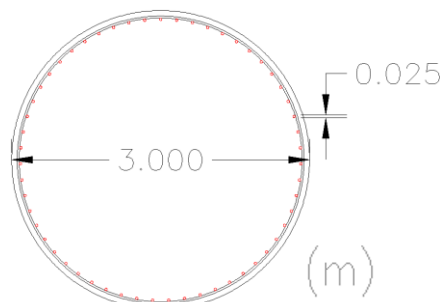


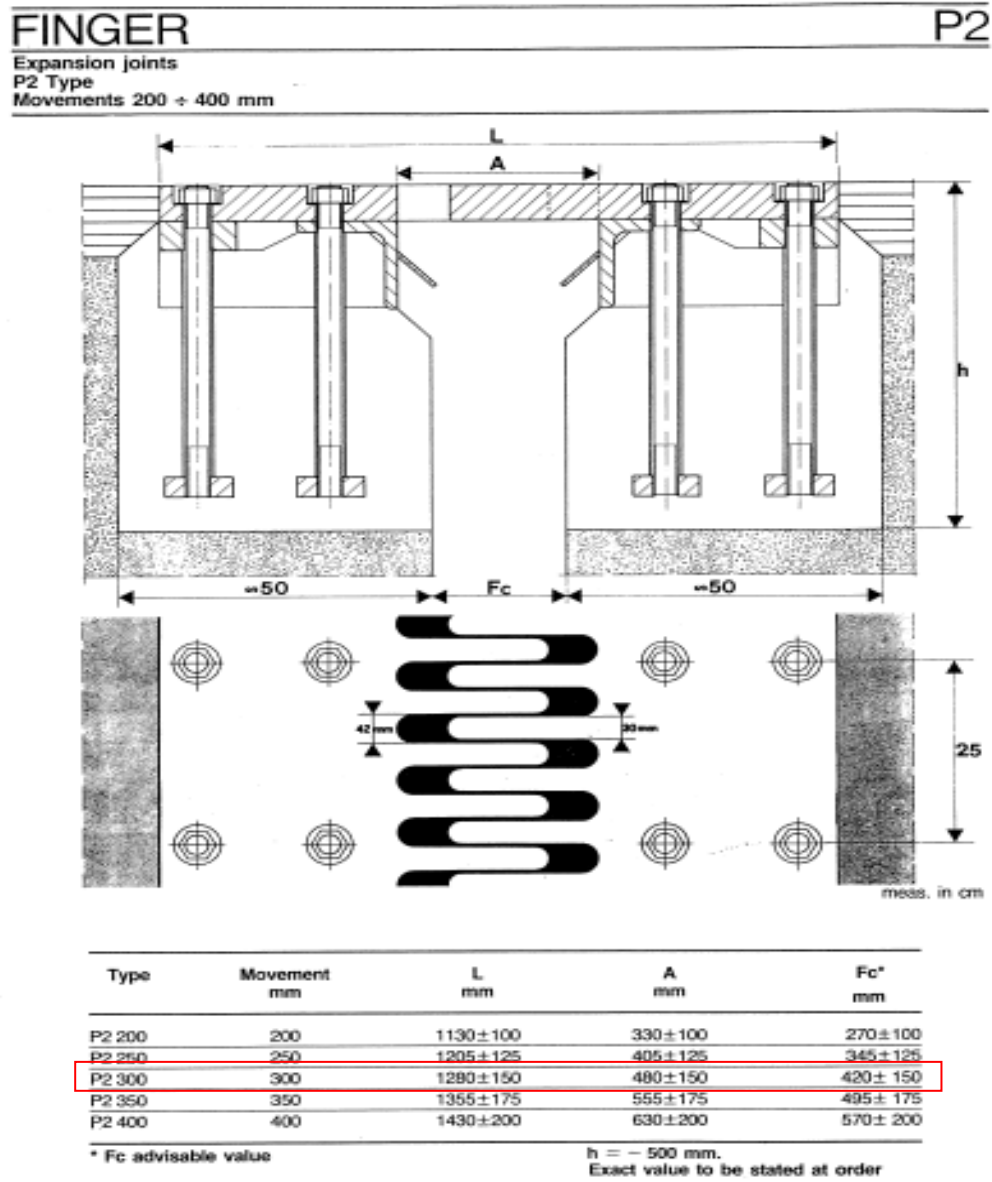
Figure 152 – Column shared between the bowstring and the approach viaduct. Detail of the main reinforcement - 55 $\phi$ 25.

## References and Appendixes



## Appendix E – Expansion Joint Definition

Adopted expansion joint: FINGER P2 300.



Technical modifications reserved.

alga  
via Olona 12  
20123 MILANO  
Tel. 02/49.87.946 (ric. aut.)  
Fax 02/28.10.21.11